On the occurrence and modeling of surface water floods

Inauguraldissertation
der Philosophisch-naturwissenschaftlichen Fakultät
der Universität Bern

vorgelegt von

Daniel Benjamin Bernet

von Grindelwald

Leiter der Arbeit:

Prof. Dr. R. Weingartner
Dr. V. Prasuhn

Geographisches Institut der Universität Bern
Agroscope, Zürich

On the occurrence and modeling of surface water floods

Inauguraldissertation
der Philosophisch-naturwissenschaftlichen Fakultät
der Universität Bern

vorgelegt von

Daniel Benjamin Bernet

von Grindelwald

Leiter der Arbeit:

Prof. Dr. R. Weingartner
Dr. V. Prasuhn

Geographisches Institut der Universität Bern
Agroscope, Zürich

Von der Philosophisch-naturwissenschaftlichen Fakultät angenommen.

Bern, 5. Oktober 2017

Der Dekan:
Prof. Dr. G. Colangelo

Floods are 'acts of God,' but flood losses are largely acts of man.

—Gilbert F. White, 1942

Abstract

Triggered by devastating flood events, surface water floods (SWFs) have received increasing attention in the more recent past. Nonetheless, the general process-related knowledge about this flood type is still rather limited. The eminent lack of data at a high spatial and temporal resolution, as well as coverage, hampers the study of the involved processes' characteristics and impairs the development and evaluation of new tools. Thus, the main objectives of this thesis are, firstly, to compile a representative data set of flood damage records and to devise new methods allowing the classification thereof according to the triggering flood type, i.e., SWFs or fluvial floods. Secondly, the classified data are analyzed with respect to the floods' occurrences in space and time in order to infer salient features of SWFs. Thirdly, in order to contribute to the increasing consideration of SWFs in hazard assessments, a commonly applied modeling approach is evaluated in relation to its reliability with which observed inundations of rural areas can be predicted with models of varying complexity within diverse settings.

The first part of this thesis elaborates the occurrence of SWFs based on spatially explicit records of buildings damaged by floods. For that matter, a data set comprised of records from 14 different public insurance companies for buildings (PICB) was collated. The data were harmonized and geocoded. Each record contains the damage date, the damage location, as well as the incurred losses. The buildings' direct tangible losses were corrected for inflation, as of 2013. Moreover, the number of buildings and the total sum insured were estimated in order to account for the effects of socio-economic development on the damage values. With these ancillary data, the relative number of damage claims and associated relative losses were assessed. Overall, the collated data set contains 63'117 damage claims, covers periods of 10 to 33 years depending on the PICB, and overall covers 48 % of all Swiss buildings.

For the exploitation of this type of data, a method has been drafted in a pilot study, in order to associate each record either with SWFs or fluvial floods, respectively. The pragmatic classification scheme is based on the location of each damaged object and additional spatial information, i.e., fluvial flood hazard maps as well as a river network. Based on findings from the pilot study, the scheme was further refined by a simple consideration of the topography, requiring a digital elevation model as an additional input. The classification scheme produces a robust, lower estimate of the damage caused by SWFs, induced by the limitation that the two flood types cannot be differentiated automatically from each other within the overlapping flood domains, i.e., within the areas prone to fluvial floods around watercourses.

The data's analyses highlight the significance of SWFs in Switzerland. Namely, 45 % of the damage claims could be associated with SWFs. In terms of the incurred losses, SWFs contribute to 23 % of the total flood losses, which is due to the lower losses per claim in comparison to the increased losses caused by fluvial floods. Some regions suffer from more damage than others. For instance, the Swiss lowlands are affected the most in terms of relative and absolute values, while the alpine regions are affected the

least. The distribution of the relative damage within these regions indicate that urban areas are affected just as rural areas are, too. By far the most damage is caused in the summer months, save a few exceptions. Within the period 1993–2013, the time series of normalized SWF damage does not show a significant upward trend, highlighting the dominant role of socio-economic development driving the ongoing increase of damage in absolute numbers.

The second part of this thesis elaborates how well inundation extents of SWFs in rural areas, inferred from various sources, can be reproduced with a common modeling approach based on single deterministic simulations of flood inundation models. Three hydrodynamic flood inundation models with varying complexity (i.e., "FLO-2D", "FloodArea", and "r.sim.water") were selected. They were complemented by a multiple flow direction algorithm ("MFD"). Firstly, all four models were applied to four artificial surfaces, each representing a characteristic slope form (i.e., a plane, an ellipsoid, an inverse ellipsoid, and a saddle) and each including an incised street. This modeling exercise highlighted inherent model differences, foremost in relation to the predicted flow patterns downslope of the incised street. Furthermore, the models' disagreement was highest for the prediction of flow over the ellipsoid characterized by a convex slope form. Secondly, the four models were applied to eight real-world case studies covering diverse geographical and meteorological settings. The models' performances were low for all case studies, indicating that reliable predictions of rural areas' inundations caused by SWFs are not (yet) feasible with the employed modeling approach and the available input data. Thereby, the need for model calibration and/or validation is highlighted, in addition to the requirement of better observational data. Moreover, the application of various models to diverse case studies has allowed more general insights regarding modeling SWFs in rural areas.

Finally, in the third and last part, the thesis' main findings are summarized and synthesized. The results of this thesis provide unambiguous proof that SWFs are a significant natural hazard in Switzerland. Although this thesis has made valuable contributions in relation to the better quantification and characterization of SWFs based on damage records, as well as concerning the modeling of SWFs in rural areas, further research is still required to form a basis on which well-informed decisions can be made in the future. Furthermore, tools for assessing and managing such SWF risks need to be improved, developed, and tested. For all these endeavors, better observational data are required, be it more accessible insurance records of higher quality, emerging data sources coupled with data mining techniques, or field observations collected at SWF-prone monitoring sites.

Contents

List of Figures

List of Tables

1 Introduction

In various European countries devastating surface water flood (SWF) events triggered, or at least supported, political, practical and scientific endeavors to recognize and investigate aspects of SWFs, for instance in France (e.g., Davy, 1990; Andrieu et al., 2004), the UK (e.g., Pitt, 2008; Coulthard & Frostick, 2010), Denmark (e.g., Haghighatafshar et al., 2014), the Netherlands (e.g., Gaitan et al., 2015; Spekkers et al., 2017) and Germany (e.g., Rözer et al., 2016; Spekkers et al., 2017). The most prominent example of an individual SWF event is likely the flooding of Hull, UK, in 2007 (Pitt, 2008; Coulthard & Frostick, 2010). However, an earlier event in the fall of 2000 has spawned efforts to better understand and manage SWF hazards in the UK (Hankin et al., 2008).

In Switzerland, on the other hand, the first published testimony of SWFs seems to be Weiss & Wyss (1992), who realized, rather by chance, that SWFs are causing a substantial amount of damage. In the quarter century since, several events characterized by SWFs have been observed and reported in Switzerland (e.g., Aller & Petrascheck, 2008; Scherrer et al., 2013). Although these events may have been the trigger for the development of a few practical methods and guidelines (e.g., Egli, 2007; Rüttimann & Egli, 2010; Kipfer et al., 2012), they have not led to coordinated and target-oriented actions at the federal level to explicitly study and manage SWFs, in contrast to events caused by other natural hazards. In fact, prominent events including earthquakes, avalanches, mass movements, and fluvial floods have spawned governmental efforts to minimize adverse effects caused by these perils over the past century (Zimmermann et al., 2005). The need for a more coordinated and integrated approach has been identified at the turn of the last century, which has led to the development and implementation of an approach based on the risk management cycle, which addresses the mentioned natural hazards in an integrative manner (PLANAT, 2005; Zimmermann et al., 2005; FOEN, 2011). Therein, natural hazards such as avalanches and mass movements are considered, which are rather insignificant in comparison to floods in terms of the incurred monetary losses (e.g., Hilker et al., 2009; Imhof, 2011; Hausmann et al., 2012). Thus, not just economic losses, but also many other factors such as fatalities, general public perception, corresponding process understanding, etc., determine whether actions are taken to mitigate adverse effects from a particular hazardous process, or not. This might explain why in an alpine country such as Switzerland, processes have been prioritized, which have had apparent impacts in terms of fatalities (cf. Hilker et al., 2009) and/or losses (Imhof, 2011; Hausmann et al., 2012), at least at the local scale, in contrast to SWFs, which have been difficult to grasp.

Nevertheless, there are indications that overland flow, as SWFs are commonly referred to in Switzerland, is finally recognized as a serious peril at the highest political level (Der Bundesrat, 2016). Therein, the lack of hazard maps regarding overland flow was specifically mentioned and was proposed to be addressed. According to Zimmermann et al. (2005), such maps are the primary management tool used for spatial planning. Moreover, the map can be used for emergency planning, risk assessment, or for demanding structural protection measures. Following this incentive, the first SWF hazard indication

map for the whole canton of Lucerne has been produced recently (Kipfer et al., 2015), based on single deterministic simulations of design rainfalls with the hydrodynamic flood inundation model "FloodArea". Nevertheless, beyond anecdotal evidence regarding the significance of SWFs, there have been hardly any scientific studies regarding SWFs in Switzerland.

In contrast, on an international level, SWFs have been receiving increasing attention regarding various aspects, including, but not limited to, modeling this flood type in urban areas (e.g., Maksivomić et al., 2009; Sampson et al., 2013; de Almeida et al., 2016) or in the urban-rural interface (e.g., Yu & Coulthard, 2015; Tyrna et al., 2017). Moreover, early warning systems concerning SWFs have been developed and tested (e.g., Priest et al., 2011; Hurford et al., 2012). Additionally, the prediction of damage has been addressed (e.g., Jongman et al., 2012; Spekkers et al., 2014) and tools for SWF risk assessment as well as risk management have been proposed (e.g., Kaźmierczak & Cavan, 2011; Blanc et al., 2012; Zhou et al., 2012; Löwe et al., 2017). At the same time, the lack of observational data is generally a major constraint for most studies (e.g., Blanc et al., 2012; Neal et al., 2012; Yu & Coulthard, 2015; Gaitan et al., 2016; Rözer et al., 2016).

Owed to the fact that SWFs are a relatively new research topic, there exist many open questions including, but not limited to, the hazard's monitoring, its inherent characteristics, its effects on society, its prediction as well as its management. Thus, with the overarching goal to increase our understanding of SWFs, ultimately enabling a better management of the risks emanating from SWFs, this thesis' main objectives are threefold: Firstly, a contribution regarding the eminent lack of data shall be made by exploiting the previously untapped potential of Swiss insurance claim records. To this end, a corresponding data set is compiled and methods are devised to analyze such spatially explicit data with respect to SWFs. Secondly, this data set is analyzed concerning the occurrences of SWFs in space and time, in order to infer inherent characteristics of this flood type. Such knowledge is deemed crucial to foster better predictions of SWFs, in the future. Related to that, the third objective of this thesis is to evaluate whether a current approach applied in practice to simulate SWFs can reliably reproduce observed inundations in rural areas caused by SWFs.

Reflecting these objectives, the thesis is structured in three parts: Firstly, the collection, exploitation and analyses of a unique data set of spatially explicit Swiss flood insurance claims are elaborated (Chapt. 2–3). Secondly, current issues related to deterministically modeling SWFs in rural areas are addressed by presenting modeling exercises (Chapt. 4). Thirdly, the findings from the first two parts are synthesized in order to draw this thesis' conclusions and to provide an outlook (Chapt. 5).

References

Aller, D., & Petrascheck, A. (2008). Schadensentwicklung im Kanton Aargau. In G. R. Bezzola, & C. Hegg (Eds.), *Ereignisanalyse Hochwasser 2005, Teil 2 — Analyse von Prozessen, Massnahmen und Gefahrengrundlagen* Umwelt-Wissen Nr. 0825 (pp. 82–92). Bern, Schweiz: Bundesamt für Umwelt and Eidgenössische Forschungsanstalt für Wald Schnee und Landschaft.

de Almeida, G. A. M., Bates, P., & Ozdemir, H. (2016). Modelling urban floods at sub-metre resolution: challenges or opportunities for flood risk management? *J. Flood Risk Manage.*, (pp. 1–11). doi:10.1111/jfr3.12276.

Andrieu, H., Browne, O., & Laplace, D. (2004). Les crues en zone urbaine: des crues éclairs? *La Houille Blanche*, (pp. 89–95). doi:10.1051/lhb:200402010.

Blanc, J., Hall, J. W., Roche, N., Dawson, R. J., Cesses, Y., Burton, A., & Kilsby, C. G. (2012). Enhanced efficiency of pluvial flood risk estimation in urban areas using spatial-temporal rainfall simulations. *J. Flood Risk Manage.*, *5*, 143–152. doi:10.1111/j.1753-318X.2012.01135.x.

Coulthard, T. J., & Frostick, L. E. (2010). The Hull floods of 2007: implications for the governance and management of urban drainage systems. *J. Flood Risk Manage.*, *3*, 223–231. doi:10.1111/j.1753-318X.2010.01072.x.

Davy, L. (1990). La catastrophe nîmoise du 3 Octobre 1988: était-elle previsible? *Bull. Soc. Languedoc. Geogr.*, *24*, 133–162.

Der Bundesrat (2016). *Umgang mit Naturgefahren in der Schweiz: Bericht des Bundesrats in Erfüllung des Postulats 12.4271 Darbellay vom 14.12.2012*. Bern, Schweiz: Schweizerische Eidgenossenschaft.

Egli, T. (2007). *Wegleitung Objektschutz gegen meteorologische Naturgefahren*. Bern, Schweiz: Vereinigung Kantonaler Feuerversicherungen. URL: http://vkf.ch/VKF/Downloads.

FOEN (2011). *Living with natural hazards: Objectives and priorities for action of the Federal Office for the Environment (FOEN) in dealing with natural hazards*. Bern, Switzerland: Swiss Federal Office for the Environment. URL: www.bafu.admin.ch/ud-1047-e.

Gaitan, S., van de Giesen, N. C., & ten Veldhuis, J. A. E. (2016). Can urban pluvial flooding be predicted by open spatial data and weather data? *Environ. Modell. Softw.*, *85*, 156–171. doi:10.1016/j.envsoft.2016.08.007.

Gaitan, S., ten Veldhuis, J. A. E., & van de Giesen, N. (2015). Spatial distribution of flood incidents along urban overland flow-paths. *Water Resour. Manag.*, *29*, 3387–3399. doi:10.1007/s11269-015-1006-y.

Haghighatafshar, S., la Cour Jansen, Jes, Aspegren, H., Lidström, V., Mattsson, A., & Jönsson, K. (2014). Storm-water management in Malmö and Copenhagen with regard to climate change scenarios. *Vatten*, *70*, 159–168.

Hankin, B., Waller, S., Astle, G., & Kellagher, R. (2008). Mapping space for water: screening for urban flash flooding. *J. Flood Risk Manage.*, *1*, 13–22. doi:10.1111/j.1753-318X.2008.00003.x.

Hausmann, P., Kurz, C., & Rebuffoni, G. (2012). *Floods in Switzerland — an underestimated risk*. Zurich, Switzerland: Swiss Re.

Hilker, N., Badoux, A., & Hegg, C. (2009). The Swiss flood and landslide damage database 1972–2007. *Nat. Hazard Earth Sys.*, *9*, 913–925. doi:10.5194/nhess-9-913-2009.

Hurford, A. P., Parker, D. J., Priest, S. J., & Lumbroso, D. M. (2012). Validating the return period of rainfall thresholds used for Extreme Rainfall Alerts by linking rainfall intensities with observed surface water flood events. *J. Flood Risk Manage.*, *5*, 134–142. doi:10.1111/j.1753-318X.2012.01133.x.

Imhof, M. (2011). *Analyse langfristiger Gebäudeschadendaten: Auswertung des Datenbestandes der Schadenstatistik VKF*. Bern, Schweiz: Interkantonaler Rückversicherungsverband. URL: http://irv.ch/IRV/Download.

Jongman, B., Kreibich, H., Apel, H., Barredo, J. I., Bates, P. D., Feyen, L., Gericke, A., Neal, J., Aerts, J. C. J. H., & Ward, P. J. (2012). Comparative flood damage model assessment: Towards a European approach. *Nat. Hazard Earth Sys.*, *12*, 3733–3752. doi:10.5194/nhess-12-3733-2012.

Kaźmierczak, A., & Cavan, G. (2011). Surface water flooding risk to urban communities: Analysis of vulnerability, hazard and exposure. *Landscape Urban Plan.*, *103*, 185–197. doi:10.1016/j.landurbplan.2011.07.008.

Kipfer, A., Kienholz, C., & Liener, S. (2012). Ein neuer Ansatz zur Modellierung von Oberflächenabfluss. In G. Koboltschnig, J. Hübl, & J. Braun (Eds.), *INTERPRAEVENT 2012 — Conference Proceedings* (pp. 179–189). International Research Society INTERPRAEVENT.

Kipfer, A., Schönthal, E., Liener, S., & Gsteiger, P. (2015). *Oberflächenabflusskarte Kanton Luzern: Bericht*. Bern, Schweiz: geo7 AG.

Löwe, R., Urich, C., Sto. Domingo, N., Mark, O., Deletic, A., & Arnbjerg-Nielsen, K. (2017). Assessment of urban pluvial flood risk and efficiency of adaptation options through simulations — A new generation of urban planning tools. *J. Hydrol.*, *550*, 355–367. doi:10.1016/j.jhydrol.2017.05.009.

Maksivomić, Č., Prodanović, D., Boonya-Aroonnet, S., Leitão, J. P., Djordjević, S., & Allitt, R. (2009). Overland flow and pathway analysis for modelling of urban pluvial flooding. *J. Hydraul. Res.*, *47*, 512–523. doi:10.3826/jhr.2009.3361.

Neal, J., Villanueva, I., Wright, N., Willis, T., Fewtrell, T., & Bates, P. (2012). How much physical complexity is needed to model flood inundation? *Hydrol. Process.*, *26*, 2264–2282. doi:10.1002/hyp.8339.

Pitt, M. (2008). *The Pitt Review: Learning lessons from the 2007 floods: An independent review by Sir Michael Pitt*. London, UK: Cabinet Office.

PLANAT (2005). *Protection against natural hazards in Switzerland — Vision and strategy: Executive summary english/deutsch/français/italiano*. PLANAT-Serial 1/2005. Biel, Switzerland: National Platform for Natural Hazards. URL: http://www.planat.ch/fileadmin/PLANAT/planat_pdf/alle_2012/2001-2005/PLANAT_2005_-_Protection_against_Natural_Hazards.pdf.

Priest, S. J., Parker, D. J., Hurford, A. P., Walker, J., & Evans, K. (2011). Assessing options for the development of surface water flood warning in England and Wales. *J. Environ. Manage.*, *92*, 3038–3048. doi:10.1016/j.jenvman.2011.06.041.

Rözer, V., Müller, M., Bubeck, P., Kienzler, S., Thieken, A., Pech, I., Schröter, K., Buchholz, O., & Kreibich, H. (2016). Coping with pluvial floods by private households. *Water*, *8*, 304. doi:10.3390/w8070304.

Rüttimann, D., & Egli, T. (2010). *Wegleitung punktuelle Gefahrenabklärung Oberflächenwasser*. St. Gallen, Schweiz: Naturgefahrenkommission des Kantons St. Gallen.

Sampson, C. C., Bates, P. D., Neal, J. C., & Horritt, M. S. (2013). An automated routing methodology to enable direct rainfall in high resolution shallow water models. *Hydrol. Process.*, *27*, 467–476. doi:10.1002/hyp.9515.

Scherrer, S., Margreth, M., & Kienzler, P. (2013). Spannungsfeld Prozesswissen — Hydrologische Modellierung aufgezeigt an einem vielseitigen Beispiel aus den Schweizer Voralpen. In R. Weingartner, & B. Schädler (Eds.), *Wasserressourcen im globalen Wandel* Forum für Hydrologie und Wasserbewirtschaftung. Fachgemeinschaft Hydrologische Wissenschaften in der DWA.

Spekkers, M., Rözer, V., Thieken, A., ten Veldhuis, M.-c., & Kreibich, H. (2017). A comparative survey of the impacts of extreme rainfall in two international case studies. *Nat. Hazard Earth Sys.*, *17*, 1337–1355. doi:10.5194/nhess-17-1337-2017.

Spekkers, M. H., Kok, M., Clemens, F. H. L. R., & ten Veldhuis, J. A. E. (2014). Decision-tree analysis of factors influencing rainfall-related building structure and content damage. *Nat. Hazard Earth Sys.*, *14*, 2531–2547. doi:10.5194/nhess-14-2531-2014.

Tyrna, B., Assmann, A., Fritsch, K., & Johann, G. (2017). Large-scale high-resolution pluvial flood hazard mapping using the raster-based hydrodynamic two-dimensional model FloodAreaHPC. *J. Flood Risk Manage.*, *42*, 19. doi:10.1111/jfr3.12287.

Weiss, H. W., & Wyss, R. (1992). Überflutungsgefährdung Kanton Bern. In G. Fiebiger, & F. Zollinger (Eds.), *Schutz des Lebensraumes vor Hochwasser, Muren und Lawinen* (pp. 167–178). International Research Society INTERPRAEVENT volume 3.

Yu, D., & Coulthard, T. J. (2015). Evaluating the importance of catchment hydrological parameters for urban surface water flood modelling using a simple hydro-inundation model. *J. Hydrol.*, *524*, 385–400. doi:10.1016/j.jhydrol.2015.02.040.

Zhou, Q., Mikkelsen, P. S., Halsnæs, K., & Arnbjerg-Nielsen, K. (2012). Framework for economic pluvial flood risk assessment considering climate change effects and adaptation benefits. *J. Hydrol.*, *414–415*, 539–549. doi:10.1016/j.jhydrol.2011.11.031.

Zimmermann, M., Pozzi, A., & Stoessel, F. (2005). *Vademecum — Hazard maps and related Instruments: The Swiss system and its application abroad*. Bern, Switzerland: National Platform for Natural Hazards. URL: http://www.planat.ch/fileadmin/PLANAT/planat_pdf/alle_2012/2001-2005/PLANAT_2005_-_Vademecum.pdf.

Part I

Occurrence of surface water floods

2 Exploiting damage claim records of public insurance companies for buildings to increase knowledge about the occurrence of overland flow in Switzerland

Daniel B. Bernet[1], Volker Prasuhn[2] and Rolf Weingartner[1]

[1]*Institute of Geography and Oeschger Centre for Climate Change Research and Mobiliar Lab for Natural Risks, University of Bern, Hallerstrasse 12, 3012 Bern, Switzerland*
[2]*Agroscope, Research Division, Agroecology and Environment, Reckenholzstrasse 191, 8046 Zurich, Switzerland*

INTERPRAEVENT 2016 — Conference Proceedings, pp. 221–230

Abstract

Overland flow is difficult to assess because direct data is missing. As Swiss public insurance companies for buildings cover overland flow along with other hazards, we exploited their records to investigate the occurrence of overland flow indirectly. With a novel classification scheme, it is possible for the first time, to distinguish claims related to overland flow from inundations caused by watercourses. We analyzed gapless data records from 1991 to 2013 of the cantons Neuchâtel, Fribourg, Nidwalden and Graubünden, each representing a different typical Swiss landscape. Altogether, roughly 40–50 % of the damage claims can be associated with overland flow, which account for 20–30 % of total loss in that period. However, the inter-cantonal differences are large and reflect the embedment of overland flow in the landscape's geographic setting. Finally, looking at averages per km^2 and year, we found that pre-alpine Fribourg is affected most by overland flow. As an outlook, we are confident that the presented method can be used to start studying overland flow from a more process-oriented perspective.

2.1 Introduction

Post-damage analyses in the field of flood hydrology highlight that not only overtopping rivers and lakes cause a substantial amount of loss. Reportedly, about fifty percent of all damages to buildings are caused by overland flow (Bezzola & Hegg, 2008). Overland flow propagates over the land surface as thin sheet flow or anastomosing braids of rivulets and trickles, until the flow reaches or is concentrated into recognizable channels (Chow et al.,

1988; Ward & Robinson, 2000). Thus, overland flow is not constrained to a riverbed, but occurs diffusely in the landscape. Furthermore, overland flow is generally associated with a short response time and practically no advance warning, which makes it difficult to observe and study the process directly. Maybe that is the reason why, in spite of the existence of several practical tools to assess the hazard of overland flow (Kipfer et al., 2012; Rüttimann & Egli, 2010; Bernet, 2013), little is known about where and when overland flow occurred in the past and will occur in the future.

As there is no direct information about the occurrence of overland flow in space and time, traces of the flow's propagation can be found wherever the process has caused detectable damages, or claims thereof. These can be used as a proxy for the occurrence of overland flow. Data sources implicitly containing such information are house owners' damage claims recorded by Swiss public insurance companies for buildings (PICB).

Our overarching goal is to improve the process understanding of overland flow. In this paper, we want to demonstrate that damage claim records can provide very useful, indirect information about the occurrence of overland flow in space and time. Furthermore, by looking at the total number of claims as well as total loss related to overland flow and inundation from watercourses respectively, we want to highlight the relative relevance of these processes. For these purposes, we have analyzed damage claim records of the PICB of Neuchâtel (NE), Fribourg (FR), Nidwalden (NW) and Graubünden (GR). These cantons approved our data enquiry and are chosen for this pilot study, as they cover different landscape patterns typical for the whole Switzerland.

2.1.1 Terms and definitions

Terms used by scientists, insurers or practitioners to describe processes that can lead to water related damages to buildings may differ. Thus, hereafter, some important terms are defined:

- In accordance to the definition above, overland flow is understood as surface runoff that propagates unchannelled over the land surface until it reaches the next river or lake.
- Damages to buildings caused by water entering the structure at ground level (this excludes penetrating groundwater, backwater from the sewer system and rainfall directly entering the building through its envelope) are, hereafter, referred to as water damages.
- For reasons of readability, we abbreviate floods and inundations from rivers and lakes, explicitly excluding overland flow, by simply referring to inundations from watercourses. Thus, the term watercourse always refers to both rivers and lakes.
- In this paper, we make use of two different flood hazard maps (Swiss flood hazard maps and Aquaprotect, S. 2.3). The former includes assessment perimeters, whereas the latter does not. Both indicate areas that are at hazard complemented by hazard-free zones. All hazardous areas, regardless of the hazard level and the map source, are referred to as flood zones.

2.2 Data

In Switzerland, PICB are present in 19 out of the total 26 cantons, within which they each hold a monopoly position. In addition, it is (with a few exceptions) mandatory for

all house owners to insure their buildings against natural hazards including avalanches, snow pressure and -load, hail, storm, land- and rockslides, falling rocks and inundation processes. Concerning the latter, hazards associated with water entering the building at ground level are covered. Consequently, all damages caused by overland flow are insured and recorded by one single institution. Unfortunately, PICB generally do not distinguish different inundation causes and, thus, the responsible process for the claimed damages, namely overland flow or inundation from watercourses, must be identified.

2.2.1 Data harmonization

For the present pilot study, we have analyzed records of house owners' damage claims related to flood processes of the PICB of Neuchâtel (NE), Fribourg (FR), Nidwalden (NW) and Graubünden (GR), representing the most typical landscapes of Switzerland. The data delivered by the different PICB were quite heterogeneous and, thus, needed to be harmonized. The most important variables used in this study were the address, geocode, total loss, processing status of the damage claim, as well as the occurrence date of the claimed damage:

- All four PICB provided geocoded damage claims. Claims with missing spatial reference were geocoded using the provided addresses, whenever possible.
- The loss of each damage claim was calculated by adding the payout and the corresponding deductible. Then, the losses were indexed to 2014. Note that in case of a covered damage, all PICB calculate the payout according to the reinstatement costs (value as new), except Fribourg. In the latter canton, reinstatement costs are determined according to (for us untraceable) depreciated values.
- The damage dates were checked for plausibility manually. The last year with complete records is 2013 for all four PICB. The complete records start in 1983 in Fribourg (31 y), 1987 in Nidwalden (27 y), 1988 in Neuchâtel (26 y) and 1991 in Graubünden (23 y), respectively.
- The status of the damage claims were categorized commonly. For this paper, only completed damage claims, i.e., claims with an actual payout, are considered. This ensures that only damage claims of an insured risk (i.e., overland flow and inundation from watercourses) are analyzed.

Overall, the data comprises 15'200 inundation related damage claims, of which 11'239 are justified and geocoded. For analyses concerning each canton separately (i.e., the compilation of percentiles, cf. Sect. 2.3), the geocoded, justified claims are used. For the comparison between the cantons (i.e., number and total loss of the different classes per canton, cf. Sect. 2.4), only the overlapping period 1991–2013 is considered (23 y), counting a total of 9'451 damage claims.

2.3 Methods

To differentiate damage claims that are associated either with overland flow or inundations from watercourses, we have developed a classification scheme (Fig. 2.1). The scheme is not directly applicable to single damage claims, as it neglects important influencing factors such as micro and macro topography, the circumstances of a loss, etc. However, by applying it to a large dataset and computing summary statistics, the method is robust

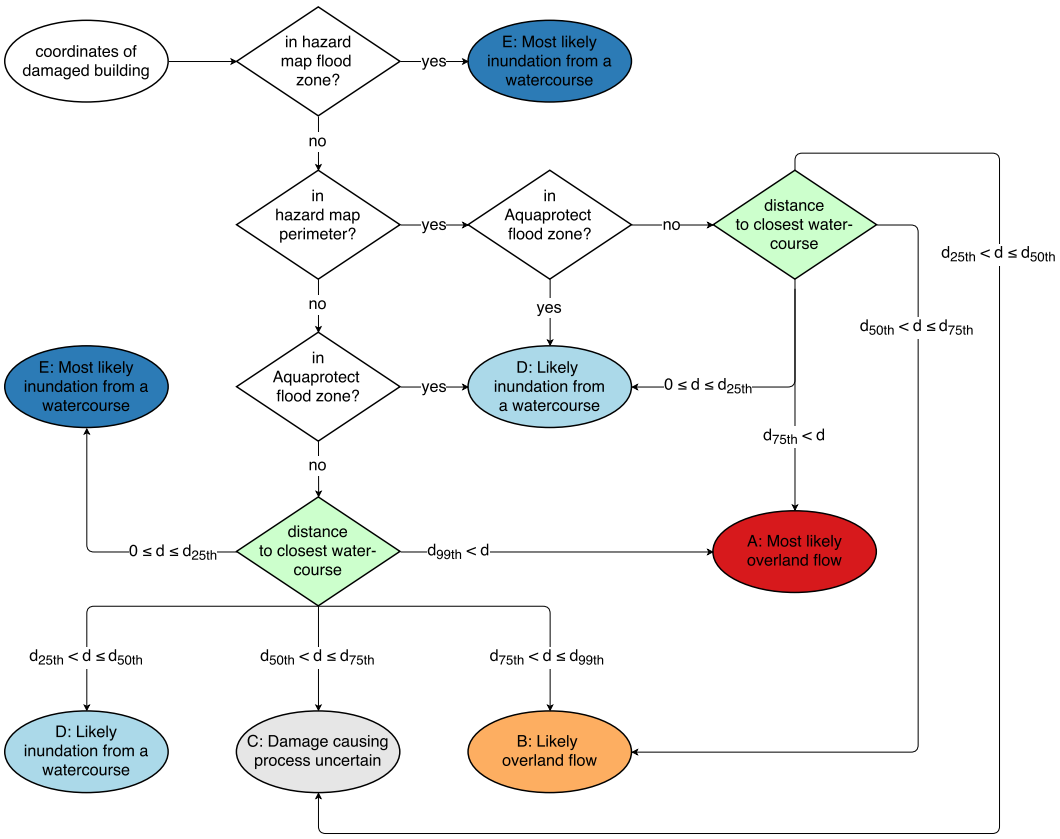

Fig. 2.1: Each geocoded damage claim is categorized according to the displayed classification scheme. The white rhombuses each represents a "yes" or "no" test, checking whether the coordinates of the affected building are within 25 m of the corresponding spatial object (that takes the uncertainty of the buildings represented as point objects into account). Only coordinates located outside of the flood zones (hazard map and Aquaprotect) reach either of the green rhombuses. For each of these claims, the distance d between the claim's point location and the closest watercourse is compared to the 25^{th}, 50^{th}, 75^{th} and the 99^{th} percentiles of the corresponding cumulative distribution of the claims within flood zones (Fig. 2.2, blue curve and percentiles). In this way, all claims outside of the flood zones are classified depending on the percentile range they fall in. All possible paths of the classification scheme are schematically shown in Fig. 2.3. The colors of the ellipses are used throughout the paper to denote overland flow (A: red and B: orange), inundation from watercourses (E: dark blue and D: light blue) or damage claims that could not be associated with either process (C: gray).

and produces productive results.

The scheme makes use of existing flood hazard maps, as mentioned in the introduction. The rationale of the scheme is to use these maps directly for claims located within indicated flood zones. From this claim subset, we can then infer characteristics and use them for the classification of claims outside of the flood zones. For the latter claims, we make the following assumption: The distance to the closest watercourse from a flooded building determines how likely that particular building has been affected by inundation from a watercourse or by overland flow. Understandably, if the building is located close to a watercourse, the responsible process has most likely been inundation from that particular watercourse. On contrary, if the building is located far away from any watercourse, overland flow has most likely caused the damage.

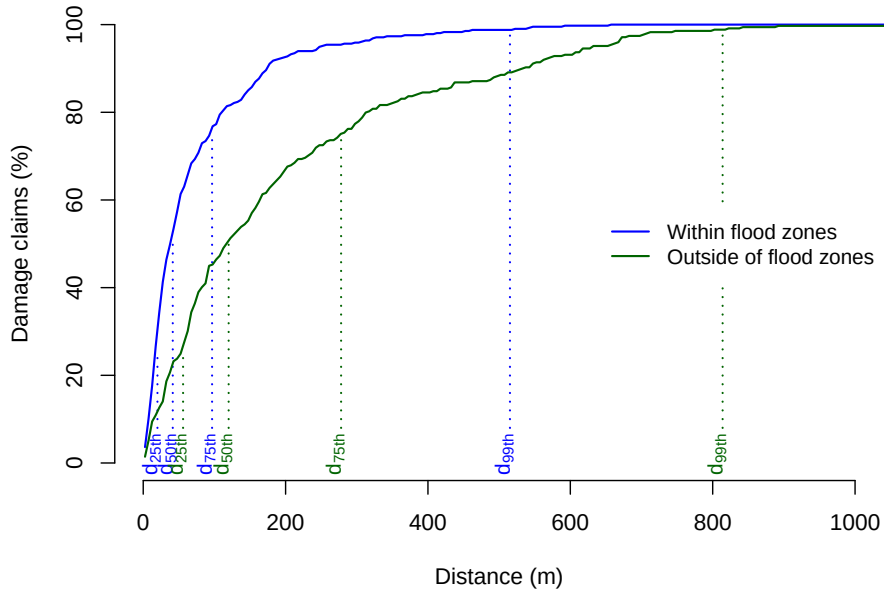

Fig. 2.2: Exemplary cumulative distribution of all damage claims of Graubünden within flood zones that are closest to a medium sized river (SSO: 2–3), plotted against the distance to the corresponding river (blue curve). As a comparison, the cumulative distribution of all damages outside of the flood zones are displayed (green curve). Additionally, the corresponding percentiles (25^{th}, 50^{th}, 75^{th} and 99^{th}) of both curves are indicated (dotted lines). Note that for each of the three SSO classes (1–2: small rivers; 2–3: medium rivers; 4–9: large rivers) as well as for each canton, the percentiles of the claims within flood zones are computed and applied separately to reflect the different geographical and hydrological setting of each canton.

The Swiss flood hazard maps provide detailed information about hazardous zones related to inundation from watercourses (Petrascheck & Loat, 1997). However, these maps were compiled for a predefined perimeter, which is generally constricted to construction zones. Moreover, the hazard maps were compiled with differing methodologies in each canton. To smooth out these differences and to increase the spatial coverage, Aquaprotect, a flood zone map covering the whole Switzerland, provided by the Swiss Federal Office for the Environment (FOEN), is used in addition to the hazard maps. Assessed with a coarse but standardized method, Aquaprotect indicates flood zones of the larger watercourses associated with return periods of 50, 100, 250 and 500 years, while neglecting existing flood control measures. The dataset referring to a return period of 250 years is chosen, as the Swiss flood hazard maps consider a return period of maximal 300 years. Although it is possible that overland flow occurs within a mapped flood zone, it can be assumed that the predominant damage causing process in these areas are inundations from watercourses. Thus, the distribution of affected buildings located within flood zones in relation to the closest watercourse is used to classify damage claims located outside of these flood zones. Thereby we assume, that the patterns of damages caused by inundations from watercourses within the mapped flood zones are the same for damages located outside of these zones.

Clearly, the zone of influence of a watercourse depends on the geographical and geological properties of the landscape, as well as on the size of the river. For that reason, we compiled distance distributions for each canton and river size class separately. The latter is feasible, as the FOEN provides a dataset (referred to as FLOZ) that can be

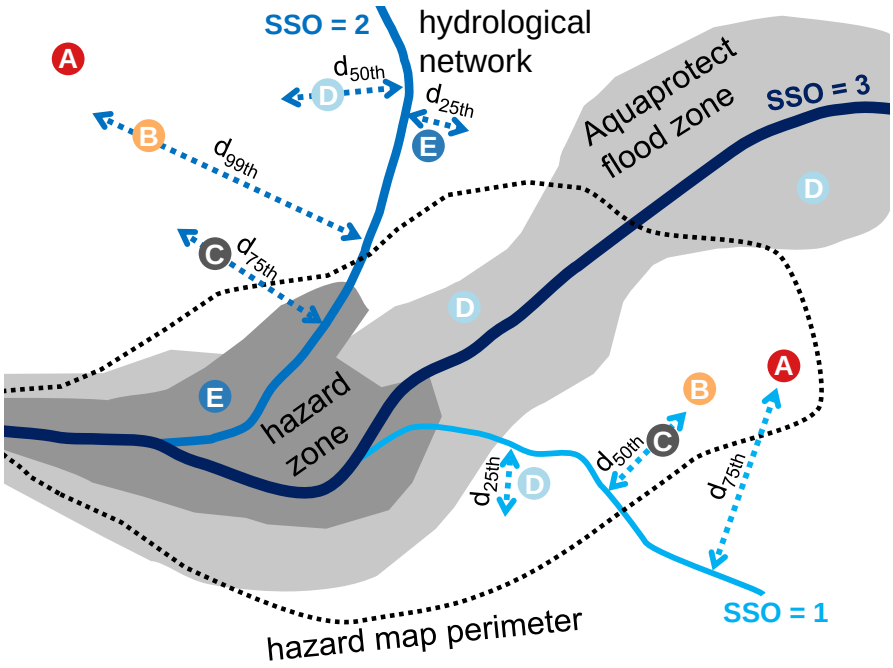

Fig. 2.3: Each displayed point corresponds to a distinct path in the classification scheme (Fig. 2.1) and denotes the corresponding process responsible for the caused damage (A: Most likely overland flow; B: Likely overland flow; C: Damage causing process uncertain; D: Likely inundation from a watercourse; E: Most likely inundation from a watercourse). The arrows show how the percentiles of the cumulative distribution of damage claims within flood zones to the next watercourse are applied in practice. Furthermore, the display indicates that the percentiles are computed for each river class formed by the Strahler Stream Orders (SSO; 1–2: small rivers; 2–3: medium rivers; 4–9: large rivers) as well as for each canton separately.

linked to the Swiss hydrological network of the product "VECTOR25" provided by swisstopo. In that way, each river section is assigned to the corresponding Strahler Stream Order SSO (Strahler, 1964), which can be used as a proxy for the river's size. The SSO takes discrete numbers, which range from 1 to 9 in Switzerland. According to Weissmann et al. (2009) a SSO of 1 refers to small, 2–3 to medium and 4–9 to large Swiss rivers.

Figure 2.2 displays the cumulative distribution of the damage claims within or outside of the mapped flood zones, depending on the distance to the next river of a certain SSO. The blue curve, corresponding to the claims within the flood zones, rises sharply within the vicinity of watercourses but levels off quickly with increasing distance. On the other hand, the green curve, referring to damage claims outside the flood zones, rises more gradually and levels off at a much higher distance. We interpret this behavior as the superposition of damages caused by inundation from watercourses (small distances) and by overland flow (farther away from the watercourses). To obtain an objective way to disentangle these processes we take the distance to the next watercourse that correspond to the 25^{th}, 50^{th}, 75^{th} and the 99^{th} percentiles of the cumulated damage claims located within the flood zones (Fig. 2.2). As mentioned before, such curves are compiled for each canton and river class separately.

The coordinate pair of each damage claim is classified using the scheme shown in

Fig. 2.1. As a depiction thereof, all possible cases are illustrated in Fig. 2.3. We distinguish five classes, each referring to the dominant process responsible for the claimed water damage with a qualitative indication of how certain the classification is:

- A: Most likely overland flow
- B: Likely overland flow
- C: Damage causing process uncertain
- D: Likely inundation from a watercourse
- E: Most likely inundation from a watercourse

2.4 Results

Our analyses show that 43 % of all claims are likely and most likely associated with overland flow and 47 % with inundations from watercourses (Fig. 2.4). The remaining 10 % cannot be associated with either process. Looking at the numbers from the individual cantons, it becomes apparent that the fractions differ greatly from canton to canton. In Neuchâtel and Fribourg, more than half of the damage claims relate to overland flow. However, in Fribourg the classification is associated with a larger uncertainty, i.e., 18 % could not be classified as either overland flow or inundation from watercourses.

In Graubünden 59 % of the claims are associated with inundation from watercourses, while more than every third claim relates to overland flow. The classification in Nidwalden shows a completely different picture. The vast share of 92 % of all claims is caused most likely by inundations from watercourses, while the remaining classes each account for only a few percent of all claims. Although Nidwalden has the lowest amount of damage claims amongst the cantons in numbers, the total loss is almost as high as in Graubünden in the same period (Fig. 2.4). The opposite is the case for Fribourg. It ranks highest amongst the cantons in terms of number of claims, but has a relatively low associated cumulated loss. Neuchâtel, although ranking in the same range as Nidwalden and Graubünden in terms of damage claim numbers, it had to cope with the smallest amount of loss.

To get an idea about the density of these processes in space and time, the numbers can be related to the size of each canton (Table 2.1). For this simple assessment, we have neglected the vulnerability, elements at risk and other possibly relevant factors: In Fribourg, damage claims are most frequently associated with overland flow and cause a yearly average loss of CHF 451.00 per km^2, followed by Neuchâtel. Although in Graubünden overland flow accounts for almost 40 % of all damage claims (Fig. 2.4) the density, both in terms of occurrence but also in terms of yearly loss per area, is by far the lowest. Graubünden also ranks last when looking at inundations from watercourses, however unlike the average occurrence of overland flow, the loss density is in the same order as in Fribourg, and Neuchâtel. Nidwalden, on the other hand, clearly stands out. With more than 0.2 damage claims amounting to more than 7000 CHF and per km^2 and year, the values are by far the highest.

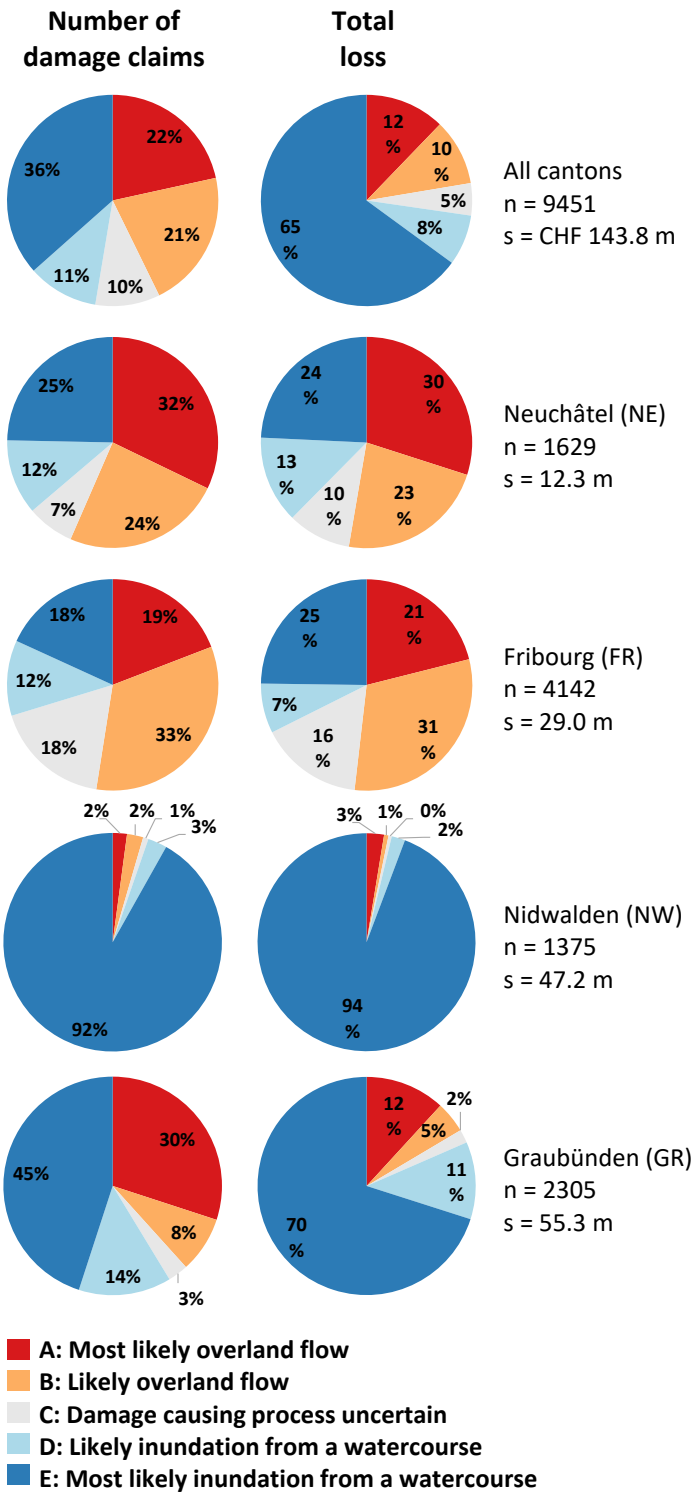

Fig. 2.4: Relative distributions of the number of damage claims as well as total water damage loss (indexed as per 2014) for each canton separately and for the cantons in total. Note that number of claims (n) as well as the total loss (s) in million Swiss Francs correspond to the statistics of the overlapping period 1991–2013.

Table 2.1: Yearly rates at which each canton is affected by overland flow (class A + B + $\frac{1}{2}$ C) or inundation from watercourses (class $\frac{1}{2}$ C + D + E, cf. Fig. 2.4), obtained by dividing the absolute numbers by the area of the respective canton and the record length of 23 years (1991–2013). The rows are ordered according to the yearly rate of buildings affected by overland flow.

Canton	**Area**	**Overland flow**		**Inundation from watercourses**	
	(km^2)	($n/km^2/a$)	($CHF/km^2/a$)	($n/km^2/a$)	($CHF/km^2/a$)
FR	1'671	0.068	451.00	0.040	304.00
NE	803	0.053	382.00	0.035	282.00
NW	276	0.011	259.00	0.205	7'173.00
GR	7'105	0.006	59.00	0.008	279.00

2.5 Discussions

Based on several case studies, it is stated that about half of all (justified) water damage claims are caused by overland flow (Bezzola & Hegg, 2008). Our analyses based on gapless claim records of the last 23 years show that with 43 %, less than half of the claims can be associated clearly with overland flow. Nevertheless, the share is highly significant. In terms of loss, it also underlines previous case studies and assumptions respectively, revealing that on average, the loss associated with overland flow is lower than loss associated with inundation from watercourses. However, our results also show that this is not the case for all areas. The regional differences, as illustrated by Fig. 2.4, can be explained by the different landscapes of the studied cantons. The geographical and geological patterns are reflected by the results: Based on several case studies, it is stated that about half of all (justified) water damage claims are caused by overland flow (Bezzola & Hegg, 2008). Our analyses based on gapless claim records of the last 23 years show that with 43 %, less than half of the claims can be associated clearly with overland flow. Nevertheless, the share is highly significant. In terms of loss, it also underlines previous case studies and assumptions respectively, revealing that on average, the loss associated with overland flow is lower than loss associated with inundation from watercourses. However, our results also show that this is not the case for all areas. The regional differences, as illustrated by Fig. 2.4, can be explained by the different landscapes of the studied cantons. The geographical and geological patterns are reflected by the results:

- In Fribourg, representative for the Pre-Alps, overland flow occurs most frequently (Table 1), which can also be explained by the geological features, favoring overland flow (Weingartner, 1999). Further, the prevalence of many underground rivers that go partly back to extensive melioration in the past century promote overland flow. Inundation from watercourses are frequent as well, but less intense than in more alpine regions.
- As expected, in Neuchâtel with its typical karstic landscape, damage claims are more frequently caused by overland flow than by inundations from watercourses.
- Nidwalden, a canton with steep slopes, mostly less permeable soils, resulting in a dense river network, together with densely populated valley floors, is exposed heavily to inundation processes from watercourses (Fig. 2.4). Although, overland flow may be responsible for certain damage claims, the dominant process is inundation from watercourses by far.
- Graubünden, the largest canton in Switzerland, is mountainous and overall loosely

populated. Thus, the relative occurrence of claims related to inundations from watercourses, but even more so for overland flow, are very low. However, the associated losses are very high due to the devastating floods of mountain torrents.

2.6 Conclusions

Indubitably, overland flow causes frequent damages to buildings in Switzerland. For the first time, we can support this with a gapless data record covering representative areas of Switzerland, as we have collected and harmonized damage claim records of 4 Swiss PICB each representative for typical Swiss regions and covering the last 23 years. Due to the large dataset, the numbers are robust. However, it has to be noted that our novel method to disentangle water damages to buildings only works for large numbers and cannot be applied to single damage claims.

We have demonstrated that it is feasible and worthwhile to analyze damage claim data from public insurance companies, even more so, as it is, to our best knowledge, the only source that indicates overland flow over a large part of Switzerland within a longer period. The next step forward is to use the disentangled dataset, in order to analyze spatial and temporal patterns of the occurrence of overland flow. In this way, we can move towards more process-based investigations that are required to better understand and, ultimately predict, overland flow in the future.

Acknowledgments

The authors would like to thank the public insurance companies for buildings of the cantons Neuchâtel, Fribourg, Nidwalden and Graubünden for their support and for providing the data used in this study. Moreover, we would like to thank the two anonymous referees for their valuable comments and suggestions.

References

Bernet, L. (2013). *Gebäudeschäden durch Schlammeintrag infolge von Bodenerosion durch Wasser in der Schweiz: Entwicklung eines GIS-Modells zur Gefahrenabschätzung auf der Basis der Erosionsrisikokarte*. Masterarbeit Universität Bern, Schweiz.

Bezzola, G. R., & Hegg, C. (Eds.) (2008). *Ereignisanalyse Hochwasser 2005, Teil 2 — Analyse von Prozessen, Massnahmen und Gefahrengrundlagen*. Umwelt-Wissen Nr. 0825. Bern, Schweiz: Bundesamt für Umwelt and Eidgenössische Forschungsanstalt für Wald Schnee und Landschaft.

Chow, V. T., Maidment, D. R., & Mays, L. W. (1988). *Applied hydrology*. McGraw-Hill series in water resources and environmental engineering. New York, USA: McGraw-Hill.

Kipfer, A., Kienholz, C., & Liener, S. (2012). Ein neuer Ansatz zur Modellierung von Oberflächenabfluss. In G. Koboltschnig, J. Hübl, & J. Braun (Eds.), *INTERPRAEVENT 2012 — Conference Proceedings* (pp. 179–189). International Research Society INTERPRAEVENT.

Petrascheck, A., & Loat, R. (1997). *Berücksichtigung der Hochwassergefahren bei raumwirksamen Tätigkeiten: Empfehlungen 1997*. Biel, Schweiz: Bundesamt für Wasserwirtschaft and Bundesamt für Raumplanung and Bundesamt für Umwelt, Wald und Landschaft.

Rüttimann, D., & Egli, T. (2010). *Wegleitung punktuelle Gefahrenabklärung Oberflächenwasser*. St. Gallen, Schweiz: Naturgefahrenkommission des Kantons St. Gallen.

Strahler, A. N. (1964). Quantitative geomorphology of drainage basin and channel networks. In V. T. Chow (Ed.), *Handbook of applied hydrology* (pp. 439–476). New York, USA: McGraw-Hill.

Ward, R. C., & Robinson, M. (2000). *Principles of hydrology*. (4th ed.). London, UK: McGraw-Hill.

Weingartner, R. (1999). *Regionalhydrologische Analysen — Grundlagen und Anwendungen* volume Nr. 37 of *Beiträge zur Hydrologie der Schweiz*. Bern, Schweiz: Schweizerische Gesellschaft für Hydrologie und Limnologie.

Weissmann, H. Z., Könitzer, C., & Bertiller, A. (2009). *Strukturen der Fliessgewässer in der Schweiz: Zustand von Sohle, Ufer und Umland (Ökomorphologie); Ergebnisse der ökomorphologischen Kartierung. Stand: April 2009*. Umwelt-Zustand Nr. 0926. Bern, Schweiz: Bundesamt für Umwelt.

3 Surface water floods in Switzerland: what insurance claim records tell us about the caused damage in space and time

Daniel B. Bernet[1], Volker Prasuhn[2] and Rolf Weingartner[1]

[1]*Institute of Geography and Oeschger Centre for Climate Change Research and Mobiliar Lab for Natural Risks, University of Bern, Hallerstrasse 12, 3012 Bern, Switzerland*
[2]*Agroscope, Research Division, Agroecology and Environment, Reckenholzstrasse 191, 8046 Zurich, Switzerland*

Natural Hazards and Earth System Sciences, accepted for publication
https://doi.org/10.5194/nhess-2017-136

Abstract

Surface water floods (SWFs) have received increasing attention in the recent years. Nevertheless, we still know relatively little about where, when and why such floods occur and cause damage, largely owed to a lack of data, but to some degree also because of terminological ambiguities. Therefore, in a preparatory step, we summarize related terms and identify the need for unequivocal terminology across disciplines and international boundaries in order to bring the science together. Thereafter, we introduce a large (n=63'117), long (10–33 years) and representative (48 % of all Swiss buildings covered) data set of spatially explicit Swiss insurance flood claims. Based on registered flood damage to buildings, the main aims of this study are twofold: First, we introduce a method to differentiate damage caused by SWFs and fluvial floods based on the geographical location of each damaged object in relation to flood hazard maps and the hydrological network. Second, we analyze the data with respect to their spatial and temporal distributions aimed at quantitatively answering the fundamental questions of how relevant SWF damage really is, as well as where and when it occurs in space and time.

This study reveals that SWFs are responsible for at least 45 % of the flood damage to buildings and 23 % of the associated direct tangible losses, whereas lower losses per claim are responsible for the lower loss share. The Swiss lowlands are affected more heavily by SWFs than the alpine regions. At the same time, the results show that the damage claims and associated losses are not evenly distributed within each region either. Damage caused by SWFs occurs by far most frequently in summer in almost all regions. The normalized SWF damage of all regions shows no significant upward trend between 1993–2013. We conclude that SWFs are in fact a highly relevant process in

Switzerland that should receive similar attention like fluvial flood hazards. Moreover, as SWF damage almost always coincides with fluvial flood damage, we suggest to consider SWFs, just as fluvial floods, as integrated processes of our catchments.

3.1 Introduction

In Switzerland, there seems to be a growing awareness that just as overtopping rivers and lakes pose substantial flood risks for society, so too does flooding that takes place far away from watercourses. All across Europe, there are well-known examples of such inland flood events. In 1988, for instance, a devastating flood occurred in Nîmes, France (e.g., Davy, 1990; Andrieu et al., 2004). In 2007, Hull UK was affected by flooding (e.g., Pitt, 2008; Coulthard & Frostick, 2010). One year later Dortmund, Germany, experienced wide-spread flooding (e.g., Grünewald, 2009). In 2011, the Danish capital Copenhagen was affected heavily by flooding (e.g., Haghighatafshar et al., 2014). The Swiss canton of Schaffhausen was affected severely in 2013 (e.g., Scherrer et al., 2013). At the same day in 2014, the Dutch capital Amsterdam (e.g., Gaitan et al., 2016; Spekkers et al., 2017) as well as Münster, Germany, experienced substantial flooding (Spekkers et al., 2017). These events in Europe share a common thread, which stems from their origin as inland floods, triggered by heavy precipitation, but mostly unrelated to watercourses.

As the definition of such floods is not straightforward, we adopt the term of surface water floods (SWFs) for now, use it for non-fluvial floods in general and discuss the terminology in Sect. 3.2 in detail. Inherently, SWFs are not constrained to areas close to watercourses, but can occur practically anywhere in the landscape (Kron, 2009). Consequently, such floods are difficult to document, study and forecast (e.g., Pitt, 2008; Steinbrich et al., 2016) and related data are scarce (e.g., Hankin et al., 2008; Douglas et al., 2010; Blanc et al., 2012; Grahn & Nyberg, 2017). Spekkers et al. (2014) mention the lack of data as well as the impact on small spatial scales as possible explanations why relatively little scientific research has been dedicated to such SWF in comparison to fluvial floods. In contrast, gray literature covers the topic of SWFs rather extensively, which is reflected by the availability of many guidelines and manuals discussing how to prepare for and manage such floods, for instance for single objects in Switzerland (Egli, 2007), or on communal or regional levels in Germany (e.g., Castro et al., 2008; DWA, 2013; LUBW, 2016) or France (e.g., CEPRI, 2014). This might exemplify that the scientific flood risk community is indeed quite oblivious of resourceful gray literature (Uhlemann et al., 2013). In any case, it indicates that the topic is a concern for the people, the responsible authorities and other stakeholders. In order to reduce the risk, an effective approach is to focus on the physical protection of exposed objects (e.g., Kron, 2009; DWA, 2013). Although this strategy is certainly pointing into the right direction, we have to be conscious about the basis on which current and future decisions concerning SWFs are made. Undoubtedly, the lack of quantitative data and studies hampers our process understanding (Grahn & Nyberg, 2017). Therefore, the underlying crucial question is "how can we reduce losses from natural hazards when we do not know (...) when and where they occur?" (Gall et al., 2009).

Owing to vast river discharge time series, fluvial floods can be well predicted along gauged rivers (Steinbrich et al., 2016). As there are no such data concerning SWFs (Steinbrich et al., 2016), we must exploit other data sources in order to quantify the

relevance of this flood type in space and time. Possible data sources include, but are not limited to, insurance claim records (e.g., Spekkers et al., 2013; Zhou et al., 2013; Moncoulon et al., 2014; Bernet et al., 2016; Grahn & Nyberg, 2017), disaster data bases (e.g., Gall et al., 2009; Kron et al., 2012), press reports (e.g., Hilker et al., 2009) and interviews with or reports from affected people (e.g., Thieken et al., 2007; Evrard et al., 2007; Gaitan et al., 2016). All data sources are probably subjected to a varying degree of a so-called "threshold bias", which refers to the bias introduced due to varying damage inclusion criteria (Gall et al., 2009). Disaster data bases only list events that exceeded predefined loss and/or fatality thresholds (Kron et al., 2012). Similarly, damage data based on news reports are subjected to unknown thresholds, as damage is only reported if it is found to be interesting enough. As interview campaigns are more likely to be initiated after devastating flood events, such data are biased towards more extreme events, as well (Elmer et al., 2010). Insurance claim records are likely affected the least by a threshold bias, as long as the related insurance policy stays the same, insured objects are not changing greatly over time and the deductibles are low or can be accounted for.

Damage claim records of insurance companies are therefore a profitable data source. Not surprisingly, they have been the base for several studies related to SWFs (e.g., Cheng et al., 2012; Spekkers et al., 2013; Zhou et al., 2013; Moncoulon et al., 2014; Spekkers et al., 2015; Bernet et al., 2016; Grahn & Nyberg, 2017). Unfortunately, insurance claim data are generally difficult to collect, since most insurance companies do not publish or provide loss data due to confidentiality issues (Boardman, 2010; Grahn & Nyberg, 2017). Furthermore, analyses based on such data are often impaired by the data's spatial or temporal aggregations. For instance, the limited usefulness of monthly aggregated data was demonstrated by Cheng et al. (2012). On the other hand, Spekkers et al. (2014) pointed out some limitations of insurance data aggregated to administrative units, which do not have homogeneous topographical properties. As insurance companies usually do not assess and record detailed information for each damage claim, it is difficult to verify and differentiate the cause of each damage without at least knowing the explicit location of the damaged object. This is particularly important, as the corresponding data often cover different processes without explicit classification: For instance, Grahn & Nyberg (2017) had to exclude all damage records with dates that coincided with dates of known fluvial flood events to obtain a subset of SWF-related claims. Spekkers et al. (2013) chose a more elaborate method by applying a statistical filter based on the assumption that rainfall-related damage is clustered around wet days, while other causes of damage are occurring on any day throughout the year. Finally, even though many or even all buildings are insured against floods in several countries (e.g., in Sweden (Grahn & Nyberg, 2017) or in the Netherlands (Spekkers et al., 2014)), usually only a subset of all objects are covered by the obtained data records. This is owed to the fact that the objects are usually insured by many different companies, each having a different (unknown) market share. In addition, these shares are generally not constant over time either, but may fluctuate heavily over time and space, as exemplified by Spekkers et al. (2014). These spatial and temporal changes need to be taken into account, which is often not trivial.

Luckily, most of these limitations are not applicable for damage claim records of the Swiss public insurance companies for buildings (PICB). In Switzerland, PICB are present in 19 out of the 26 cantons, whereas each company insures (almost) all buildings within the respective canton due to their monopoly position and because the insurance

is generally mandatory for all house owners (e.g., Schwarze et al., 2011). Beside other natural hazards, the insurance covers damages caused by floods, which includes both fluvial floods as well as SWFs. Data records of PICB are, therefore, exceptionally interesting for analyzing floods in general, and SWFs in particular. Most PICB have shown a general interest about research on this topic and, thus, were willing to provide flood claim records including the address of each damaged object.

Based on these data, the first aim of this study is to provide a method, with which each claim can be classified as being caused by SWFs or fluvial floods, respectively. Second, based on the classified claim records, we aim at answering the fundamental question of how relevant damage caused by SWFs is, as well as where and when such damage occurs in space and time. The underlying data set stems from 13 PICB and covers 48 % of all buildings in Switzerland. Thus, the data set is representative for most of Switzerland, except for southern Switzerland (i.e., Western Inner Alps and Southern Alps). The analyzed data records all end in 2013 and extent back to at least 2004, but even up to 1981 depending on the PICB. As the PICB, safe a few exceptions, insure only property and not its contents, this study only considers damage to buildings. More specifically, this study is limited to direct tangible flood damages to buildings, i.e., monetary losses caused by the buildings' direct contact with flood water (Merz et al., 2010). Thereby, we acknowledge that these damages only constitute a portion of the total flood losses.

We have identified a lack of a common terminology concerning SWFs. Therefore, we dedicate the following Sect. 3.2 to a short overview of terms that are currently being used to address flood types that could be categorized as SWFs, as mentioned before. In Sect. 3.3 we describe the data in detail and introduce a method to differentiate SWF damage from fluvial flood damage. Thereafter, in Sect. 3.4, we present general characteristics of the number of claims as well as associated loss caused by SWFs in comparison to fluvial floods. Furthermore, we present the spatial and temporal characteristics of damage caused by SWFs in Switzerland during the last decades and discuss the results in Sect. 3.5. Finally, by providing concluding remarks, we conclude the study (Sect. 3.6).

3.2 Terminology

Flooding is a complex interlinked system, affecting many aspects of the physical, economic and social environments acting at different spatial and temporal scales (Evans et al., 2004; Barredo, 2009). As such, flooding involves a wide range of interconnected hydraulic subsystems and processes (Evans et al., 2004). Therefore, the classification of such a complex process like flooding is not trivial, particularly in practice. At the same time, many of the terms used to address flood types or involved hydrological processes in relation to SWFs are either used ambiguously in the literature or are not well-defined. To prevent terminological ambiguities, we first introduce relevant hydrological processes, which helps to distinguish SWFs and fluvial floods. Thereafter, we elaborate related flood terms for a clearer definition of SWFs and provide recommendations for these terms' future reference.

SWFs are characterized by overland flow and ponding, which can be defined as follows. As precipitation reaches the land surface, different runoff generation mechanisms determine whether water starts to pond and whether overland flow is generated (e.g.,

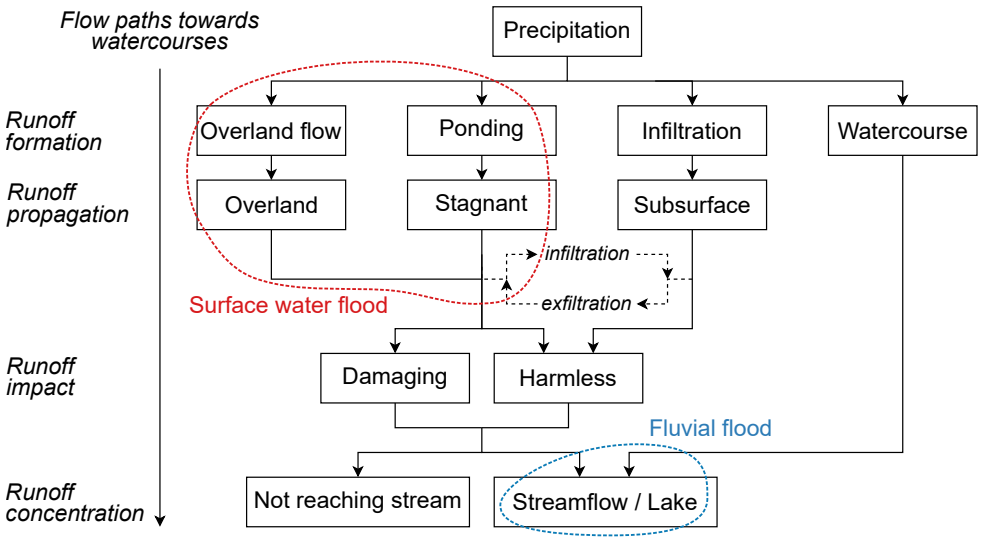

Fig. 3.1: Interrelation of hydrological processes that may lead to a SWFs (red ring) and/or a fluvial flood (blue ring).

Fiener et al., 2013). The water may then take several routes towards the stream channels (Ward & Robinson, 2000), as depicted in Fig. 3.1. The flow path along the land surface is sometimes ambiguously referred to as "surface runoff", but is better defined by the widely-used term "overland flow" (Ward & Robinson, 2000). However, in the literature, this distinction is inconsistently made, whereas either of the terms or even both are used. We adopt the term overland flow and, thereby, mean the transport of water downhill at the land surface as thin sheet flow or anastomosing braids of rivulets and trickles until the water reaches or is concentrated into recognizable streams (Chow et al., 1988; Ward & Robinson, 2000; Brutsaert, 2005).

The propagation and accumulation (i.e., ponding) of overland flow can be considered as a flood, which in the glossary of Field et al. (2012) is defined as "the overflowing of the normal confines of a stream or other body of water, or the accumulation of water over areas that are not normally submerged". As long as the water is directed towards a watercourse, but has not yet reached it, the flood can be regarded as a SWF, as defined later. Thus, the notable difference between a SWF and a fluvial flood is that in the former case, water is making its way towards a watercourse, whereas in the latter case flooding stems from a watercourse (Fig. 3.1).

As outlined before, different flood terms are used in relation with SWFs. For a better distinction of these terms, we discuss each term and give recommendations about their future reference. A summary of the terms is presented in Table 3.1.

"Pluvial floods" are caused by intense rainfall that, due to whatever reason, cannot be drained by natural or artificial drainage systems, thereby ponds in local depressions or propagates along the surface as overland flow (Pitt, 2008; Hurford et al., 2012), before it possibly, but not necessarily, reaches or is concentrated into regular watercourses. The term pluvial flood is often used synonymously with SWF, although according to Falconer et al. (2009), SWFs have a broader meaning. Namely, in addition to pluvial floods as defined above, the term SWF also includes flooding from sewer systems, small open channels, culverted watercourses or flooding from groundwater springs (Hankin

et al., 2008; Falconer et al., 2009). Therefore, SWFs can be regarded as the most general definition of rainfall-related (pluvial) floods. For future studies, we recommend using these two terms distinctively, depending on the corresponding context.

The term "muddy flooding" is well-established and refers to floods, which are formed by muddy runoff from agricultural fields that damage adjacent properties downslope (Boardman, 2010; Ledermann et al., 2010). Here, the term is mentioned to point out that this flood type is implicitly included by the definition of SWFs and pluvial floods, respectively.

The term "flash floods" is used quite ambiguously in the literature (van Campenhout et al., 2015). Traditionally, it refers to fluvial floods triggered by short, intense and local storm events (e.g., Merz & Blöschl, 2003; Gaume et al., 2009; Falconer et al., 2009; Ruiz-Villanueva et al., 2012). However, the term may include other causes as well (Castro et al., 2008; Priest et al., 2011; Gourley et al., 2013). Moreover, the term has increasingly been used in relation to pluvial flood types (cf. Kron et al., 2012; Steinbrich et al., 2016). Apparently, the term is often used in this context by publications in German using the translated term "Sturzflut" (cf. Castro et al., 2008; Kron, 2009; DWA, 2013). For future reference, we recommend to adopt the term flash flood only in the traditional sense and use the applicable term, i.e., pluvial flood or SWF, for all other cases.

The term "urban" or "intra-urban" are mainly used as a specifier of the geographical extent of a flood or the main focus of the corresponding study (cf. Evans et al., 2004; Andrieu et al., 2004; Douguédroit, 2008; Hankin et al., 2008; DWA, 2013; Zhou et al., 2013). If applicable, the use of this term as a specifier in combination with other flood terms can be recommended, since the corresponding flood type is thus better defined. However, we suggest refraining from the isolated usage of the term, as in "urban flood" for instance, since the flood type is thereby not unequivocally defined. In case the term is intentionally used in such a broad context, we recommend mentioning this explicitly.

Finally, we deem it necessary to introduce a further distinction for a better understanding of this study's results. Namely, it is important to note that the term "flood" is sometimes implicitly used in the hydrological sense, but sometimes also in the context of "damaging floods" (Barredo, 2009). In the former case, any inundation of land is considered, while in the latter case, the flood necessarily interacts with the societal system causing adverse effects (Barredo, 2009). Thus, our results represent only damaging floods, as this study is based solely on the exploitation of damage data. Note that this

Table 3.1: Summary of flood terms related to SWFs. The column "Type" indicates whether the corresponding term refers to a rainfall-related (pluvial) or fluvial flood type. The information is taken from the sources cited in Sect. 3.2.

Flood term	Type	Main sources
Surface water flood	Pluvial	Water that could not be drained; surcharged sewer or culverted watercourse; overtopping open channel; groundwater spring
Pluvial flood	Pluvial	Water that could not be drained
Sewer flood	Pluvial	Sewer surcharge or backup
Muddy flood	Pluvial	Muddy runoff from agricultural fields
Urban flood	Fluvial/Pluvial	Any source contributing to inundation in urban areas
Flash flood	Fluvial/(Pluvial*)	Watercourses / (cf. surface water flood*)

* Recently increasingly used to address pluvial flood types

distinction is visualized in Fig. 3.1.

3.3 Materials and methods

The compiled data set is based on flood damage claim records from 14 different PICB. In addition, we obtained similar records from the Swiss Mobiliar, a cooperative insurance company, hereafter referred to as CIC. The corresponding data records were solely used to support the parametrization of the classification scheme. Thus, they were not part of the data analyses, as elaborated in more detail in Sect. 3.3.1.

As mentioned before, each PICB holds a monopoly position and, thus, insures virtually every single building within the respective canton against various natural hazards including flooding. Therefore, damage caused by water entering the building envelope at the surface is insured, while damage associated with direct intrusion of groundwater or backwater from the sewer, as well as flooding from dams or other artificial water structures is generally excluded. In consequence, water-related damage covered by PICB is either caused by SWFs or fluvial floods, whereas the insurance companies themselves do not differentiate the two processes (Imhof, 2011). Therefore, similar to other studies

Table 3.2: Summary of the specific input data used for the classification and normalization of the flood damage claims, in the order of appearance in Fig. 3.2. Note that all links were last checked on 3 March 2017.

Input data	Name	Description	source
Address data base	GeoPost Coordinates	Register of all geocoded postal addresses of Switzerland as of 2015, provided by the national postal service Swiss Post	*https://www.post.ch/en/business/a-z-of-subjects/maintaining-addresses-and-using-geodata/address-and-geodata*
River network	swissTLM3D	Feature TLM_FLIESSGEWAESSER of the Swiss topographical landscape model, v1.4, provided by the Federal Office of Topography (swisstopo)	*https://shop.swisstopo.admin.ch/en/products/landscape/tlm3D*
Flood hazard maps (main)	Flood hazard maps	Official Swiss (fluvial) flood hazard maps (e.g., Zimmermann et al., 2005; de Moel et al., 2009) compiled to a single data set and provided by the Swiss Mobiliar	*https://www.bafu.admin.ch/bafu/en/home/topics/natural-hazards/state/maps.html*
Flood map (ancillary)	Aquaprotect	Simple flood map for the whole of Switzerland, produced by the Swiss Federal Office for the Environment (FOEN) in collaboration with the Swiss reinsurance company Swiss Re	*https://www.bafu.admin.ch/bafu/en/home/state/data/geodata/natural-hazards--geodata.html*
Building footprints	swissTLM3D	Feature TLM_GEBAEUDE_FOOTPRINT, see river network for details	see river network
Digital elevation model	swissALTI3D	High precision digital elevation model (DEM) as of 2013 with a regular grid size of 2 by 2 m, provided by swisstopo	*https://shop.swisstopo.admin.ch/en/products/height_models/alti3D*
Digital surface model	DSM	Digital surface model, last updated in 2008, provided by swisstopo	*https://shop.swisstopo.admin.ch/en/products/height_models/DOM*
Residential buildings	BDS	Buildings and dwellings statistic, as of 2013, provided by the Swiss Federal Statistical Office	*https://www.bfs.admin.ch/bfs/en/home/statistics/construction-housing/surveys/gws2009.assetdetail.8945.html*
PICB characteristics	–	Total number of insured buildings and total sum insured of each considered PICB as of the end of 2013, taken from their annual reports	available online for most PICB

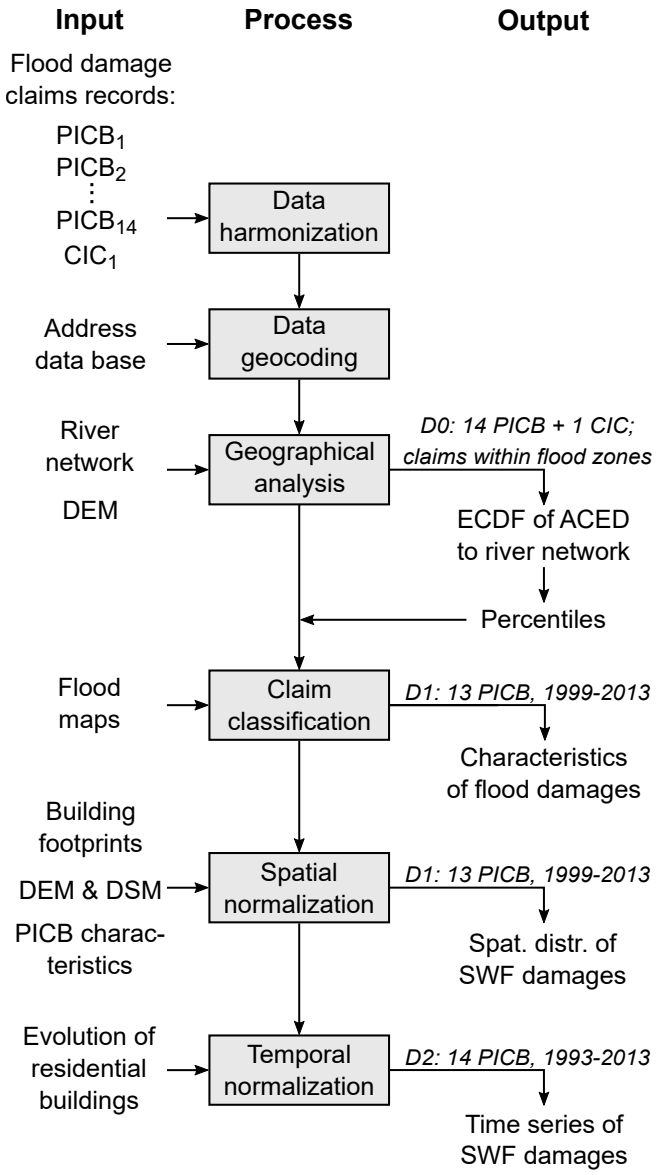

Fig. 3.2: Illustration of the main data processing steps (boxes) as well as the required input data, which are further specified in Table 3.2. *D0*, *D1* and *D2* refer to the data (sub-) sets, which were used to produce the output, illustrated by this study's tables and figures. Note that *D0* constitutes the complete data set including data from 14 PICB in addition to data from a CIC, whereas *D1* and *D2* consist of PICB data only, limited to the indicated periods (cf. Table 3.3). The empirical cumulative distribution function (ECDF), as well as the altitude constrained Euclidean distance (ACED) between each claim and the next river are abbreviated (cf. Sect. 3.3.2).

(e.g., Spekkers et al., 2013, 2015; Grahn & Nyberg, 2017), the data have to be classified first. However, in contrast to the aforementioned studies, the claim records were provided in a spatially explicit way, enabling a classification based on each claim's geographical context.

Following the data processing procedure depicted in Fig. 3.2, we first describe the compiled data set as well as the harmonization and geocoding thereof (Sect. 3.3.1).

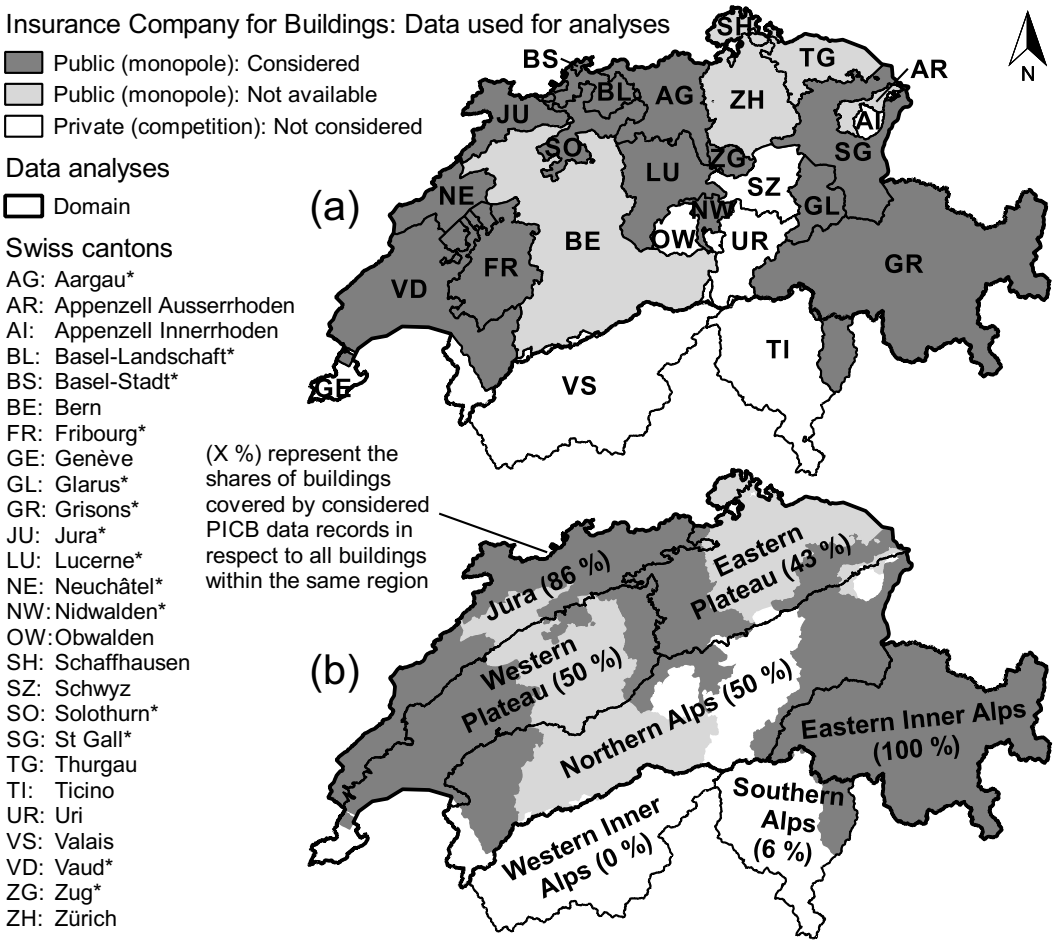

Fig. 3.3: Overview of the compiled data set *D1* (cf. Table 3.3). **(a)** Cantons with and without a PICB, as well as an indication which PICB provided data. The latter are additionally marked with an asterisk (*) in the legend. **(b)** Natural landscape units based on Grosjean (1975), which are used to analyze the data on a regional scale. As almost no buildings are insured by PICB within the Western Inner Alps as well as the Southern Alps, these two regions are excluded from the data analyses, as indicated by the domain.

Following, we introduce a method to differentiate claims associated with SWFs and fluvial floods (Sect. 3.3.2) and, thereafter, we discuss the necessary normalizations of the data (Sect. 3.3.3). Note that the classification scheme is described as generally as possible, to make its application to other contexts and countries as straightforward as possible. However, it could not be prevented that the classification scheme is adapted to some national characteristics, in particular concerning the properties of the considered Swiss flood maps. The specific input data for each data processing step listed in Fig. 3.2 are described in detail in Table 3.2.

3.3.1 Data

Figure 3.3 gives an overview of the compiled data set and illustrates all 19 cantons with a PICB, while the 14 PICB that provided data are highlighted additionally. As the cantons' borders have mostly administrative meaning, we adapted the natural landscape

Table 3.3: Characterization of the claim records reporting flood damage to buildings provided by 14 different PICB in addition to claims of content and buildings provided by a CIC. The absolute number of localized claims is presented in addition to the fraction relating to the total number of claims. The columns *D0*, *D1*, *D2* each represents a data (sub-) set and indicates the temporal coverage of each data record (*D0*) or a specific limitation thereof (*D1* and *D2*), respectively.

Company	Canton	Localized claims	*D0*	*D1*	*D2*
$PICB_1$	Solothurn (SO)	4'456 (90 %)	1981–2013	1993–2013	1999–2013
$PICB_2$	Glarus (GL)	463 (56 %)	1982–2013	1993–2013	1999–2013
$PICB_3$	Fribourg (FR)	5'494 (96 %)	1983–2013	1993–2013	1999–2013
$PICB_4$	Nidwalden (NW)	1'383 (97 %)	1987–2013	1993–2013	1999–2013
$PICB_5$	Neuchâtel (NE)	1'959 (99 %)	1988–2013	1993–2013	1999–2013
$PICB_6$	Aargau (AG)	9'024 (73 %)	1989–2013	1993–2013	1999–2013
$PICB_7$	Grisons (GR)	2'258 (95 %)	1991–2013	1993–2013	1999–2013
$PICB_8$	Basel-Stadt (BS)	243 (86 %)	1992–2013	1993–2013	1999–2013
$PICB_9$	Lucerne (LU)	7'848 (79 %)	1993–2013	1993–2013	1999–2013
$PICB_{10}$	Vaud (VD)	3'275 (56 %)	1994–2013	1994–2013	1999–2013
$PICB_{11}$	Basel-Landschaft (BL)	1'820 (89 %)	1999–2013	1999–2013	1999–2013
$PICB_{12}$	Jura (JU)	809 (83 %)	1999–2013	1999–2013	1999–2013
$PICB_{13}$	St Gall (SG)	4'764 (74 %)	1999–2013	1999–2013	1999–2013
$PICB_{14}$	Zug (ZG)	761 (85 %)	2004–2013	2004–2013	
CIC_1	All (build. & cont.)	18'560 (100 %)	2004–2014		
Total		63'117 (85 %)	63'117	40'233	31'711

units from Grosjean (1975), while constraining the borders to hydrological catchment boundaries. In this study, the data are analyzed with respect to these regions (Fig. 3.3). Overall, 43–100 % of the buildings are covered by our data set, with the exception of the Western Inner Alps (0 %) and the Southern Alps (6 %). The low values of the latter two regions are owed to the fact that practically no buildings are insured by a PICB within these areas. Consequently, these areas are excluded from this study's analyses, even though some claims provided by the CIC covered this region.

The CIC's data contain flood damage claim records of content and, additionally, of property in cantons with no PICB. These records have quite similar characteristics as the data provided by the PICB, but are not limited to certain cantons and, thus, extend over the whole of Switzerland. However, unlike PICB, the CIC does not hold a monopoly position. Consequently, the corresponding data records cover only the objects that are not insured by another private insurance company. Such records that are subjected to certain (unknown) market shares are much more challenging to interpret, as pointed out in the introduction. Nevertheless, the data are useful to set up the classification scheme, because every additional claim generally increases the method's robustness (cf. Sect. 3.3.2). The data from the CIC are part of the data set *D0*, which is used solely for parametrizing the classification scheme (cf. Table 3.3 and Fig. 3.2).

The minimal information of each flood damage claim includes the damage date, the location of the damage (address or coordinates) as well as the associated direct tangible loss to the respective building. As the claim data stem from 15 different data sources (14 PICB and data from a CIC), the provided raw data are heterogeneous and need to be harmonized first, as indicated in Fig. 3.2 (cf. Bernet et al., 2016, for details). During this procedure, the data were quality checked. Obvious errors such as address misspellings or flipped coordinate pairs were corrected. Furthermore, we removed duplicated entries, as well as records with incomplete (e.g., missing address) or invalid data (e.g., invalid

damage date). In terms of loss, we assessed total loss values, i.e., the sum of the registered pay offs and applicable deductibles. Since the insurance coverage is not limited to an upper bound, the maximal total loss for each building equals its sum insured. Applicable deductibles vary between the different PICB, whereas no deductibles at all, a fixed participation of a few hundred Swiss francs or a variable participation of 10 % within a fixed range with a maximum value of CHF 4000 are applied. Finally, the total loss values were corrected for inflation as of 2013 by applying the respective construction output price index considered by each PICB, in case the source data had not been indexed already.

During the next step, each damage claim is geocoded (Fig. 3.2). The coordinates of each damaged building could be obtained by matching the corresponding address with a geocoded register of all Swiss postal addresses (cf. Table 3.2). Notably, only the claims with a unique match were analyzed later. As the data quality of the addresses varies among the different PICB, the amount of claims that could be localized at the building level varies as well (Table 3.3). Nevertheless, most of all PICB claims (79 %) could be localized. A summary of the compiled (sub-) data set is given in Table 3.3.

3.3.2 Classification

The basic idea behind the classification scheme is simple: In case a building (and/or its content) has been damaged by flooding and was located far away from any watercourse, it is very likely that the damage was caused by a SWF. The opposite is not necessarily true: Overland flow is propagating over the land surface towards the watercourses and might cause damage along the flow path until it reaches the next watercourse (Fig. 3.1). Thus, for damaged objects close to a watercourse it is difficult to deduce the responsible flood type without studying each case in detail. Given the size of the data set, detailed manual classification is not practical, in addition to the fact that the data generally do not contain additional information about the responsible damage causes.

In order to classify the claims pragmatically, we exploit the damage claims' known locations as follows: We assume that the dominant damage process in known fluvial flood zones are fluvial floods and, thus, damaged objects located within such zones were likely affected by this process. As these damage claims are inherently clustered around watercourses, we make use of this characteristic by assessing the distance between these claims and the next river. We then classify the damage claims outside of known flood zones based on how their own distance to the next river relates to the typical distances obtained from fluvial flood claims. However, the question is how this distance should be measured and how a representative cut-off distance can be determined.

We tested different distance measures, whereas the Euclidean distance performed well for instance, but neglected topography altogether. For instance, a building on a ridge can be associated with a short Euclidean distance to the next river, in spite of being safe from river flooding due to the building's elevated location. We therefore chose the following approach to address this issue, while at the same time making use of the Euclidean distance's simplicity: Before calculating the Euclidean distance to the next river, we first hide all parts of the river network that are located at lower altitudes than the respective object. For this task, we create a raster mask indicating cells that are located at lower altitudes than the corresponding object, based on a digital elevation model (DEM, Table 3.2). The Euclidean distance to the river network is then assessed by

Table 3.4: Percentile values (d_X, whereas X stands for the Xth percentile) obtained from the ECDF of ACEDs between claims within flood zones and the closest river for each respective region. The column n represents the sample size of each underlying ECDF.

Region	n (#)	d_{25} (m)	d_{50} (m)	d_{75} (m)	d_{99} (m)
Jura	5'508	58	135	315	1'360
Western Plateau	5'810	47	108	237	1'259
Eastern Plateau	10'167	56	135	285	1'084
Northern Alps	7'532	65	137	298	1'198
Eastern Inner Alps	891	29	61	112	643

using the raster mask, which hides all river sections at lower altitudes than the respective object. The obtained quantity is hereafter referred to as "altitude constrained Euclidean distance" (ACED).

Typical distances for all fluvial flood damage claims can then easily be obtained by analyzing the ACEDs of all claims located within known flood zones. For that matter, we selected all claims within such flood zones and compiled the empirical cumulative distribution function (ECDF) of the ACEDs. Based on the large data set, we can be confident that the claims located farther away from the closest river than the 99th percentile of the respective ECDF were caused by SWFs. Considering that fluvial floods become generally more probable the closer we get to the rivers, we chose evenly spaced percentiles, i.e., the 25th, the 50th, 75th and the 99th percentile, respectively. The percentiles are calculated for each region separately (Table 3.4). As the regions themselves represent areas with similar orographic and climatic characteristics (Grosjean, 1975), we thereby implicitly take these regional geographical characteristics into account.

Inherently, the flood claims also include damage caused by overflowing lakes, which could not be distinguished easily from fluvial floods. Consequently, damage related to lakes will be associated with a certain distance to the next river, even though the corresponding river was not the cause of the damage. A visual check of such claims revealed that they tend to be located closer to the corresponding lake than the next watercourse. Technically, this shifts the ECDF of distances to the right and, accordingly, renders higher percentile values (cf. Fig. 3.4 and Table 3.4). In turn, applying the classification scheme with increased percentile values, leads to more claims being associated with fluvial floods instead of SWFs. However, as the number of claims associated with overflowing lakes is low in comparison to claims associated with overtopping rivers, it is safe to assume that this influence is negligible. At most, it might lead to a slightly more conservative classification of SWF claims. Besides, the claims associated with overflowing lakes are directly and correctly classified as fluvial floods, because the hazard of overflowing lakes is consistently considered in the fluvial flood maps (cf. Fig. 3.5).

Using the precompiled percentiles (Table 3.4) as well as fluvial flood maps (Table 3.2) as input, the damage claims can then be classified by means of the classification scheme presented in Fig. 3.5. Five different classes are differentiated ranging from *most likely surface water flood (A)* to *most likely fluvial flood (E)* (cf. Fig. 3.5). The qualitative confidence levels reflect that in general it is becoming gradually more unlikely that an object is affected by fluvial floods the farther away an object is located from a river.

As outlined in Fig. 3.5, we make use of two particular fluvial flood maps, i.e., the

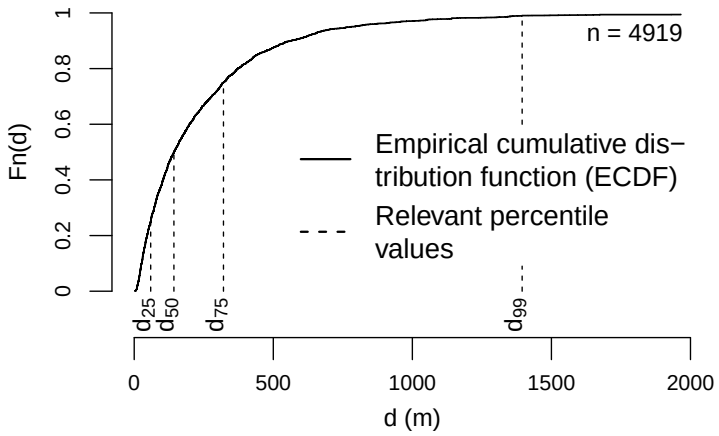

Fig. 3.4: ECDF of all ACEDs of the claims within flood zones in the region Jura. Such ECDFs were compiled separately for all five analyzed regions in Switzerland (cf. Fig. 3.3). The corresponding percentiles are used for the classification of the claims (Fig. 3.5), and are listed in Table 3.4.

"official" Swiss flood hazard maps (Zimmermann et al., 2005; de Moel et al., 2009) and an ancillary map available for the whole of Switzerland called Aquaprotect (Table 3.2). As for the Swiss flood hazard maps, the Swiss Mobiliar collected all available maps from each canton and, in agreement with the responsible authorities, provided the data as per December 2016. The data contain the perimeters for which fluvial flood hazards have been mapped in detail. Within these perimeters, the fluvial flood hazards are indicated using four different so-called danger levels (de Moel et al., 2009), whereas we define the flood hazard zone as the combined area of *low*, *medium* and *elevated danger*, while excluding the area categorized as *residual danger* (cf. Zimmermann et al., 2005). As indicated by de Moel et al. (2009), the flood hazard maps are available for almost the entire Swiss territory. In fact, 88 % of all claims are covered by the flood hazard maps as of 2016, i.e., they are located within the hazard maps' perimeters. The number has increased rapidly over the recent years. Nevertheless, there are still cantons where more than 60 % of the claims are located outside of the perimeters. Thus, to increase the coverage, we used the aforementioned map called Aquaprotect (Table 3.2). It contains coarse fluvial flood extension maps compiled for return periods of 50, 100, 250 and 500 years. We chose the map representing a return period of 250 years, as it best matches the return period of up to 300 years considered by the flood hazard maps. As indicated in Fig. 3.6, Aquaprotect is only used for the territory not covered by the flood hazard maps. Namely, the hazard map perimeters have been extracted from the Aquaprotect layer using common GIS tools.

It should be noted that the areas not covered by flood zones, i.e., the hazard-free zones, have similar implications for the two different sources. Consistently, headwaters and small tributaries are not covered by Aquaprotect. Yet, no information about the specific exclusion criterion could be found. This also holds true for the flood hazard maps, as the study of a few examples revealed. Moreover, the flood hazard maps are produced independently by the regional governments (de Moel et al., 2009), i.e., cantons. Consequently, the applied methods vary between the different cantons and, thus, general statements cannot be made. Nevertheless, the level of detail of the Swiss flood hazard maps far exceeds the one of Aquaprotect. We considered this by empirically choosing

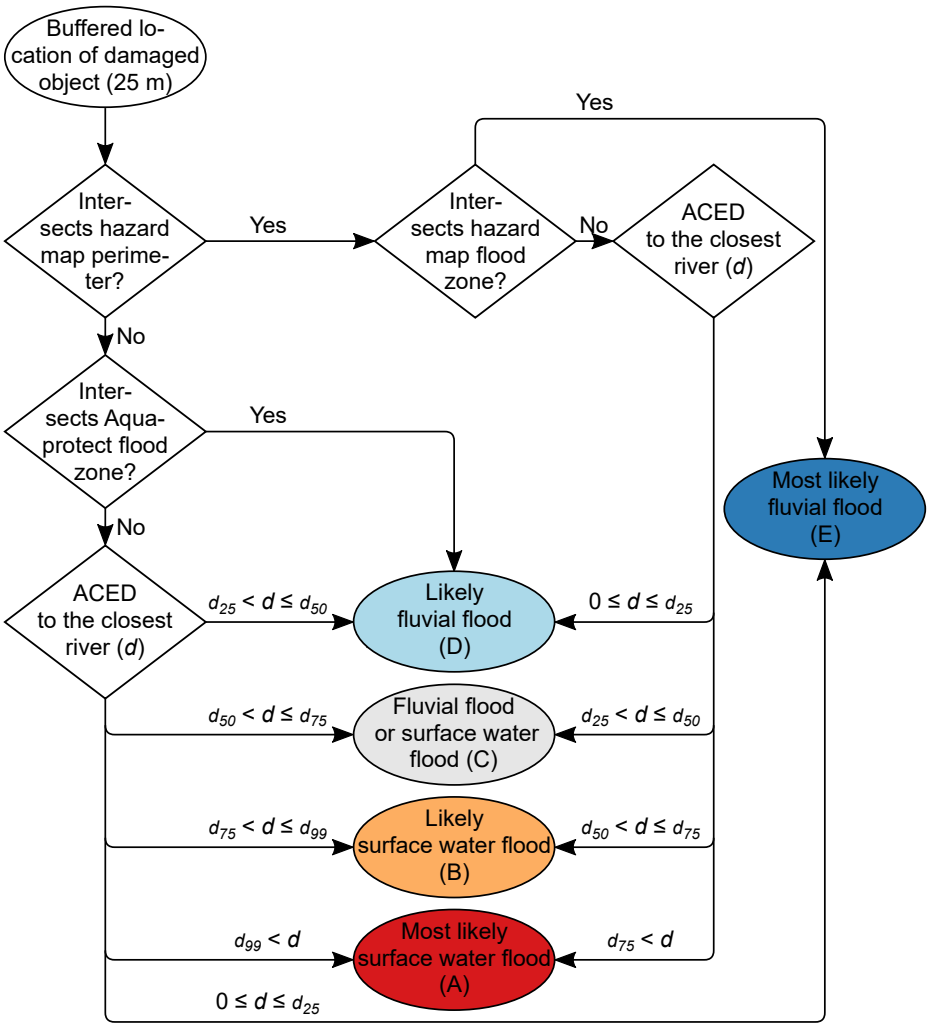

Fig. 3.5: Classification scheme applied to all localized damage claims. As indicated, each claim's point location is buffered by 25 m, corresponding to an average building width. This accounts for the fact that in reality the buildings have a certain spatial extent. The claims are classified as *most likely fluvial flood (E)* in case their buffered location intersect the hazard map flood zone or as *likely fluvial flood (D)*, if it intersects the ancillary flood map Aquaprotect, respectively. The different qualitative confidence levels reflect the level of detail of the two different flood maps (cf. Table 3.2). In all other cases, the specific ACED (d) of each claim is compared to the typical ACEDs of fluvial flood damage (d_{25}, d_{50}, d_{75} and d_{99}, cf. Table 3.4). The classification scheme is further illustrated by Fig. 3.6.

lower percentile levels for claims located within the flood hazard perimeters, as shown in Fig. 3.5 and 3.6.

3.3.3 Normalization

Reported increasing trends of flood losses (e.g., Kron et al., 2012; Grahn & Nyberg, 2017) might be misleading. In fact, there is evidence that increasing flood losses are mainly owed to socio-economic development rather than trends in the flood processes itself (Barredo, 2009). Increasing losses caused by natural hazards such as flooding can,

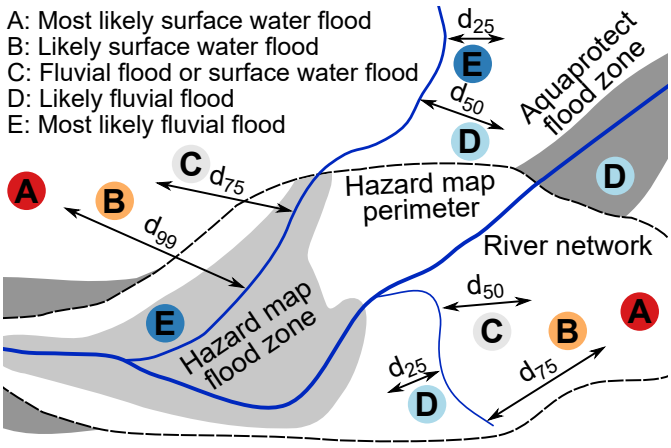

Fig. 3.6: Schematic visualization of the classification scheme. Note that each of the shown classified damage claims corresponds to one of the 11 unique paths of the classification scheme depicted in Fig. 3.5.

thus, mostly be attributed to increasing population and expansion into hazardous areas (e.g., Cutter & Emrich, 2005; Barredo, 2009; Bouwer, 2011; Kundzewicz et al., 2014), as well as increasing property values and diminishing awareness about such hazards (Kundzewicz et al., 2014) and, additionally, better documentation of cases of damage in the more recent past (Gall et al., 2009). Consequently, the loss data need to be normalized with regard to such effects, if the natural process rather than the product with the socio-economic background is of interest. The most fundamental normalization is to adjust past losses to the current values (Kron et al., 2012). However, the more difficult part is to remove the influence of socio-economic development on the observed number of damage claims as well as the associated loss. In addition, the consideration of a change in the exposed objects' vulnerabilities is even more difficult (Bouwer, 2011).

In this study, the values are adjusted for inflation during the harmonization procedure (Sect. 3.3.1). Furthermore, the absolute damage data are normalized in space by relating them to the number of buildings and the sum insured as of 2013, respectively (Appendix 3.A.1). Finally, by normalizing the data over time (Appendix 3.A.2), we obtain a time series of normalized damage caused by SWFs. At the same time, we assume that the buildings' vulnerabilities with regards to SWFs have remained constant within the last decades. This assumption seems appropriate since SWFs have not been considered by any building code, so far. Moreover, the analyzed period is several times shorter than the regular life span of Swiss buildings. Lastly, we apply the seasonal Mann–Kendall test (Hirsch et al., 1982) with a significance level of 0.1 for the resulting p-value to test whether the number of damage claims and associated losses have increased or decreased over time.

3.3.4 Validation

There are few data sets available, with which the claims' classification or normalization could be validated. Hereafter, the exploitation of available data sources for this purpose is elaborated.

First of all, the canton of Lucerne published an overland flow depth map in 2016

stemming from hydrodynamic simulations based on the method described by Kipfer et al. (2012). However, the map indicating categorized flow depth polygons is not suitable for a quantitative validation of the claims' classification. The polygons all indicate a minimal flow depth of 0.015 m and are very dense. In fact, 67 % of all building footprints of the canton of Lucerne intersect such a polygon, whereas only 6.5 % of the footprints are farther than 10 m away from the closest polygon. Consequently, neither quantitative nor a visual relationship could be found between each claim's class and the categorized flow depths.

Secondly, hazard indication maps regarding overland flow are available from two of the 14 cantons covered by our data set, i.e., from the canton of Basel-Landschaft and Aargau. However, the hazard of overland flow was not assessed comprehensibly judging from the technical reports that are publicly available. In some sub-regions, the hazard was assessed by means of GIS analysis and/or based on known past events, or the hazard was not considered at all. Consequently, these maps did not allow a direct quantitative validation either.

In fact, a systematic validation of the classification was not feasible, owed to the large number of claims and the lack of suitable data. Nevertheless, the classification was checked visually, drawing from the input data including flood maps, the river network, the DEM, etc. (cf. Table 3.2), in addition to the before mentioned hazard indication maps. The results of this qualitative and visual comparison are summarized in Sect. 3.4.1.

However, unlike for the claims' classification, it was possible to verify the overall performance of the applied normalizations. Specifically, we could compare our normalized data set with virtually the same source data that had been normalized with the corresponding property data. The reference data are a subset of the data shown in Imhof (2011). The normalization's validation is presented in Sect. 3.4.1, as well.

3.4 Results

After presenting the validation's results (Sect. 3.4.1), we quantify, characterize and compare the damage caused by SWFs with damage caused by fluvial floods (Sect. 3.4.2). Following, we present the spatial distribution of SWF damage (Sect. 3.4.3) and show how the damage evolved within the last 20 years (Sect. 3.4.4).

Note that in the following damage claims classified as A or B, i.e., *(most) likely surface water floods*, are regarded as damage caused by SWFs, if not stated otherwise. Analogously, damage claims classified as D or E, i.e., *(most) likely fluvial floods*, are counted as damage caused by fluvial floods. Claims of class C, i.e., *fluvial flood or surface water flood*, are neither counted for one, nor the other flood type, unless total values are presented.

3.4.1 Validation

The visual comparison of the classified damage claims with overland flow indication maps of the canton of Basel-Landschaft and Aargau revealed that many claims associated with overland flow are clearly located outside areas for which the hazard of overland flow have been assessed or documented. In contrast, the indicated hazard zones were either covering SWF claims or were at least located close to such claims. This might highlight that the corresponding claims were the cause for the delineation of these zones,

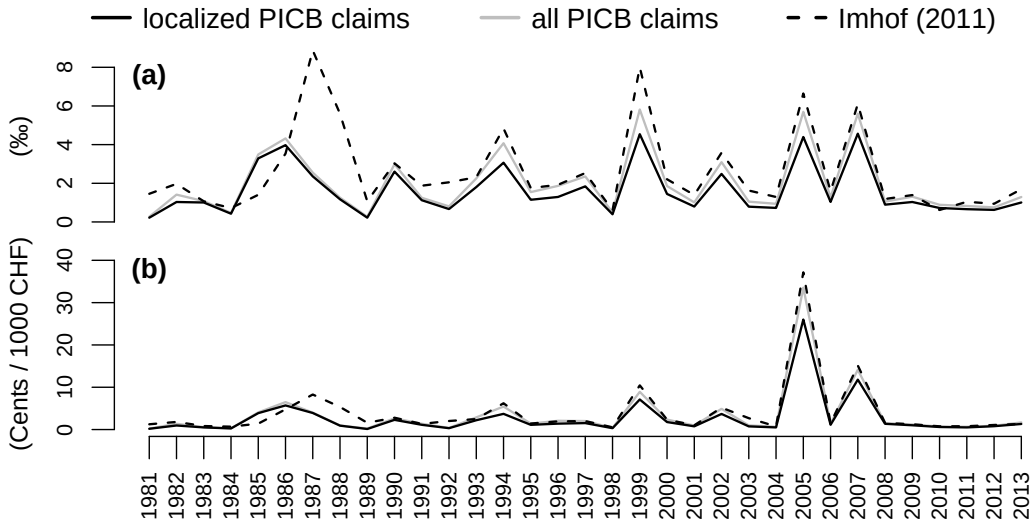

Fig. 3.7: Validation of the normalized damage data. **(a)** Aggregated normalized number of claims in relation to the total number of insured buildings. As a reference, data stemming from a subset of the data presented in Imhof (2011) are shown. As the data are spatially aggregated, all the data including claims without a geocode could be shown, in addition to the localized claims. **(b)** Aggregated normalized loss in relation to the total sum insured.

but at the same time, it also indicates that the classification scheme produces meaningful results.

Overall, the classification scheme rendered reliable and plausible results based on the visual validation. Most importantly, claims classified as A or B, i.e., *(most) likely surface water floods*, are consistently located far away from any watercourse or the topographical location of the claims strongly suggest that these claims were not influenced by a watercourse. Note that the strengths and weaknesses of the classification scheme are elaborated in Sect. 3.6.

As outlined in Sect. 3.3.4, we could validate the normalization of the damage data with reference data based on Imhof (2011). The reference data show aggregated number of flood claims per number of insured buildings (Fig. 3.7a), as well as the loss per total sum insured (Fig. 3.7b). The reference data consist of (almost) the complete records of the 14 corresponding PICB, whereas our data set contains less and less records, as we move back in time (cf. Table 3.3). As we are looking at relative numbers, the comparison is still valid, but the different data coverages have to be kept in mind.

In fact, Fig. 3.7 highlights that before 1989, the data sets are badly matching, but have very similar patterns thereafter. Together with the fact that after 1993 all regions are satisfactorily represented, these are the reasons why we have limited the time series of SWF damage to the period 1993–2013 (cf. Table 3.3 and Fig. 3.14).

The clear bias of the localized claims in comparison to the reference data can mainly be attributed to the 21 % of the claims that could not be localized, i.e., the curves aline much better, when also considering the claims without a precise geocode (Fig. 3.7). However, a small bias persists, to a larger degree for the number of claims and to a smaller degree for the loss values, respectively. The remaining deviations are probably due to the coverage that becomes increasingly different in earlier years as well as the applied normalization procedure using auxiliary data. Notably, given the simple applied

methods, the normalization works exceptionally well.

3.4.2 Relevance of surface water flood damage

Figure 3.9 reveals that SWFs were responsible for 45 % of all localized flood damage claims between 1999–2013 based on the data set *D2* that covers 48 % of all Swiss buildings (cf. Table 3.3). In terms of loss, however, SWFs only account for 23 % of the total loss. The regional loss shares vary only slightly, i.e., between 15 and 25 %, except in the Western Plateau, where SWFs account for 51 % of the total loss. In the same region, SWFs caused two-thirds of all damage claims. In the Jura, roughly half of all claims could be associated with SWFs. The share is lower in the Eastern Inner Alps and the Eastern Plateau with 43 % and 39 %, respectively. In the Northern Alps, SWFs are only responsible for 24 % of the flood claims.

The distribution of loss per claim explains why almost half of all claims are only responsible for roughly one-quarter of the total loss. As shown in Fig. 3.8, the mean loss per SWF claim is considerably lower than the mean loss per claim related to fluvial floods. This is most pronounced when comparing claims of class A (*most likely surface water floods*) with class E (*most likely fluvial floods*): For class A, 95 % of all claims are less or equal to CHF 32'349, while for class E, the 95 % percentile is CHF 120'330.

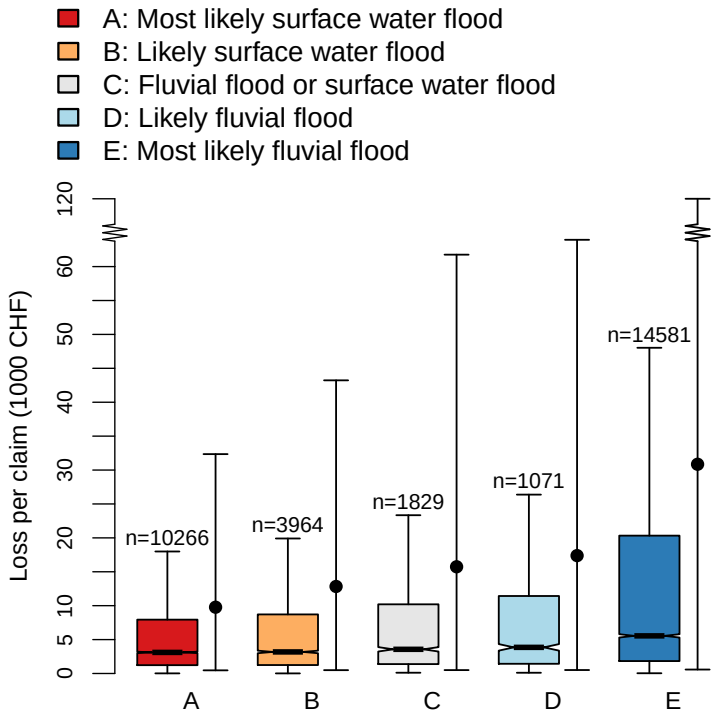

Fig. 3.8: Box plots of losses per claim showing the interquartile range, i.e., the range from the 25 % to the 75 % percentile, as well as the median (bold horizontal line). Non-overlapping notches indicate significantly differing medians, while the whiskers extent to 1.5 times the interquartile range. Note that the outliers are not plotted. Instead, the 5–95 % percentile range is plotted on the right of each box plot, while the mean value is indicated by the solid dot. Furthermore, note that the y-axis is compressed between CHF 60'000 and 120'000. The plot is based on the data set *D2* (cf. Table 3.3).

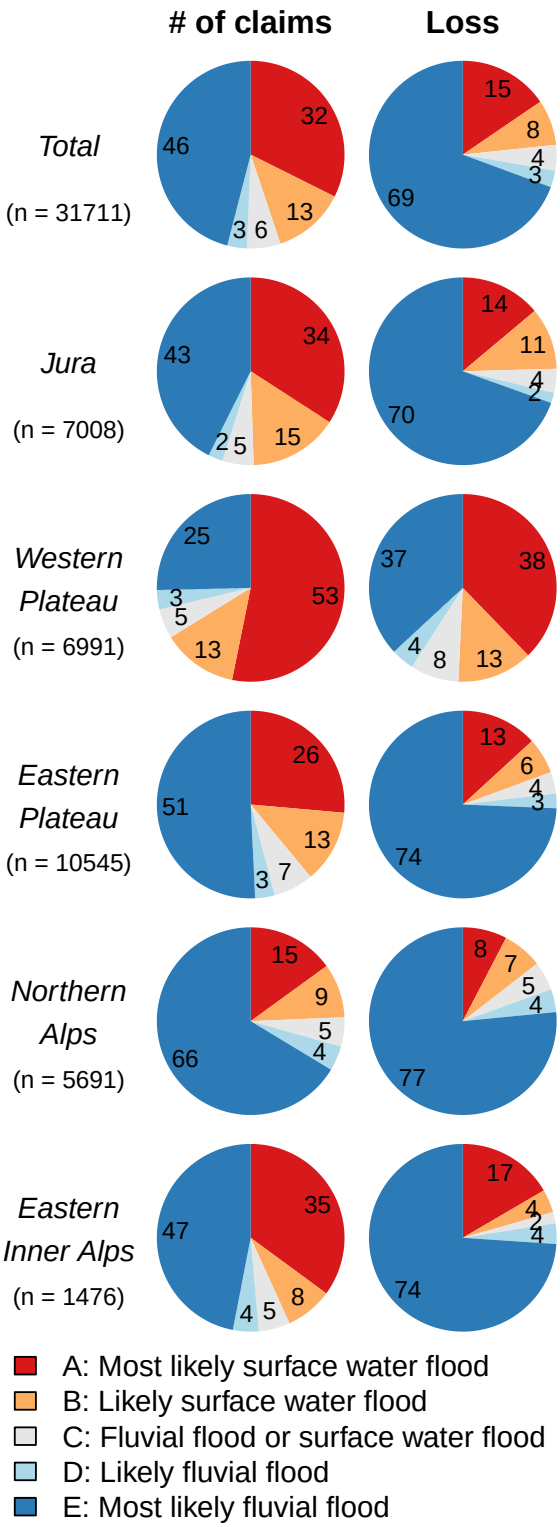

Fig. 3.9: Number of claims as well as corresponding losses in total, and separately for each region. The values stem from the data set *D2*, which contains seamless claim records of 13 PICB covering the period 1999–2013 (cf. Table 3.3). The numbers indicate the shares in %, while n represents the sample size.

Although there is a significant difference, the medians are relatively low for claims of class A and E with values of CHF 3'113 and CHF 5'554, respectively. Thus, the majority of the claims of all classes are associated with a rather low amount of loss, while the minority of the claims report extreme losses. However, by far the highest losses are associated with claims of class E (Fig. 3.8). Grahn & Nyberg (2017) have found similarly skewed distributions caused by pluvial floods in Sweden.

So far, an unanswered question has been, how the number of damage claims and associated losses are distributed in relation to the size of the corresponding event. Supposedly, frequent damage associated with low loss values might add up to a substantial sum in the end, as suggested by Kron (2009), for instance. For that matter, we have stratified the data according to the total number of claims per day using five categories

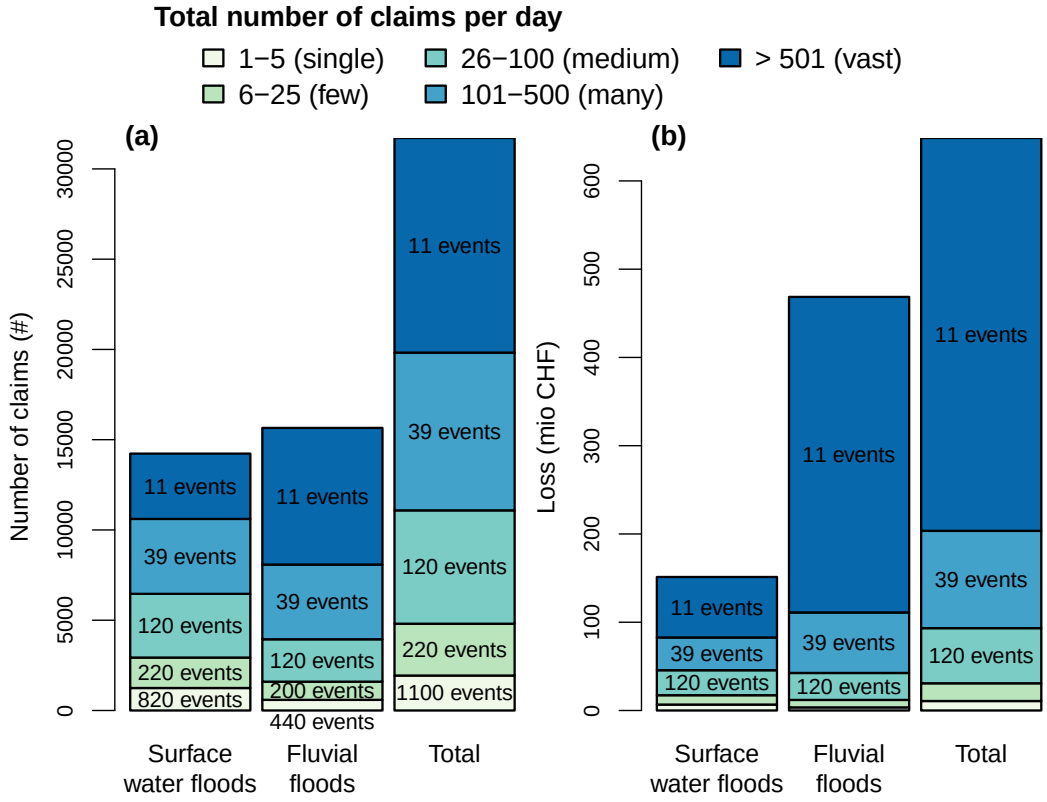

Fig. 3.10: The total number of claims and loss categorized according to the size of the corresponding event, based on the data set *D2* (cf. Table 3.3). **(a)** Each claim was categorized according to the total number of flood damage claims that occurred on the same day. For instance, all claims that occurred on 21 June 2007 fall into the category *vast*, since 1'162 damage claims were registered for that day in total. Thus, all these claims belong to one of the 11 largest events within the period 1999–2013. As each claim was classified (Sect. 3.3.2), we can further group the data as claims related to SWFs (class A and B) or fluvial floods (class D and E), respectively. For the lowest two categories, i.e., *single* and *few*, the number of events of SWFs is larger than the number of fluvial flood events. This is due to the fact that some of these events consist of claims categorized as SWFs only. For all other categories, the event numbers match, indicating that for each of these days, some of the claims were classified as SWFs, while some were classified as fluvial floods. **(b)** The same stratification is applied to the associated loss. Note that the indication of the number of events for the smallest two event categories, i.e., *single* and *few*, were omitted for better readability. However, the values are identical to the values shown in panel a.

ranging from *single* (1–5 claims per day) to *vast* (>501 claims per day). We defined an event as a day with at least one claim of any class (A–E), which amounts to a total of 1'490 events in the period 1999–2013. Obviously, this is a pragmatic definition of an event. Specifically, separate local events occurring at the same day are counted as a single event, while events spanning over several days are counted as individual events. Nevertheless, the pragmatic definition is sufficient for the purpose of a first simple analysis, presented hereafter.

The stratified number of claims (Fig. 3.10a, *Total*) confirms that smaller events are more frequent than larger events, i.e., 1'100 events of the smallest category (*single*) are opposing 11 events of the largest category (*vast*). Interestingly, days with *single* and *few* claims only account for a small share of SWF and fluvial flood claims, although for SWFs the shares are larger. Strikingly, 11 events within the last 15 years with more than 500 claims each, account for almost half of the claims caused by fluvial floods, but only to one-quarter of the claims associated with SWFs. In contrast, the same 11 events accounted for 45 % of the loss caused by SWFs, and even 76 % of the loss caused by fluvial loss, respectively (Fig. 3.10b). Based on this analysis, we can infer some important characteristics about the damage caused by SWFs:

- SWF damage occurs more frequently during small events, whereas the majority of fluvial flood damage is caused during large events.
- The largest events cause most of the losses, whereas small events only account for insignificant losses in comparison.

Figure 3.10 has hinted at the fact that each event causes SWF damage alongside fluvial flood damage, except a few of the smallest events. This is further explored by Fig. 3.11. For each event, i.e., a day with at least one flood damage of any class, the number of claims classified as SWFs is plotted against the number of claims classified as fluvial floods. As expected, most of the events are clustered around the origin, owed to the fact that events with up to 5 claims account for 74 % (1'100) of the total number of events (1'490) within the period 1999–2013.

The most severe floods within the last 15 years within the study domain are highlighted in Fig. 3.11, which highlights that these flood events are also associated with high numbers of SWF damage, even though these events are mostly known for being devastating fluvial floods. Thus, our analyses show that fluvial flood damage generally coincide with SWF damage. This has been noted before (e.g., Blanc et al., 2012) and can be explained by the fact that both flood types are generated by the same rainfall input. Particularly, during extreme rainfall events, we can expect fluvial flood damages as well as SWF damage. However, the shares of SWF damage in comparison to fluvial flood damage are different, which might be linked to the type of rainfall. For instance, the damage on the 20–21 June 2007 was caused by widespread thunderstorms with local rainfall intensities as high as 73 mm^{-1} (Hilker et al., 2008) and is associated with a larger share of SWF damage claims (Fig. 3.11). All other highlighted extreme flood events were triggered by long-duration rainfalls and, at the same time, larger numbers of fluvial flood damage claims. This could be an indication that the type of rainfall, and in particular the rainfall intensity, is an important driver of SWF damage, as noted for instance by Spekkers et al. (2013), as well.

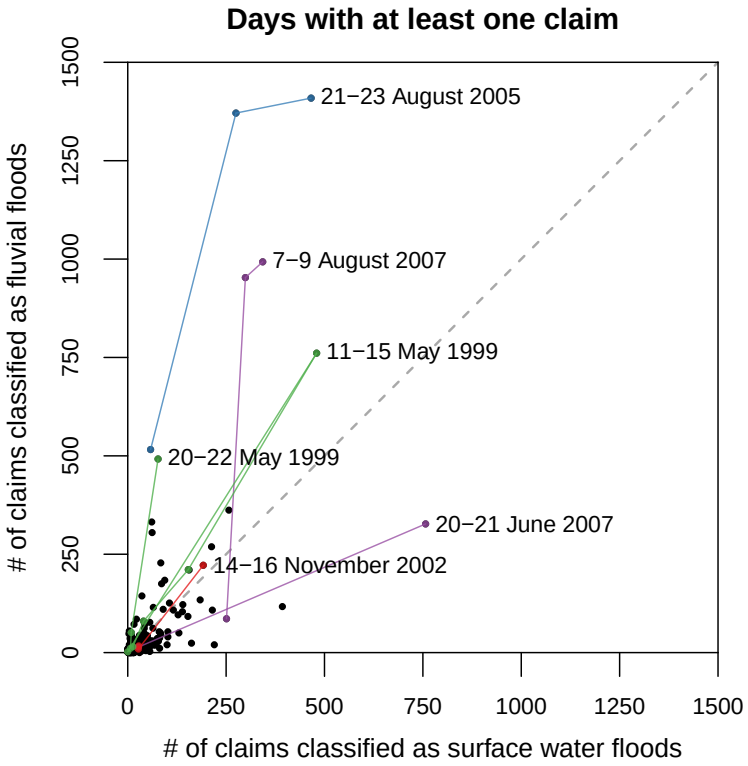

Fig. 3.11: Scatterplot between the number of claims classified as SWFs (class A and B) against claims classified as fluvial floods (class D and E) based on the data set *D2* (cf. Table 3.3). Each point represents an event, i.e., a day with at least one flood damage of any class. Along the dashed gray line, the number of SWF claims and fluvial flood claims are identical. Thus, claims below the line indicate events with more SWF than fluvial flood claims, and events above the line indicate the opposite. The severest flood events within the period 1999–2013 are highlighted, in addition to the event in November 2002 that was the most significant event for the Eastern Inner Alps (cf. Fig. 3.13). Moreover, all dates that belong to the same event are connected with lines, and severe events of the same year are shown in the same colors. The event dates are based on Hilker et al. (2008, 2009).

3.4.3 Spatial distribution

Thanks to the spatially explicit input data, we can get a good overview of damage claims triggered by SWFs in space, as shown in Fig. 3.12. In general, it can be observed that the Swiss Plateau (2 and 3) is exposed most to SWFs, both in relative and absolute terms. Also in the Jura (1), many buildings are affected by SWFs. In contrast, the alpine regions of Switzerland, i.e., the Northern Alps (4) and also the Eastern Inner Alps (5) are exposed the least.

The visualization of relative values has advantages. For instance, in Bernet et al. (2016), low inundation rates by overland flow were reported for Grisons, i.e., the Eastern Inner Alps, and high values for Fribourg, which lies mostly in the Western Plateau. Fig. 3.12 supports these findings, but presents a more differentiated picture, as differences within the mentioned regions can be grasped, as well. In particular, we can see that the relative values, i.e., the number of damage claims in relation to the number of buildings within the same raster cell, are not evenly distributed in space. The most affected regions

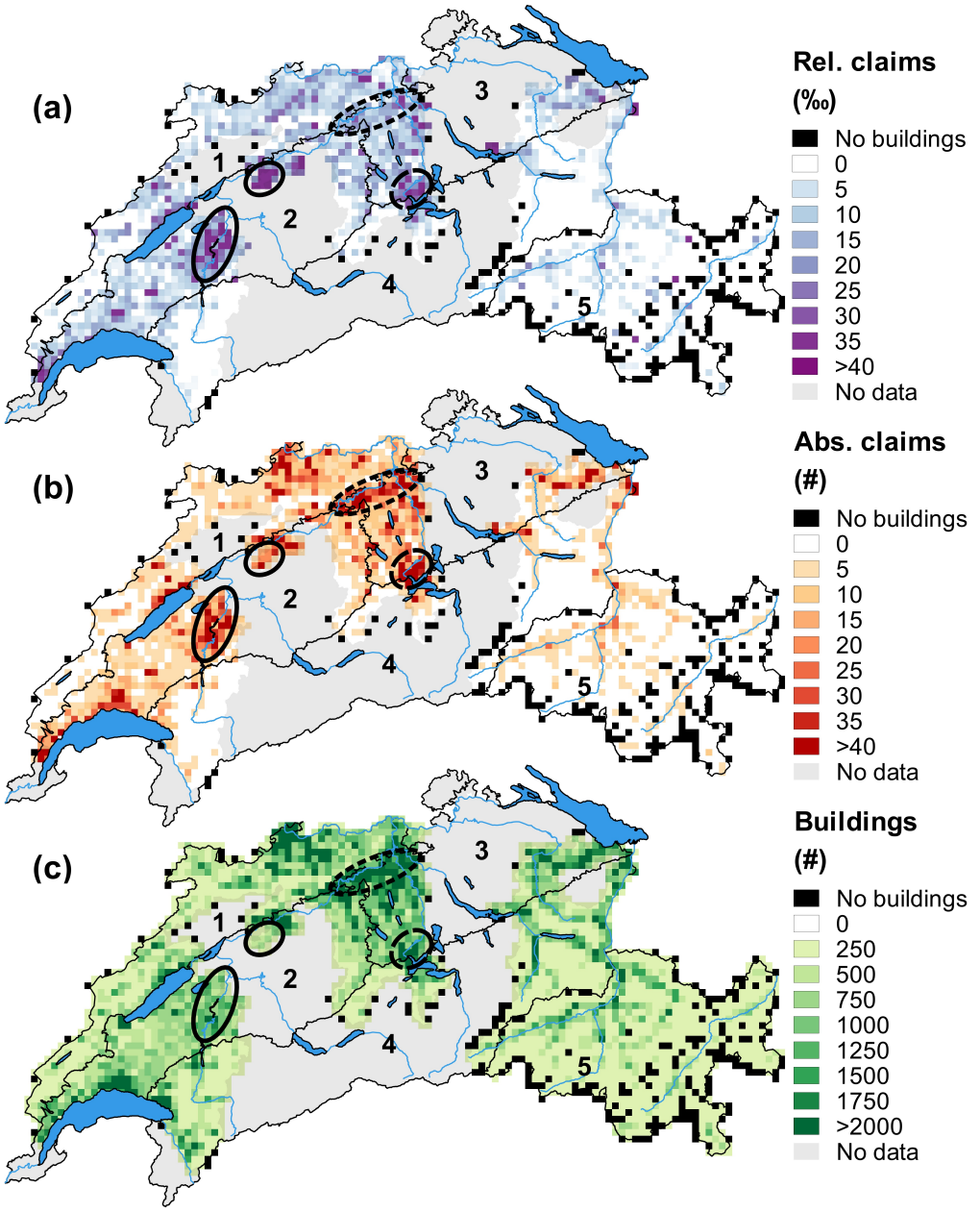

Fig. 3.12: Relative (**a**) and absolute (**b**) number of damage claims caused by SWFs based on the data set *D2* covering the period 1999–2013 (cf. Table 3.3), aggregated to regular grids of 3 by 3 km. In addition, the absolute number of buildings per cell are shown (**c**). The solid ellipses highlight two less populated areas with high relative and absolute number of damage claims. The dashed ellipse indicates a highly populated area with high absolute and relative values, whereas the dotted ellipse marks a densely populated area with high absolute number of damage claims, but comparatively low relative values. The numbers indicate the corresponding region, i.e., Jura (1), Western Plateau (2), Eastern Plateau (3), Northern Alps (4) and Eastern Inner Alps (5).

are certainly those with high relative, as well as absolute number of claims, such as the areas indicated by the solid and dashed ellipses in Fig. 3.12. In addition, we see that such areas do not necessarily coincide with the most densely populated areas (dashed ellipse),

but may lie in less populated areas (solid ellipses). Moreover, we can also identify areas that suffer from high absolute number of damage claims but are exposed less in relative terms (dotted ellipse).

3.4.4 Temporal evolution

To obtain an idea about the distribution of the damage throughout the year, we have plotted the number of claims as well as associated losses against the month in which they occurred in form of spider plots (Fig. 3.13). In relation to SWFs, by far the most damage occurs in the summer months from June to August in all regions, except in the Eastern Inner Alps. In the latter region, the maximum number of damage claims were

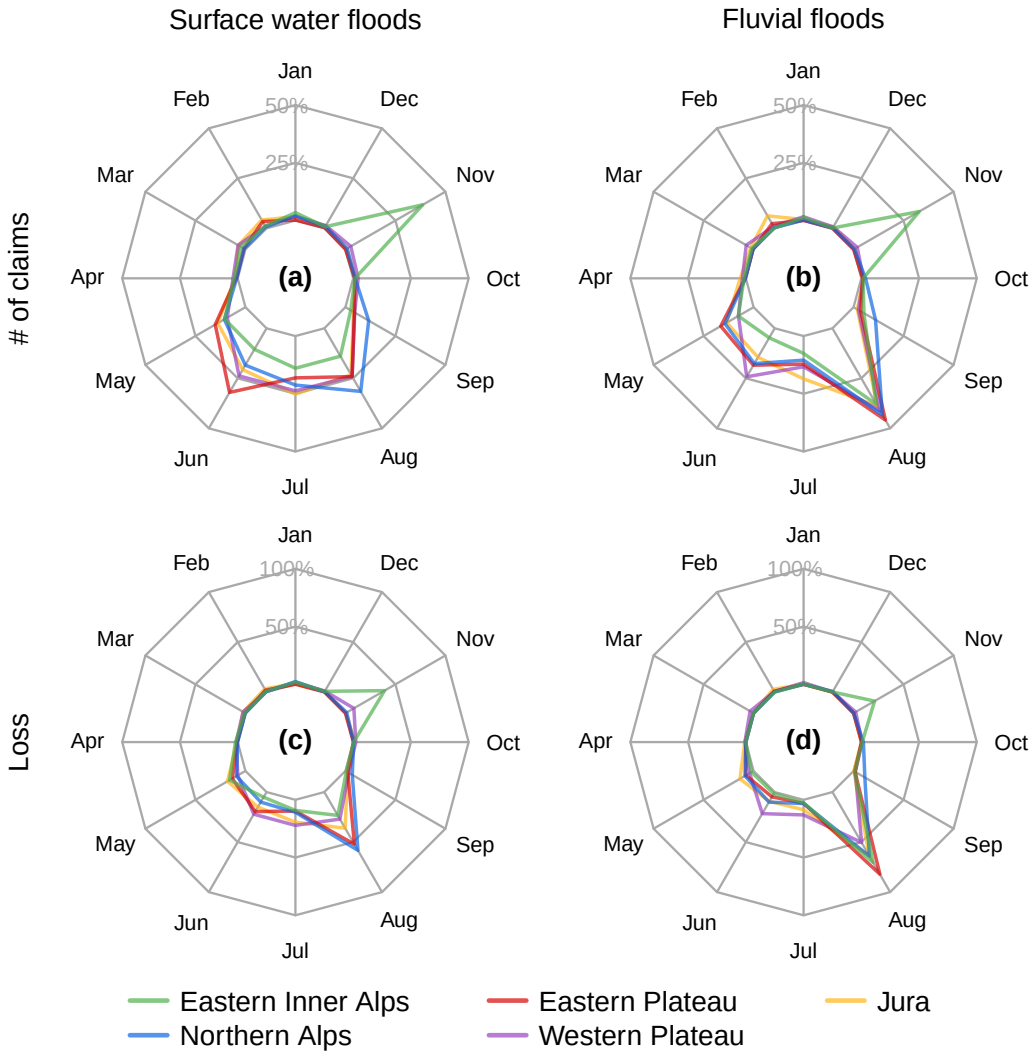

Fig. 3.13: Spider plots indicating the relative number of damage claims and associated losses for each month. Separate plots are shown for SWFs (class A and B) and fluvial floods (class D and E). The data set *D2* constitutes the underlying data and covers the period 1999–2013 (cf. Table 3.3). Note that the scale for the number of claims ((**a**) and (**b**); 0–50 %) is not the same as the scale for the loss ((**c**) and (**d**); 0–100 %).

registered in November, which can be attributed to a single event that occurred on 14–16 November 2002 (Romang et al., 2004), which is highlighted in Fig. 3.11, as well. The remaining damage claims occurred also mainly in summer, but due to the devastating event in fall 2002, the values are much lower in comparison to the other regions.

Overall, the number of claims are elevated in the last month in spring, i.e., May, and to a smaller degree in the first month of fall, i.e., September, for most regions. During the rest of the year, i.e., from October to April, very few damage claims are caused, except for the Eastern Inner Alps in November, as discussed before.

Analogous to the number of damage claims, SWFs cause most of the associated losses in the summer months (Fig. 3.13c). Interestingly, the losses in the Eastern Plateau and the Northern Alps have larger shares in August, compared to the other regions, but also compared to the corresponding number of claims (Fig. 3.13a). This can be explained by the particularly high losses during the August 2005 flooding, as indicated in Fig. 3.12.

The number of claims and associated losses of fluvial floods are highly concentrated in August in all regions (Fig. 3.13b and 3.13d). The event in November 2002 that affected the Eastern Inner Alps is also showing up prominently for fluvial floods, as elaborated before.

Finally, it is interesting to have a look at the time series of damage caused by SWFs. Based on the normalized values covering the period 1993–2013, we are able to show the relative number of claims and losses related to SWFs, individually for each region (Fig. 3.14). The seasonally aggregated values show a distinct pattern. The relative

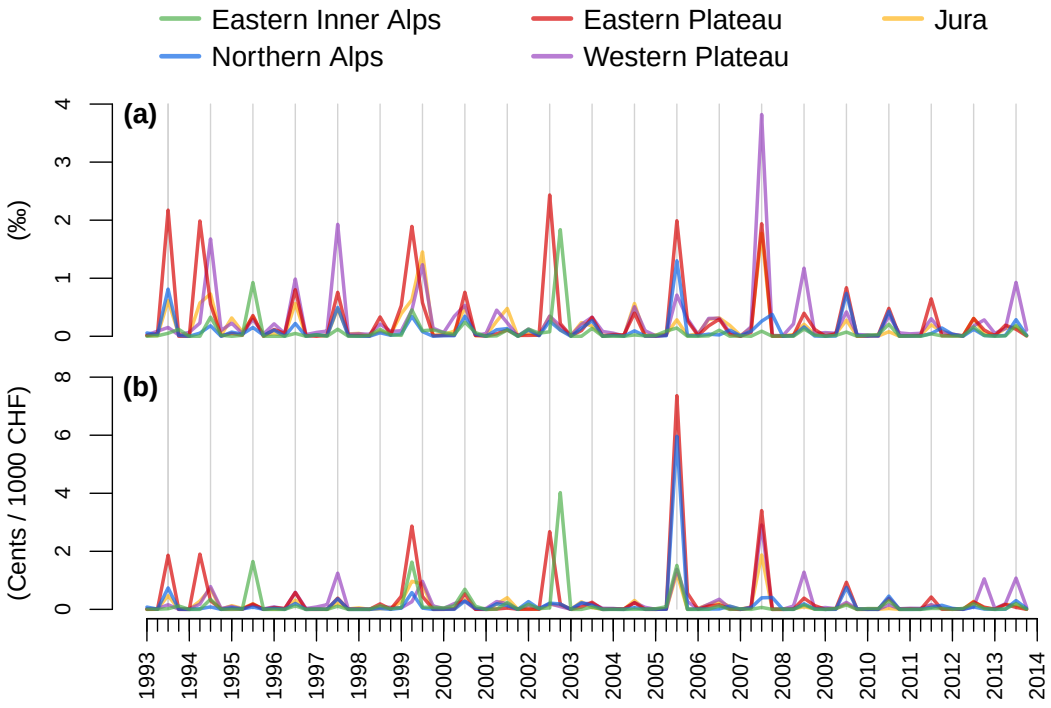

Fig. 3.14: Time series showing the normalized number of SWF damage claims (**a**) as well as associated losses (**b**), based on the data set *D1* (cf. Table 3.3). As pointed out in Sect. 3.4.1, not all data records cover the whole period, thus the representativeness is decreasing starting from 2003 as we move back to 1993. Nevertheless, as the aggregated values match well with the reference values (cf. Fig. 3.7), and only relative values are considered here, the values are still meaningful.

number of claims were almost always highest during the summer, i.e., in June, July and August, which supports the results discussed before. However, there are a few exceptions such as the spring of 1994 and 1999, where corresponding values exceeded the highest values of the same year. Interestingly, in both cases high values were also observed in the following summer, but in other regions. In 2002, a high value in summer that affected the Eastern Plateau was followed by severe damage in the Eastern Inner Alps in November 2002 (Romang et al., 2004), which corresponds to the highest observed value in that region during the whole studied period. High values occurred frequently in the Eastern Plateau, but also in the Western Plateau, where in 2007 almost 4 ‰ of claims per buildings were registered. The highest values in the Jura occurred in summer 1999 and 2005. A value higher than 1 ‰ was observed in the Northern Alps only once, namely in 2005.

The values in terms of loss are in line with the claims per buildings, however, they are scaled differently. Most pronounced are certainly the high values in the Eastern Plateau and the Northern Alps in 2005. Other high values are observed in spring 1999, summer and fall 2002 as well as in summer 2007.

Furthermore, the data do not exhibit any trends of SWF damage claims in the period 1993–2013 based on the seasonal Mann–Kendall test at a significance level of 0.1, except for the Jura. In that region, the number of claims have been decreasing ($p = 0.006$). In contrast, the relative losses in Jura do not exhibit such a trend ($p = 0.52$). The absence of any increasing trend might be a surprising result, as increasing damage trends are often reported (e.g., Kron et al., 2012; Grahn & Nyberg, 2017). However, it is important to note that in this study we are talking about normalized, relative values, while in the aforementioned publications, the trends of the absolute numbers are considered.

3.5 Discussions

The key to the exploitation of the insurance data with regards to SWFs lies in the classification of the damage claims (beside the provision of the data in the first place). The classification scheme, as introduced in this study, is based on the geographical location of each damage with respect to known fluvial flood zones and the hydrological network. On the one hand, this obviously requires spatially explicit damage data. On the other hand, it provides a reproducible, objective and most importantly, an independent classification. These characteristics are important, as the following examples highlight: Grahn & Nyberg (2017) had to exclude damage that occurred on the same day as known fluvial floods in order to distinguish pluvial from fluvial flood claims. However, our results show that fluvial flood damage almost always coincides with damage caused by SWFs. Consequently, excluding damage occurring on the same day as fluvial floods likely introduces a bias. Another example is the statistical model applied by Spekkers et al. (2013) in order to differentiate rainfall-related damage clustered around wet days from non-rainfall related damage occurring throughout the year. Thereby, the classification of each claim is not independent anymore, but depends on how many other damage claims occurred on the same day.

Although, the classification scheme presented in this study has striking advantages, it has the following short-coming: As overland flow propagates over the land surface, it may eventually reach a watercourse (cf. Fig. 3.1). Areas alongside watercourses, where

the overland flow joins the river, may be a flood hazard zone. If so, all claims in that specific area are classified as a fluvial flood, even though, possibly, the claim might have been caused by incoming overland flow. However, a more qualified classification entails likely event-specific, time-consuming manual assessments. In fact, it is extremely difficult to disentangle the different flood types, even more so for events in the more distant past and if no data with that particular focus are available. In contrast, for claims that are located far away of any watercourse, it is very unlikely that they are affected by watercourses at all. Therefore, our method renders a lower boundary of claims associated with SWFs, in essence. In reality, the numbers are likely higher, but as mentioned before, disentangling the flood types within their overlapping domains is difficult.

By applying the classification scheme to the harmonized damage data, we could show that SWFs caused almost the same number of damage claims as fluvial floods. Thereby, our results confirm anecdotal evidence that indicated similar numbers. For instance, one of the few quantitative studies about SWFs in Switzerland reported that at least half of the flood damage claims in the canton of Aargau were caused by overland flow (Aller & Petrascheck, 2008). However, the study is neither comprehensible in terms of applied methods, nor the underlying data, and covers only a small part of Switzerland. Thus, for the first time, we can present sound evidence about the relevance of SWFs in Switzerland based on a large data set including more than 30'000 damage claims covering 15 years and 48 % of all Swiss buildings.

Despite the remarkably high number of damage claims caused by SWFs, our results show that SWFs only account for roughly one-quarter of the total loss, which is inline with results from the pilot study (i.e., Bernet et al., 2016). Nevertheless, the associated yearly loss is highly significant, as the following numbers exemplify: The median of total yearly losses to buildings caused by fluvial floods within the considered regions is even slightly lower (5.0 mio CHF y^{-1}) than the median of SWF losses (5.9 mio CHF y^{-1}) based on the data set *D2* covering the period 1999–2013 (cf. Table 3.3). However, the mean yearly loss of fluvial floods is more than 3 times the loss caused by SWFs (i.e., 31.3 mio CHF y^{-1} versus 10.1 mio CHF y^{-1}, respectively). The difference between the maximum yearly losses caused by each flood type is even more pronounced: While the maximum loss of SWFs amounts to 38.3 mio CHF y^{-1} in 2005, fluvial floods caused 234.3 mio CHF y^{-1} in the same year, which corresponds to a factor of roughly 6.

These observation concerning annual flood losses are supported by the characteristics of the individual losses. Their exploration (Fig. 3.8) expressed that the range of loss per claim is much narrower for SWFs than for fluvial floods. As SWFs are expected to be associated with significantly lower flow depth than fluvial floods, this might be one of the main reasons for the lower associated loss, since water depth is among the most significant single impact parameters for structural damage to residential buildings (e.g., Kreibich et al., 2009; Merz et al., 2013). Interestingly, the median loss of each claim associated with fluvial floods is also rather low, although significantly higher than the median loss of claims related to SWF. Yet, the highest losses per claim are caused by fluvial floods during the most severe events within the study domain (Fig. 3.10). As during extreme events, larger areas are affected and the associated shares of objects inundated by large water depths are higher (Elmer et al., 2010), higher losses per claim can be expected. Along the same lines, Hilker et al. (2009) report that the most severe events contribute to more than half of the estimated total loss and Barredo (2009) found an even higher share for flood losses in the whole of Europe. Undoubtedly, loss ratios are

higher during more extreme events (Elmer et al., 2010). Although, this probably also holds true for damage caused by SWFs, such damage certainly seems less influenced by the severity of the event (cf. Fig. 3.8 and 3.10). Consequently, SWFs may rarely cause the total destruction of a building, and associated loss ratios may, thus, mostly be well below 1.

As outlined in the introduction, this study is limited to direct tangible loss to buildings. Therefore, the absolute loss values are low in comparison to other loss estimations that include other losses, as well. For instance, Hilker et al. (2009) report a mean financial loss of 317.2 mio CHF y^{-1} between 1972–2007, which is roughly 7 times higher than the mean of all flood losses to buildings, as represented by our data set. For one, the data published by Hilker et al. (2009) cover the whole of Switzerland and consider a longer period. More importantly, however, these estimates also include damage to infrastructure, forestry and agricultural land, in addition to damage to buildings and their content. Therefore, the associated losses are inherently higher than the numbers presented in this study. This exemplifies that one has to be careful when comparing values from different data sources (Kron et al., 2012). Moreover, it highlights the fact that damage to buildings are associated with just a small fraction of the total loss caused by SWFs for the society. Nevertheless, these data serve well for assessing the relevance of SWF damage in Switzerland, especially when considering relative values.

The spatial distribution of damage caused by SWFs can be deceiving: Obviously, an area with a higher building density will likely result in a larger number of damage claims compared to an area that is less populated (Fig. 3.12b versus 3.12c). Therefore, it is important to have a look at relative values, as well (Fig. 3.12a). Thereby, the effect of higher values caused by a denser number of buildings is considered. However, the relative values are quite sensitive in sparsely populated areas. A damaged house with virtually no other houses in the vicinity will produce a high relative value or a low value, respectively, if the same is not affected. In contrast, in more populated areas, the relative value will not change much in case a building is more or less damaged. Thus, to obtain a complete picture, the relative and absolute values should be considered alongside the building density. In that way, the most exposed areas can be identified, like the two highlighted areas in the Western Plateau that are associated with high relative and absolute numbers of damage claims (Fig. 3.12).

Furthermore, it is important to keep in mind that in case an area has no registered damage, it does not necessarily mean that the area has not been affected by a floods at all. It just indicates that either no buildings were in the vicinity of the flooded area or the buildings were properly protected against such floods. Therefore, damage records can only indicate floods that lead to some sort of damage and never to the occurrence of floods in the hydrological sense, as discussed in the introduction (cf. Fig. 3.1). However, understanding the characteristics of damaging floods can open the stage to understand the process in a broader context, as well.

The temporal distribution of claims related to SWFs exhibits a distinct seasonality (Fig. 3.13 and 3.14). Similar to the flood losses reported by Hilker et al. (2009), most damage clearly occurs in summer, with a few exceptions. Therefore, thunderstorms associated with short but intense rainfall are certainly an important driver of SWF damage. Nevertheless, long duration rainfall events are also responsible for a large share of SWF damage claims, highlighted by the most severe events that are mostly associated with long duration precipitation. In contrast, much fewer damage claims are

caused in spring and fall, and virtually no damage claims are caused in winter. Damage to buildings in winter can likely be attributed to rather local events coinciding with conditions promoting overland flow generation such as rain on frozen soils. Overall, these observations have important implications for assessing the hazard of SWFs. In particular, simply focusing on high intensity rainfall events may lead to an underestimation of the risk of SWFs.

Although the time series is relatively short, the data do not exhibit any increasing trends of SWF damage in the period 1993–2013. Obviously, the general increase of absolute loss in time, which can be found in our data as well, is eliminated when the data are normalized. Thus, as suggested for instance by Kundzewicz et al. (2014), the increase in loss can be mainly attributed to the socio-economic development. However, we did not consider further aspects that could have an influence on such trends, such as a change in vulnerability (Bouwer, 2011). Moreover, insurance or local governmental policies that might have changed over time were not taken into account either. Nevertheless, it is important to note that increasing absolute losses are most likely not attributable to climate change, but to socio-economic factors (e.g., Cutter & Emrich, 2005; Barredo, 2009; Bouwer, 2011; Kundzewicz et al., 2014). Consequently, the major associated risks related to SWF damage is not climate change, but the increased exposure due to population growth and increasing wealth. This has implications for decision and policy makers, as well as for insurance companies and similar stakeholders.

Indeed, the flood processes are a complex interlinked system, as Evans et al. (2004) stated. In fact, the insurance data illustrated that damage caused by SWFs occur (almost) always alongside claims caused by fluvial floods (cf. Fig. 3.11). Be it a short and intense thunderstorm or a long duration event, rainfall is the main trigger of every SWF, as well as (almost) every fluvial flood. Understandably, if there is enough rainfall to cause a SWF, it may as well cause or at least contribute to a fluvial flood, once part of the water reaches the next watercourse. Undoubtedly, severe events that include hundreds or thousands of damage claims entail a combination of flood processes, while, of course, some local events may be associated with a single flood process only.

3.6 Conclusions

In this study, we have presented a simple and pragmatic approach of how spatially explicit insurance data records can be exploited to investigate damage caused by SWFs. The method provides a robust lower estimate of SWF damage. Using the presented percentile values (Table 3.4), the method is applicable for classifying any claim in Switzerland, except in the Western Inner Alps and Southern Alps, where data were lacking. For these regions, appropriate values could be approximated. Moreover, the method is transferable to other regions and countries, but has to be adapted to locally available flood hazard maps.

There seems to be a consensus among practitioners and experts that SWFs are responsible for a large share of all flood damage. However, this perception does not stem from quantitative research, but rather from single case studies or practical experience and, thus, lacks evidence. With the study at hand, we are able to quantify the striking relevance of SWFs in Switzerland based on a sound data basis, regionally representing 39–100 % of all buildings over a period of 15 years. The data reveal that SWFs cause

nearly as many damage claims as fluvial floods. In contrast, SWFs account for roughly one-quarter of the direct tangible losses, driven by lower losses per SWF claim. This hints at the different processes' characteristics with generally low flow depths associated with SWFs, opposed to both low and high, static and dynamic, flow depths during fluvial floods that are additionally sensitive to the severity of an event.

The most affected areas are clearly the Western Plateau, both in relative and absolute terms, followed by the Eastern Plateau and the Jura. The more mountainous regions, i.e., the Northern Alps and the Eastern Inner Alps, are affected less. Notably, there are also large differences between the spatial distribution of damage within each region. By relating the absolute number of damage claims to the number of buildings in the vicinity, the effect of varying building densities can be considered. Nevertheless, in sparsely populated areas the relative numbers are sensitive and, thus, less robust, owed to the particularly low building densities. Furthermore, not all regions are affected by SWFs to the same extent throughout the year. Yet, in all regions most of the damage occurs in summer, safe a few exceptions.

In general, the spatial and temporal distribution of SWF damage is complex. Different factors might be responsible for high damage within certain areas or during certain periods. For instance, the meteorological forcing differ spatially and temporally, the predisposition due to unfavorable soils or landuse practices play a role, past human interventions such as the installation of drainage and the removal of small natural rivulets can have an influence, but also slightly differing practices by the insurance companies or different rules applied for buildings to be built might be relevant. Undoubtedly, we stand at the beginning of better understanding SWFs in Switzerland, and also on an international level. Meanwhile, a common terminology is the base to strengthening and extending the science within this field across the countries' borders.

This study highlights the fact that SWFs are a highly significant flood process in Switzerland. Unlike for fluvial flood hazards, there is no publicly available information about the hazard of SWFs up to date, in spite of the process's obvious relevance. Since SWFs can occur practically anywhere in the landscape, the more paramount it seems to have detailed information about local SWF hazards. Such information can help to make well-founded decisions by all different stakeholders, e.g., planning and installing appropriate property protections by house owners, applying measures to reduce overland flow generation on agricultural fields by local farmers, providing surface retention ponds by municipalities or amend regulations to prevent SWF damage by the federal government. However, as a first priority, SWFs in general and the influencing factors of SWFs in particular should be further studied, and, ultimately, better understood.

As a first step in this direction, we propose that SWFs should not be regarded as an isolated process by itself. A better way is probably to extend our focus from rivers and lakes alone to hidden rivulets, covered drains, the sewer system, impervious areas, agricultural fields and headwaters, which all contribute to the generation of SWFs. Therefore, we should regard overland flow and ponding as an integrated part of our catchments. In this manner we may start to understand the complex interlinked flood processes better in the future.

Appendix

3.A Normalization

Obviously, it would be best to normalize the damage data with the corresponding property data of the respective insurance company. However, property data are generally even more difficult to obtain than damage data, as the former contain additional sensitive and confidential information. Therefore, ancillary data are required to estimate the number of insured buildings, as well as the replacement value of each corresponding building. Moreover, as these values change over time, we need additional ancillary data to take these temporal changes into account. As outlined in Sect. 3.3.3, the spatial normalization as well as the temporal normalization of the damage data are described in detail in the following sections.

After all, we divide the number of claims by the estimated number of insured buildings, while the losses are divided by the corresponding total sum insured, respectively. For that matter, all quantities have to be spatially aggregated. For this study, we aggregated the data to regular grids and visually compared the corresponding maps. Fine resolutions produced patchy patterns, while local characteristics got lost with coarse resolutions. Thus, we chose a resolution of 3-by-3 km, which constitutes a balanced compromise between level of detail and smoothing. The point of origin of the corresponding rasters is chosen arbitrarily. We acknowledge that the choice may change the absolute values of each cell, but in general does not change the larger picture.

3.A.1 Spatial normalization

As property data were not available, we inferred the number of buildings using ancillary data. For this purpose, we made use of the terrain model swissTLM3D (Table 3.2). From this data set, the number of buildings represented by their footprints can easily be extracted. However, the data needed to be preprocessed: Invalid geometries had to be corrected and overlapping polygons were dissolved into single polygons in order to obtain a homogeneous data set as of 2013.

The definitions of a building are quite similar among the PICB (Imhof, 2011). Nevertheless, the number of footprints does not match the number of insured buildings, since a row house might be represented by one footprint, while it constitutes several buildings as defined by the respective insurance company, for instance. To consider this, we referred to publicly available annual reports of 2013 and, thereby, obtained the total number of insured buildings for each PICB. We then divided the obtained values by the number of footprints, resulting in a simple multiplication factor (f_n, Table 3.5). By multiplying the aggregated number of buildings with the factor f_n, we obtain the approximated number of insured buildings as of 2013. For each grid cell, the aggregated number of claims is then divided by the aggregated number of buildings to obtain spatially normalized damage numbers.

To normalize the loss, we need to relate the loss values to the total sum insured. There are few published methodologies to assess building values in detail, but these can be too time-consuming for applications in large study areas (Kleist et al., 2006). Given the large data set, we chose a simple approach similar to the method shown by Grünthal et al. (2006), who used the product of mean insurance values and the number

Table 3.5: Factors used for the data normalization, i.e., the dimensionless multiplication factor (f_n) relating the number of building footprints to the number of buildings as defined by each PICB, as well as the estimated insurance value per cubic meter (ρ_v). For the derivation of these factors, the number of buildings and the total sum insured was required for each PICB. The corresponding values are generally published in the publicly available annual reports. Specifically, the values from the year 2013 were extracted for the PICB of the cantons of Aargau (AG), Basel-Landschaft (BL), Basel-Stadt (BS), Fribourg (FR), Grisons (GR), Jura (JU), Neuchâtel (NE), St Gall (SG), Solothurn (SO), Vaud (VD) and Zug (ZG). The values for the PICB of Glarus (GL) and Nidwalden (NW) were not reported, so that the mean value of 1.37 was adopted for the multiplication factor f_n and the total sum insured was inferred indirectly from the respective annual reports.

	AG	BL	BS	FR	GL	GR	JU	LU	NE	NW	SG	SO	VD	ZG
f_n (-)	1.34	1.56	3.92	1.30	1.37	1.46	1.18	1.27	1.28	1.37	1.25	1.33	1.33	1.28
ρ_v (CHF m^{-3})	720	734	1056	577	582	868	449	575	656	706	628	664	733	1'029

of buildings to estimate the replacement costs of residential buildings. However, instead of the buildings' footprint area, we considered the buildings' volume, which we expect to be a more representative measure for estimating building values.

Specifically, we first assessed the mean altitude of each building's footprint by using common zonal statistic functions of a GIS as well as a digital elevation model as input (Table 3.2). The top of each building was then assessed by the same method, but using a digital surface model, instead. The approximated building height resulted from the difference of the two values. Implausible results were corrected, i.e., values below 3.5 m or above 100 m were set to the standard building height of 3.5 m. Thus, a standard height of 3.5 m is assigned for buildings that might have been built after the last update of the DSM in 2008 (cf. Table 3.2). Following, the building volumes are obtained by multiplying the building's footprint area with the mean building height. The total building volume for each canton is assessed and divided by the respective total sum insured, in order to obtain the insurance value per cubic meter (ρ_v, Table 3.5). The product of each building's volume and ρ_v finally results in each building's value as of 2013. Analogous to the number of buildings, the loss is aggregated to regular grids and divided by the aggregated sum insured.

3.A.2 Temporal normalization

As the considered terrain model itself does not include attributes for such considerations, we used another auxiliary data set, i.e the buildings and dwellings statistic of the Swiss Federal Statistical Office as of 2013, from which the number of newly built residential buildings can be inferred (Table 3.2). The data are regularly updated, whereas the number of residential buildings can be assessed at any time by linear interpolation between the sampling points. Normalizing with the number of buildings per canton as of 2013 (Appendix 3.A.1), we obtain a dimensionless factor (f_t, Table 3.6). With the assumption that the residential buildings are representative for the development of all buildings, we obtain the temporal development of the number of buildings and the total sum insured. To that end, we multiply the interpolated factor f_t for each time step with the number of buildings and the total sum insured as per 2013, respectively.

Table 3.6: Multiplicative factor (f_t) indicating the number of buildings at a certain point in time in relation to the total number of buildings as of 2013. In this table, the factor's values at the sampling points of the source data are shown (cf. Table 3.2).

Year	AG	BL	BS	FR	GL	GR	JU	LU	NE	NW	SG	SO	VD	ZG
1980	0.58	0.63	0.91	0.53	0.78	0.66	0.70	0.56	0.74	0.61	0.65	0.63	0.67	0.55
1985	0.64	0.69	0.93	0.59	0.81	0.71	0.74	0.63	0.78	0.68	0.70	0.69	0.72	0.62
1990	0.72	0.76	0.94	0.67	0.86	0.79	0.80	0.70	0.84	0.75	0.77	0.76	0.79	0.70
1995	0.78	0.81	0.96	0.73	0.90	0.84	0.85	0.77	0.87	0.80	0.82	0.82	0.82	0.76
2000	0.85	0.88	0.97	0.80	0.94	0.89	0.89	0.84	0.91	0.86	0.88	0.88	0.86	0.84
2005	0.91	0.93	0.99	0.87	0.96	0.93	0.93	0.90	0.94	0.92	0.92	0.93	0.91	0.91
2010	0.97	0.98	1.00	0.95	0.99	0.97	0.98	0.96	0.98	0.97	0.97	0.97	0.97	0.97
2013	1.00	1.00	1.00	1.00	1.00	1.00	1.00	1.00	1.00	1.00	1.00	1.00	1.00	1.00

Acknowledgements

Funding from the Swiss Mobiliar supported the completion of this research. We thank the Swiss Mobiliar in general and the natural hazards group in particular for acquiring and compiling the flood hazard maps as well as providing claim records. Furthermore, we would like to thank the public insurance companies for buildings of the cantons Aargau, Basel-Landschaft, Basel-Stadt, Fribourg, Glarus, Grisons, Jura, Lucerne, Neuchâtel, Nidwalden, St Gall, Solothurn, Vaud and Zug for providing claim records and supporting us during the data harmonization process. Also, we would like to thank the Federal Office of Topography for providing the corresponding spatial data and the canton of Lucerne for providing the overland flow map. Last but not least, we thank Markus Mosimann for his support harmonizing the insurance data, Veronika Röthlisberger for the joint effort to collect and harmonize the insurance data in the first place, in addition to her support for the estimation of the buildings' values and, generally, we thank her and Andreas Zischg for the many valuable inputs.

References

Aller, D., & Petrascheck, A. (2008). Schadensentwicklung im Kanton Aargau. In G. R. Bezzola, & C. Hegg (Eds.), *Ereignisanalyse Hochwasser 2005, Teil 2 — Analyse von Prozessen, Massnahmen und Gefahrengrundlagen* Umwelt-Wissen Nr. 0825 (pp. 82–92). Bern, Schweiz: Bundesamt für Umwelt and Eidgenössische Forschungsanstalt für Wald Schnee und Landschaft.

Andrieu, H., Browne, O., & Laplace, D. (2004). Les crues en zone urbaine: des crues éclairs? *La Houille Blanche*, (pp. 89–95). doi:10.1051/lhb:200402010.

Barredo, J. I. (2009). Normalised flood losses in Europe: 1970–2006. *Nat. Hazard Earth Sys.*, *9*, 97–104. doi:10.5194/nhess-9-97-2009.

Bernet, D. B., Weingartner, R., & Prasuhn, V. (2016). Exploiting damage claim records of public insurance companies for buildings to increase knowledge about the occurrence of overland flow in Switzerland. In G. Koboltschnig (Ed.), *INTERPRAEVENT 2016 — Conference Proceedings* (pp. 221–230). International Research Society INTERPRAEVENT.

Blanc, J., Hall, J. W., Roche, N., Dawson, R. J., Cesses, Y., Burton, A., & Kilsby, C. G. (2012). Enhanced efficiency of pluvial flood risk estimation in urban areas using spatial-temporal rainfall simulations. *J. Flood Risk Manage.*, *5*, 143–152. doi:10.1111/j.1753-318X.2012.01135.x.

Boardman, J. (2010). A short history of muddy floods. *Land Degrad. Dev.*, *21*, 303–309. doi:10.1002/ldr.1007.

Bouwer, L. M. (2011). Have disaster losses increased due to anthropogenic climate change? *B. Am. Meteorol. Soc.*, *92*, 39–46. doi:10.1175/2010BAMS3092.1.

Brutsaert, W. (2005). *Hydrology: An introduction*. Cambridge, UK and New York, USA: Cambridge University Press.

van Campenhout, J., Hallot, E., Houbrechts, G., Peeters, A., Levecq, Y., Gérard, P., & Petit, F. (2015). Flash floods and muddy floods in Wallonia: recent temporal trends, spatial distribution and reconstruction of the hydrosedimentological fluxes using flood marks and sediment deposits. *Belgeo*, (pp. 1–22). doi:10.4000/belgeo.16409.

Castro, D., Einfalt, T., Frerichs, S., Friedeheim, K., Hatzfeld, F., Kubik, A., Mittelstädt, R., Müller, M., Seltmann, J., & Wagner, A. (2008). *Vorhersage und Management von Sturzfluten in urbanen Gebieten (URBAS): Schlussbericht des vom Bundesministerium für Bildung und Forschung geförderten Vorhabens*. Aachen, Deutschland: Hydrotec GmbH and Fachhochschule Aachen and Deutscher Wetterdienst. URL: http://www.urbanesturzfluten.de.

CEPRI (2014). *Gérer les inondations par ruissellement pluvial — Guide de sensibilisation*. Orléans, France: Centre Européen de Prévention du Risque d'Inondation. URL: http://www.cepri.net/Ruissellement_pluvial.html.

Cheng, C. S., Li, Q., Li, G., & Auld, H. (2012). Climate change and heavy rainfall-related water damage insurance claims and losses in Ontario, Canada. *J. Water Resource Prot.*, *4*, 49–62. doi:10.4236/jwarp.2012.42007.

Chow, V. T., Maidment, D. R., & Mays, L. W. (1988). *Applied hydrology*. McGraw-Hill series in water resources and environmental engineering. New York, USA: McGraw-Hill.

Coulthard, T. J., & Frostick, L. E. (2010). The Hull floods of 2007: implications for the governance and management of urban drainage systems. *J. Flood Risk Manage.*, *3*, 223–231. doi:10.1111/j.1753-318X.2010.01072.x.

Cutter, S. L., & Emrich, C. (2005). Are natural hazards and disaster losses in the U.S. increasing? *Eos Trans. AGU*, *86*, 381–389. doi:10.1029/2005EO410001.

Davy, L. (1990). La catastrophe nîmoise du 3 Octobre 1988: était-elle previsible? *Bull. Soc. Languedoc. Geogr.*, *24*, 133–162.

Douglas, I., Garvin, S., Lawson, N., Richards, J., Tippett, J., & White, I. (2010). Urban pluvial flooding: a qualitative case study of cause, effect and nonstructural mitigation. *J. Flood Risk Manage.*, *3*, 112–125. doi:10.1111/j.1753-318X.2010.01061.x.

Douguédroit, A. (2008). Précipitations extrêmes et « crues urbaines » à Marseille (France) de 1861 à 2007. *Bulletin de la Société géographique de Liège*, *51*, 105–114.

DWA (2013). *Starkregen und urbane Sturzfluten — Praxisleitfaden zur Überflutungsvorsorge* volume T1/2013 of *DWA-Themen*. Hennef, Deutschland: Deutsche Vereinigung für Wasserwirtschaft, Abwasser und Abfall (DWA).

Egli, T. (2007). *Wegleitung Objektschutz gegen meteorologische Naturgefahren*. Bern, Schweiz: Vereinigung Kantonaler Feuerversicherungen. URL: http://vkf.ch/VKF/Downloads.

Elmer, F., Thieken, A. H., Pech, I., & Kreibich, H. (2010). Influence of flood frequency on residential building losses. *Nat. Hazard Earth Sys.*, *10*, 2145–2159. doi:10.5194/nhess-10-2145-2010.

Evans, E., Ashley, R., Hall, J., Penning-Roswell, E., Saul, A., Sayers, P., Thorne, C., & Watkinson, A. (2004). *Foresight: future flooding scientific summary: volume 1 — future risks and their drivers*. London, UK: Office of Science and Technology. URL: https://www.gov.uk/government/publications/future-flooding.

Evrard, O., Bielders, C. L., Vandaele, K., & van Wesemael, B. (2007). Spatial and temporal variation of muddy floods in central Belgium, off-site impacts and potential control measures. *Catena*, *70*, 443–454. doi:10.1016/j.catena.2006.11.011.

Falconer, R. H., Cobby, D., Smyth, P., Astle, G., Dent, J., & Golding, B. (2009). Pluvial flooding: new approaches in flood warning, mapping and risk management. *J. Flood Risk Manage.*, *2*, 198–208. doi:10.1111/j.1753-318X.2009.01034.x.

Field, C. B., Barros, V., Stocker, T. F., Quin, D., Dokken, D. J., Ebi, K. L., Mastrandrea, M. D., Mach, K. J., Plattner, G.-K., & Allen, S. K. (Eds.) (2012). *Managing the risks of extreme events and disasters to advance climate change adaption: A special report of working groups I and II of the Intergovernmental Panel on Climate Change*. Cambridge, UK and New York, USA: Cambridge University Press.

Fiener, P., Auerswald, K., Winter, F., & Disse, M. (2013). Statistical analysis and modelling of surface runoff from arable fields in central Europe. *Hydrol. Earth Syst. Sc.*, *17*, 4121–4132. doi:10.5194/hess-17-4121-2013.

Gaitan, S., van de Giesen, N. C., & ten Veldhuis, J. A. E. (2016). Can urban pluvial flooding be predicted by open spatial data and weather data? *Environ. Modell. Softw.*, *85*, 156–171. doi:10.1016/j.envsoft.2016.08.007.

Gall, M., Borden, K. A., & Cutter, S. L. (2009). When do losses count? Six fallacies of natural hazards loss data. *B. Am. Meteorol. Soc.*, *90*, 799–809. doi:10.1175/2008BAMS2721.1.

Gaume, E., Bain, V., Bernardara, P., Newinger, O., Barbuc, M., Bateman, A., Blaškovičová, L., Blöschl, G., Borga, M., Dumitrescu, A., Daliakopoulos, I., Garcia, J., Irimescu, A., Kohnova, S., Koutroulis, A., Marchi, L., Matreata, S., Medina, V., Preciso, E., Sempere-Torres, D., Stancalie, G., Szolgay, J., Tsanis, I., Velasco, D., & Viglione, A. (2009). A compilation of data on European flash floods. *J. Hydrol.*, *367*, 70–78. doi:10.1016/j.jhydrol.2008.12.028.

Gourley, J. J., Hong, Y., Flamig, Z. L., Arthur, A., Clark, R., Calianno, M., Ruin, I., Ortel, T., Wieczorek, M. E., Kirstetter, P.-E., Clark, E., & Krajewski, W. F. (2013). A unified flash flood database across the United States. *B. Am. Meteorol. Soc.*, *94*, 799–805. doi:10.1175/BAMS-D-12-00198.1.

Grahn, T., & Nyberg, L. (2017). Assessment of pluvial flood exposure and vulnerability of residential areas. *Int. J. Disaster Risk Reduct.*, *21*, 367–375. doi:10.1016/j.ijdrr.2017.01.016.

Grosjean, G. (1975). *Die Schweiz: Der Naturraum in seiner Funktion für Kultur und Wirtschaft* volume U1 of *Geographica Bernensia*. Bern, Schweiz: Arbeitsgemeinschaft Geographica Bernensia.

Grünewald, U. (2009). Erkenntnisse und Konsequenzen aus dem Sturzflutereignis in Dortmund im Juli 2008. *KW — Korrespondenz Wasserwirtschaft*, *8*, 422–428. doi:10.3243/kwe2009.08.003.

Grünthal, G., Thieken, A. H., Schwarz, J., Radtke, K. S., Smolka, A., & Merz, B. (2006). Comparative risk assessments for the city of Cologne — storms, floods, earthquakes. *Nat. Hazards*, *38*, 21–44. doi:10.1007/s11069-005-8598-0.

Haghighatafshar, S., la Cour Jansen, Jes, Aspegren, H., Lidström, V., Mattsson, A., & Jönsson, K. (2014). Storm-water management in Malmö and Copenhagen with regard to climate change scenarios. *Vatten*, *70*, 159–168.

Hankin, B., Waller, S., Astle, G., & Kellagher, R. (2008). Mapping space for water: screening for urban flash flooding. *J. Flood Risk Manage.*, *1*, 13–22. doi:10.1111/j.1753-318X.2008.00003.x.

Hilker, N., Badoux, A., & Hegg, C. (2008). Unwetterschäden in der Schweiz im Jahre 2007. *Wasser Energie Luft*, *100*, 115–123.

Hilker, N., Badoux, A., & Hegg, C. (2009). The Swiss flood and landslide damage database 1972–2007. *Nat. Hazard Earth Sys.*, *9*, 913–925. doi:10.5194/nhess-9-913-2009.

Hirsch, R. M., Slack, J. R., & Smith, R. A. (1982). Techniques of trend analysis for monthly water quality data. *Water Resour. Res.*, *18*, 107–121. doi:10.1029/WR018i001p00107.

Hurford, A. P., Parker, D. J., Priest, S. J., & Lumbroso, D. M. (2012). Validating the return period of rainfall thresholds used for Extreme Rainfall Alerts by linking rainfall intensities with observed surface water flood events. *J. Flood Risk Manage.*, *5*, 134–142. doi:10.1111/j.1753-318X.2012.01133.x.

Imhof, M. (2011). *Analyse langfristiger Gebäudeschadendaten: Auswertung des Datenbestandes der Schadenstatistik VKF*. Bern, Schweiz: Interkantonaler Rückversicherungsverband. URL: http://irv.ch/IRV/Download.

Kipfer, A., Kienholz, C., & Liener, S. (2012). Ein neuer Ansatz zur Modellierung von Oberflächenabfluss. In G. Koboltschnig, J. Hübl, & J. Braun (Eds.), *INTERPRAEVENT 2012 — Conference Proceedings* (pp. 179–189). International Research Society INTERPRAEVENT.

Kleist, L., Thieken, A. H., Köhler, P., Müller, M., Seifert, I., Borst, D., & Werner, U. (2006). Estimation of the regional stock of residential buildings as a basis for a comparative risk assessment in Germany. *Nat. Hazard Earth Sys.*, *6*, 541–552. doi:10.5194/nhess-6-541-2006.

Kreibich, H., Piroth, K., Seifert, I., Maiwald, H., Kunert, U., Schwarz, J., Merz, B., & Thieken, A. H. (2009). Is flow velocity a significant parameter in flood damage modelling? *Nat. Hazard Earth Sys.*, *9*, 1679–1692. doi:10.5194/nhess-9-1679-2009.

Kron, W. (2009). Überschwemmungsüberraschung: Sturzfluten und Überschwemmungen fernab von Gewässern. *Wasserwirtschaft*, *6*, 15–20.

Kron, W., Steuer, M., Löw, P., & Wirtz, A. (2012). How to deal properly with a natural catastrophe database — analysis of flood losses. *Nat. Hazard Earth Sys.*, *12*, 535–550. doi:10.5194/nhess-12-535-2012.

Kundzewicz, Z. W., Kanae, S., Seneviratne, S. I., Handmer, J., Nicholls, N., Peduzzi, P., Mechler, R., Bouwer, L. M., Arnell, N., Mach, K., Muir-Wood, R., Brakenridge, G. R., Kron, W., Benito, G., Honda, Y., Takahashi, K., & Sherstyukov, B. (2014). Flood risk and climate change: global and regional perspectives. *Hydrolog. Sci. J.*, *59*, 1–28. doi:10.1080/02626667.2013.857411.

Ledermann, T., Herweg, K., Liniger, H., Schneider, F., Hurni, H., & Prasuhn, V. (2010). Applying erosion damage mapping to assess and quantify off-site effects of soil erosion in Switzerland. *Land Degrad. Dev.*, *21*, 353–366. doi:10.1002/ldr.1008.

LUBW (2016). *Leitfaden kommunales Starkregenrisikomanagement in Baden-Württemberg*. Karlsruhe, Deutschland: Landesanstalt für Umwelt, Messungen und Naturschut Baden-Württemberg (LUBW). URL: http://www.lubw.baden-wuerttemberg.de/servlet/is/261161.

Merz, B., Kreibich, H., & Lall, U. (2013). Multi-variate flood damage assessment: a tree-based data-mining approach. *Nat. Hazard Earth Sys.*, *13*, 53–64. doi:10.5194/nhess-13-53-2013.

Merz, B., Kreibich, H., Schwarze, R., & Thieken, A. (2010). Review article — "Assessment of economic flood damage". *Nat. Hazard Earth Sys.*, *10*, 1697–1724. doi:10.5194/nhess-10-1697-2010.

Merz, R., & Blöschl, G. (2003). A process typology of regional floods. *Water Resour. Res.*, *39*. doi:10.1029/2002WR001952.

de Moel, H., van Alphen, J., & Aerts, J. C. J. H. (2009). Flood maps in Europe — methods, availability and use. *Nat. Hazard Earth Sys.*, *9*, 289–301. doi:10.5194/nhess-9-289-2009.

Moncoulon, D., Labat, D., Ardon, J., Leblois, E., Onfroy, T., Poulard, C., Aji, S., Rémy, A., & Quantin, A. (2014). Analysis of the French insurance market exposure to floods: a stochastic model combining river overflow and surface runoff. *Nat. Hazard Earth Sys.*, *14*, 2469–2485. doi:10.5194/nhess-14-2469-2014.

Pitt, M. (2008). *The Pitt Review: Learning lessons from the 2007 floods: An independent review by Sir Michael Pitt*. London, UK: Cabinet Office.

Priest, S. J., Parker, D. J., Hurford, A. P., Walker, J., & Evans, K. (2011). Assessing options for the development of surface water flood warning in England and Wales. *J. Environ. Manage.*, *92*, 3038–3048. doi:10.1016/j.jenvman.2011.06.041.

Romang, H., Frick, E., & Krummenacher, B. (2004). Unwetterereignisse im November 2002, Graubünden, Schweiz. In L. Stepanek, B. Kohl, & G. Markart (Eds.), *INTERPRAEVENT 2004 — Conference Proceedings* (pp. 109–120). International Research Society INTERPRAEVENT volume 1.

Ruiz-Villanueva, V., Borga, M., Zoccatelli, D., Marchi, L., Gaume, E., & Ehret, U. (2012). Extreme flood response to short-duration convective rainfall in South-West Germany. *Hydrol. Earth Syst. Sc.*, *16*, 1543–1559. doi:10.5194/hess-16-1543-2012.

Scherrer, S., Frauchiger, R., & Näf-Huber, D. (2013). *Analyse und Einordnung des Hochwassers vom 2. Mai 2013 in Schaffhausen und der Umgebung: Schwerpunkt Freudentalbach, Durach und Dorfbach Herblingen*. 13/174. Reinach, Schweiz: Scherrer AG, Hydrologie und Hochwasserschutz.

Schwarze, R., Schwindt, M., Weck-Hannemann, H., Raschky, P., Zahn, F., & Wagner, G. G. (2011). Natural hazard insurance in Europe: Tailored responses to climate change are needed. *Env. Pol. Gov.*, *21*, 14–30. doi:10.1002/eet.554.

Spekkers, M., Rözer, V., Thieken, A., ten Veldhuis, M.-c., & Kreibich, H. (2017). A comparative survey of the impacts of extreme rainfall in two international case studies. *Nat. Hazard Earth Sys.*, *17*, 1337–1355. doi:10.5194/nhess-17-1337-2017.

Spekkers, M. H., Clemens, F. H. L. R., & ten Veldhuis, J. A. E. (2015). On the occurrence of rainstorm damage based on home insurance and weather data. *Nat. Hazard Earth Sys.*, *15*, 261–272. doi:10.5194/nhess-15-261-2015.

Spekkers, M. H., Kok, M., Clemens, F. H. L. R., & ten Veldhuis, J. A. E. (2013). A statistical analysis of insurance damage claims related to rainfall extremes. *Hydrol. Earth Syst. Sc.*, *17*, 913–922. doi:10.5194/hess-17-913-2013.

Spekkers, M. H., Kok, M., Clemens, F. H. L. R., & ten Veldhuis, J. A. E. (2014). Decision-tree analysis of factors influencing rainfall-related building structure and content damage. *Nat. Hazard Earth Sys.*, *14*, 2531–2547. doi:10.5194/nhess-14-2531-2014.

Steinbrich, A., Leistert, H., & Weiler, M. (2016). Model-based quantification of runoff generation processes at high spatial and temporal resolution. *Environ. Earth Sci.*, *75*, 1423. doi:10.1007/s12665-016-6234-9.

Thieken, A. H., Kreibich, H., Müller, M., & Merz, B. (2007). Coping with floods: preparedness, response and recovery of flood-affected residents in Germany in 2002. *Hydrolog. Sci. J.*, *52*, 1016–1037. doi:10.1623/hysj.52.5.1016.

Uhlemann, S., Bertelmann, R., & Merz, B. (2013). Data expansion: the potential of grey literature for understanding floods. *Hydrol. Earth Syst. Sc.*, *17*, 895–911. doi:10.5194/hess-17-895-2013.

Ward, R. C., & Robinson, M. (2000). *Principles of hydrology*. (4th ed.). London, UK: McGraw-Hill.

Zhou, Q., Panduro, T. E., Thorsen, B. J., & Arnbjerg-Nielsen, K. (2013). Verification of flood damage modelling using insurance data. *Water Sci. Technol.*, *68*, 425–432. doi:10.2166/wst.2013.268.

Zimmermann, M., Pozzi, A., & Stoessel, F. (2005). *Vademecum — Hazard maps and related Instruments: The Swiss system and its application abroad*. Bern, Switzerland: National Platform for Natural Hazards. URL: http://www.planat.ch/fileadmin/PLANAT/planat_pdf/alle_2012/2001-2005/PLANAT_2005_-_Vademecum.pdf.

Part II

Modeling surface water floods

4 Modeling surface water floods in rural areas: lessons learned from the application of various uncalibrated models

Daniel B. Bernet[1], Andreas Zischg[1], Volker Prasuhn[2] and Rolf Weingartner[1]

[1] *Institute of Geography and Oeschger Centre for Climate Change Research and Mobiliar Lab for Natural Risks, University of Bern, Hallerstrasse 12, 3012 Bern, Switzerland*
[2] *Agroscope, Research Division, Agroecology and Environment, Reckenholzstrasse 191, 8046 Zurich, Switzerland*

Submitted to Environmental Modelling and Software

Abstract

Surface water floods (SWFs) do not only increasingly threaten cities, but also affect rural areas. So far, little research has been dedicated to the prediction of SWFs in rural environments, although in practice the process is already being considered in deterministic flood hazard assessments. To test the validity of such assessments, we select four raster-based models with differing complexity and evaluate whether they reliably predict inundated areas by SWF in rural areas. The uncalibrated models are first applied to four artificial surfaces and second, to eight case studies covering manifold geographical and meteorological settings. For the case studies, the models' prediction skills are assessed based on inundated areas inferred from various sources. The models' performance is rather low for all case studies, which highlights the necessity for calibration and/or validation of such models. Moreover, the case studies provide more general conclusions concerning the modeling of SWFs in rural areas.

Software availability

- FLO-2D (cf. Sect. 4.2.1.1)
  - Details: FLO-2D Pro (Build No. 16.06.16)
  - Developers: FLO-2D Software Inc. (P.O. Box 66, Nutrioso, AZ 85932, United States)
  - Requirements: Windows 7 or higher
  - Cost: $995.00
  - URL: `https://www.flo-2d.com/flo-2d-pro/`
- FloodArea (cf. Sect. 4.2.1.2)

  - Details: FloodArea^{HPC}-Desktop 10.3 (4 Cores) on ArcGIS®10.3.0.4322
  - Developers: geomer GmbH (Im Breitspiel 11 b, 69126 Heidelberg, Germany)
  - Requirements: Windows 7 or higher and ArcGIS®10.3
  - Cost: €11'845.00
  - URL: `http://www.geomer.de/en/software/floodarea`

- r.sim.water (cf. Sect. 4.2.1.3)
  - Details: Module r.sim.water in GRASS GIS 7.2.0 (2016)
  - Developers: H. Mitasova, J. Hofierka, C. Thaxton (and GRASS Development Team)
  - Requirements: Windows, Linux or Mac OSX
  - Cost: Free of charge (GNU General Public Licence)
  - URL: `https://grass.osgeo.org/grass72/manuals/r.sim.water.html`

- MFD (cf. Sect. 4.2.1.4)
  - Details: Tool Flow Accumulation (Top-Down) with option "Multiple Flow Direction" in SAGA GIS 4.1.0 (64-bit)
  - Developers: O. Conrad and T. Grabs
  - Requirements: Windows or Linux
  - Cost: Free of charge (GNU General Public Licence)
  - URL: `http://www.saga-gis.org/saga_tool_doc/4.1.0/ta_hydrology_0.html`

4.1 Introduction

Economic losses caused by floods have been heavily increasing over the past decades in absolute terms (Thieken et al., 2007; Kron et al., 2012; Grahn & Nyberg, 2017), mostly driven by societal development (e.g., Cutter & Emrich, 2005), but possibly exacerbated by climate change (Falconer et al., 2009; Barredo, 2009; Kundzewicz et al., 2014). In particular, the frequency and the intensity of heavy rainfall is expected to increase in many places in the future (Kundzewicz et al., 2014). This has drawn growing attention to surface water floods (SWFs), which are caused by intense rainfall that cannot be drained altogether by means of natural and/or artificial drainage systems, stem from surcharged sewers, channels, culverted watercourses or groundwater springs and, consequently, result in ponded water and overland flow (Hankin et al., 2008; Falconer et al., 2009). With a particular high percentage of impermeable areas, cities are particularly prone to SWFs, as exemplified by recent devastating flood events affecting urbanized areas, such as Hull, UK (Pitt, 2008; Coulthard & Frostick, 2010), Copenhangen, DK (Haghighatafshar et al., 2014), Amsterdam, NL (Gaitan et al., 2016; Spekkers et al., 2017) or Münster, DE (Spekkers et al., 2017).

Not surprisingly, a lot of research is dedicated to urban areas in terms of modeling SWFs (e.g., Maksivomić et al., 2009; Chen et al., 2012; Sampson et al., 2013; de Almeida et al., 2016), flood loss estimation (e.g., Merz et al., 2010; Jongman et al., 2012; van Ootegem et al., 2015) as well as flood risk assessment and management (e.g., Kaźmierczak & Cavan, 2011; Blanc et al., 2012; Zhou et al., 2012; Löwe et al., 2017). In contrast, relatively little research has been dedicated to rural areas, in spite the fact that such areas are highly exposed to flooding, as examples from the European Alps point out

(Fuchs et al., 2015, 2017; Röthlisberger et al., 2017). At the same time, these areas are not only affected by fluvial floods, but similarly by SWFs (Bernet et al., 2017). Moreover, overland flow generated on rural or peri-urban areas may be transferred into urbanized areas and thereby contribute to the adverse effects of SWFs within the urban environment, as well (Andrieu et al., 2004; Yu & Coulthard, 2015). Thus, scientific studies regarding the link between SWFs and rural areas are generally lacking.

In contrast, the topic of how to prepare for and manage SWFs has been discussed outside of academia (Bernet et al., 2017). This has led to a wide range of manuals and guidelines regarding SWF hazard assessment, risk management and awareness raising at the point scale (e.g., Egli, 2007; Rüttimann & Egli, 2010), as well as on communal and regional scales (e.g., Castro et al., 2008; DWA, 2013; LUBW, 2016; CEPRI, 2014). Therein, the focus lies generally on the built environment and, thus, the rural areas are considered, as well.

In practice, the tools used for SWF hazard assessments, consist mainly of single deterministic simulations with two-dimensional (2D) flood inundation models (cf. Meon et al., 2009; Tyrna & Hochschild, 2010; Kipfer et al., 2015; Tyrna et al., 2017). This circumstance has certainly been influenced by the heavily increasing availability of high-resolution digital elevation models (DEMs), driven by advancing data collection techniques (Wechsler, 2007; Fewtrell et al., 2008; Sampson et al., 2012; Chen et al., 2012; Neal et al., 2012; Dottori et al., 2013; de Almeida et al., 2016; Savage et al., 2016a). At the same time, the applicability of hydrodynamic flood inundation models to finer resolutions has been supported by increasing computational power (Fewtrell et al., 2008; Hunter et al., 2008; Dottori et al., 2013; Savage et al., 2016b). However, the exploitation of high-resolution DEMs is still limited by computational constraints (Chen et al., 2012; Sampson et al., 2012; de Almeida et al., 2016; Savage et al., 2016a,b; Tyrna et al., 2017). Thus, rather simple flood inundation models are applied in practice for SWF hazard assessments, as they usually encompass large areas.

In general, a compromise is inevitable when applying a model, balancing spatial resolution, model complexity and computational efficiency (Horritt & Bates, 2001; Cook & Merwade, 2009; Fewtrell et al., 2008, 2011; Sampson et al., 2012; Neal et al., 2012; Dottori et al., 2013; Savage et al., 2016a,b). At the same time, it is not obvious how the specific choice influences the models' performance. Moreover, recent studies have pointed out that the uncertainty associated with flood inundation models fed with high-resolution DEMs are more complex than previously thought (Abily et al., 2016; Savage et al., 2016b). Meanwhile, the models' extreme precisions may provoke overconfidence in their results, which could ultimately lead to wrong decisions in flood risk management (Dottori et al., 2013; Savage et al., 2016a).

Wrong decisions can usually be prevented by rigorously evaluate the applied models (e.g., Jakeman et al., 2006; Bennett et al., 2013). However, appropriate data are crucial for this task. Yet, there is an eminent lack of observational data (Blanc et al., 2012; Neal et al., 2012; Spekkers et al., 2014; Yu & Coulthard, 2015; Gaitan et al., 2016; Rözer et al., 2016), which impairs the applicability of such deterministic modeling approaches. Even more so for SWFs in rural areas, where the lack of observational data is particularly pronounced (Yu & Coulthard, 2015). In practice, however, the lack of observational data does not appear to prevent the use of single deterministic simulations for SWF hazard assessments. On the contrary, examples of overland flow predictions in urban, peri-urban and rural areas indicate that it rather leads to the renouncement of model

calibration and/or validation (cf. Meon et al., 2009; Tyrna & Hochschild, 2010; Kipfer et al., 2015; Tyrna et al., 2017).

Thus, the question arises whether the deterministic tools reportedly used today in SWF hazard assessments are fit for their purpose of reliably predict areas exposed to SWF under various conditions. In particular, it is unclear how well such a modeling approach performs if such tools are not conditioned and/or evaluated due to a lack of observational data. Using this starting point, the main goal of this study is to assess the applicability of uncalibrated and unvalidated 2D models to SWF hazard assessments in rural environments. Thus, we want to assess the predictive skills of such models for various case studies at different study sites. By doing so, we are able to draw conclusions about the suitability of this modeling approach based on single deterministic simulations for SWF hazard assessments and about modeling SWFs in rural areas, in general.

For that matter, we directly explore the models' predictive skills by comparing their outputs (Teng et al., 2017). In a first step, we apply the selected models to four artificial surfaces, inspired by Zhou & Liu (2002). In this highly controlled and simplified environment, the models can easily be compared and inherent model characteristics are revealed. In a second step, the models are applied to real-world case studies. To mimic the commonly used approach in practical SWF hazard assessments, we apply similar uncalibrated 2D models with varying complexity. Thereafter, we quantitatively assess the models' predictive skills using common binary pattern performance measures (Bennett et al., 2013). For this assessment, we have reconstructed inundated areas based on various available data sources.

The seven study sites encompass various topographies, slopes, land use etc., while each of the eight case studies is associated with either relatively heavy or weak rainfall, respectively. Thus, for the purpose of this study, we relax the definition of SWFs and include not only events triggered by heavy rainfall, bot also events associated with weak rainfall. All events have in common that overland flow was produced, which led or could have led to damages to the built and unbuilt environment along the flow paths. As per definition, the inundations did not originate from overtopping watercourses, but are directly triggered by effective rainfall (cf. Bernet et al., 2017, for a discussion of related terms).

4.2 Materials and methods

4.2.1 Models

In this study, we test three raster-based, 2D hydrodynamic flood inundation models, i.e., FLO-2D, FloodArea and r.sim.water. The models have been selected such that different levels of model complexity are covered, following Neal et al. (2012). From the wealth of available 2D hydrodynamic models (cf. Teng et al., 2017), we chose FloodArea and r.sim.water since they have reportedly been used in the field of flood hazard assessment covering large areas including rural environments (cf. Kipfer et al., 2015; Tyrna et al., 2017). FLO-2D was selected as it is a "hydro-inundation model", using a term from Yu & Coulthard (2015) describing models that consider hydrological processes and overland flow routing, at the same time. Moreover, it has the most complex flow routing scheme among the selected models. Finally, the model selection was complemented by a flow accumulation algorithm, i.e., the multiple flow direction (MFD) algorithm introduced by

Table 4.1: Model feature comparison. "Yes" indicates features or modules that can be directly assessed by the respective model, "no" highlights unavailable features, while "NA" describes features that are not applicable, i.e., the rainfall-related features for the flow accumulation algorithm MFD.

Feature, modules	FLO-2D	FloodArea	r.sim.water	MFD
Flow depth	yes	yes	yes	no
Flow velocity	yes	yes	no	no
Flow barrier	yes	yes	no	no
Unsteady rain	yes	yes	no	NA
Interception	yes	no	no	NA
Infiltration	yes	no	no	NA

Freeman (1991). Such flow algorithms have manifold applications due to their striking simplicity (cf. López-Vicente et al., 2014; Alder et al., 2015). An overview of the models' features is provided by Table 4.1.

4.2.1.1 FLO-2D

FLO-2D is a distributed, physically based flood inundation model (O'Brian, 2009). Among the selected models, it is the most sophisticated one, as it makes use of the full dynamic wave approximation (O'Brian, 2009). FLO-2D has various modules which can be switched on or off, if desired. It incorporates an infiltration module with various available methods, whereas the Green-Ampt (GA) method based on Green & Ampt (1911) is the most sophisticated one.

4.2.1.2 FloodArea

FloodArea is a simplified hydrodynamic flood inundation model that is fully integrated into a Geographic Information System (GIS), i.e., ArcGIS®by ESRI, with the main purpose of calculating areas affected by floods (geomer, 2016). The model cannot directly account for losses such as interception and infiltration. Thus, these losses have to considered by reducing the corresponding rainfall input (cf. Table 4.1 and Sect. 4.2.3.5).

4.2.1.3 r.sim.water

The hydrodynamic model r.sim.water simulates overland flow with a path sampling method, which is implemented as a module in the open source GIS software GRASS (Mitasova et al., 2004; Neteler et al., 2012). Similar to FloodArea, r.sim.water cannot directly account for losses such as interception and infiltration. Moreover, unsteady rainfall cannot be modeled (cf. Table 4.1 and Sect. 4.2.3.5).

4.2.1.4 MFD

MFD is a multiple flow direction algorithm that assesses the flow paths based solely on a digital elevation model (DEM) (Quinn et al., 1991). We use the algorithm implemented in the open source System for Automated Geoscientific Analyses (SAGA) (Conrad et al., 2015). Among the selected models, MFD is the simplest approach that does not route any water, but instead assesses each cell's relative catchment area. Consequently, the model does not predict any flow depths and velocities (cf. Table 4.1), but assesses a static

characteristic of the topography, i.e., the distributed flow accumulation areas. Note that prior to applying MFD to real-world case studies, sinks and pits of the respective DEM were filled, as discussed by Wechsler (2007). For that matter, we used the algorithm by Planchon & Darboux (2002) with a value of 0.01° for the minimal slope.

4.2.2 Artificial surfaces

To assess the performance of flow routing algorithms, Zhou & Liu (2002) defined four different mathematical surfaces and compared the calculated specific catchment area with the theoretically true values. The application of such algorithms on smooth artificial surfaces reveals distinct patterns and characteristics reflecting the algorithm's differing mathematical formulations (cf. Zhou & Liu, 2002; Seibert & McGlynn, 2007; Pilesjö & Hasan, 2014). We adapt this approach to flood inundation modeling. Even without a theoretically true value, the adaptation of this approach to SWF modeling reveals inherent model characteristics that might not be apparent otherwise. Therefore, as a first exercise, we apply the selected models to four artificial surfaces, i.e., to an inclined plane (Eq. 4.1), a convex surface defined by an ellipsoid (Eq. 4.2), a concave surface given by the ellipsoid's inverse (Eq. 4.3) and a saddle (Eq. 4.4) representing the combination of a convex and a concave surface. We compiled corresponding raster DEMs of 250-by-250 cells and a resolution of 2 m. The elevations of the plane are given by

$$z = ax + by + c \tag{4.1}$$

where $a \approx -0.051$, $b \approx 0.141$, $c = 0$ for a prescribed slope of $s = 15$ % and an aspect of $a = 160°$; $0 \leq x \leq 250$, $0 \leq y \leq 250$. The ellipsoid is defined as

$$\frac{x^2}{a} + \frac{y^2}{b} + \frac{z^2}{c} = 1 \quad z > 0 \tag{4.2}$$

where $a = 998$, $b = -748.5$, $c \approx 191.5$; $0 \leq x \leq 250$, $-250 \leq y \leq 0$. The inverse ellipsoid is given by

$$\frac{x^2}{a} + \frac{y^2}{b} + \frac{z^2}{c} = 1 \quad z < 0 \tag{4.3}$$

where $a = 998$, $b = -748.5$, $c \approx 191.5$; $-250 \leq x \leq 0$ and $0 \leq y \leq 250$. Finally, the saddle is defined as

$$\frac{x^2}{a} + \frac{y^2}{b} = \frac{z}{c} \quad z < 0 \tag{4.4}$$

where $a = 998$, $b = -748.5$, $c \approx 191.5$; $-250 \leq x \leq 0$ and $-250 \leq y \leq 0$.

The artificial surfaces are further manipulated. Two rows of the corresponding DEMs are incised by a minimum of 0.3 m, in order to represents a 4 m wide street crossing the surfaces from West to East. This incision enables to test and visualize the influence of structures in the landscape that can have major effects on overland flow paths. The top views of the four artificial surfaces are shown in Fig. 4.1.

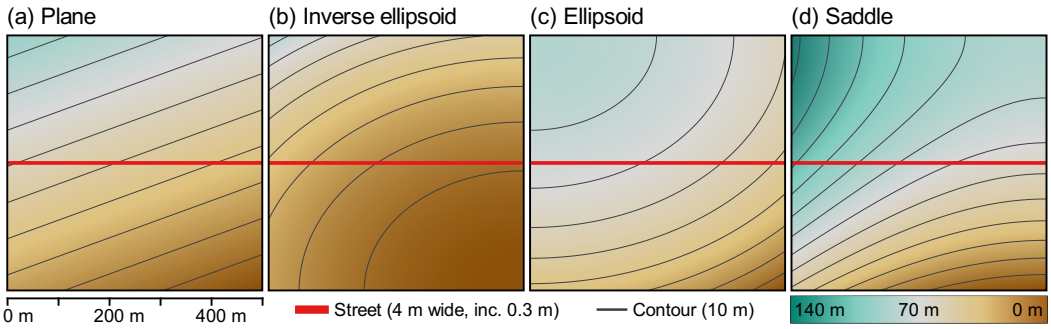

Fig. 4.1: A parallel (a), a concave (b), a convex (c) and a combination of a convex and concave (d) artificial surface used for an initial model test.

For the artificial surfaces, a rain event lasting one hour with an intensity of 50 mmh^{-1} was simulated. Infiltration and interception losses were not considered. A Manning's roughness coefficient of $n = 0.24\ \mathrm{sm}^{-1/3}$ was chosen for all artificial surfaces, which corresponds to the value recommended for dense grass by McCuen (2016). A value of $n = 0.012\ \mathrm{sm}^{-1/3}$ is chosen for the incised streets, which corresponds to the recommended value for asphalt (McCuen, 2016).

4.2.3 Real-world case studies

We elaborated eight real-world case studies at seven study sites, i.e., at one study site two different events were observed. The case studies' characteristics are summarized in Table 4.2 and 4.3, while their respective location is shown in Fig. 4.2. In the following we introduce the delineation of the study perimeters, the gathered input data, the consideration of hydrological losses, the reconstruction of overland flow paths as well as the assessment of the model performance.

In terms of hydrological losses, we account for infiltration and interception losses, but neglect evaporation, as contributions of the latter are generally particularly low (cf. Yu & Coulthard, 2015). Furthermore, we neglect the influence of the sewer system

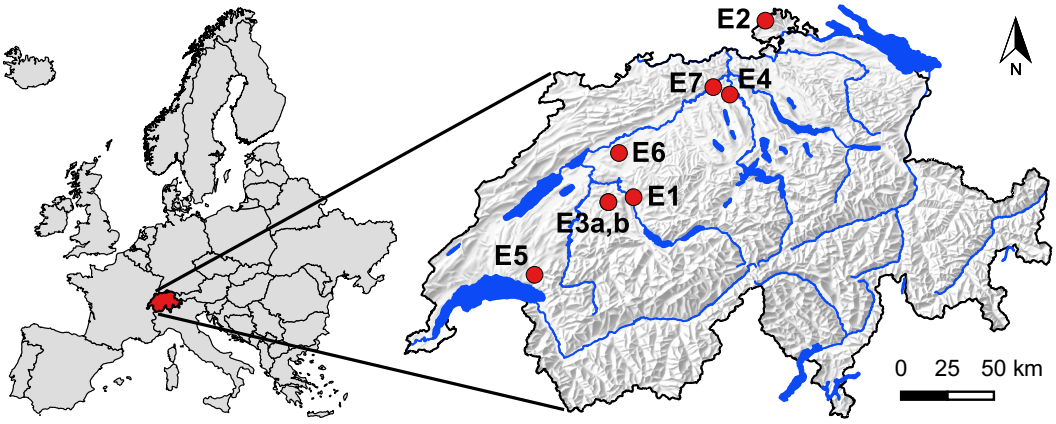

Fig. 4.2: Location of the seven study sites. Note the two case studies (E3a and E3b) were observed at the corresponding study site.

altogether and simply suppose that the system operates at full capacity, as assumed e.g., by Fewtrell et al. (2011), as well.

Table 4.2: Characteristics of the five case studies (at four study sites) triggered by relatively heavy rainfall.

Characteristic	**E1**	**E2**	**E3a / E3b**	**E4**
Date	20.07.2007	02.05.2013	12.07.2014 / 06.06.2015	08.06.2016
Town and Canton (abbr.)	Rubigen BE	Schleitheim SH	Mittelhaeusern BE	Dottikon AG
Slope: mean ± sd (%)	7.7 ± 6.4	14.7 ± 9.3	18.1 ± 8.4	17.1 ± 10.1
Altitude: mean $\pm\Delta h/2$ (m)	571 ± 25	562 ± 62	727 ± 58	505 ± 82
Perimeter P_{wsd} (km^2)	1.26	0.83	0.33	0.64
Perimeter P_{obs} (km^2)	0.61	0.22	0.33	0.33
Preconditions (-)	dry	normal	wet / dry	normal
Rainfall duration (h)	5	6	13 / 4	11
Rainfall sum (mm)	48.0	23.9	44.5 / 32.3	61.9
Max rainfall int. (mmh^{-1})	41.8	21.5	13.2 / 31.9	26.0
Mean rainfall int. (mmh^{-1})	9.6	4.0	3.4 / 8.1	5.6

Table 4.3: Characteristics of the three case studies triggered by relatively weak rainfall.

Characteristic	**E5**	**E6**	**E7**
Date	03.07.2007	13.05.2016	14.05.2016
Town and Canton (abbr.)	Bossonnens FR	Oberramsern SO	Oberflachs AG
Slope: mean ± sd (%)	12.7 ± 10.9	22.1 ± 20	22.9 ± 11.5
Altitude: mean $\pm\Delta h/2$ (m)	765 ± 42	586 ± 92	614 ± 110
Perimeter P_{wsd} (km^2)	0.28	0.25	0.54
Perimeter P_{obs} (km^2)	0.04	0.03	0.09
Preconditions (-)	wet	wet	normal
Rainfall duration (h)	49	27	68
Rainfall sum (mm)	56.5	59.7	90.1
Max rainfall int. (mmh^{-1})	6.7	7.3	6.5
Mean rainfall int. (mmh^{-1})	1.2	2.2	1.3

4.2.3.1 Domains

In order to delineate the study perimeter for each case study, the areas were considered, within which overland flow paths could be reconstructed. The corresponding study perimeters were then obtained by delineating the smallest respective watershed that would still encompass the reconstructed flow paths. Thereafter, these perimeters were buffered by at least 50 m to obtain a simulation domain that extend over the watershed's boundary. This ensures that the simulations' boundary effects within the study perimeters remain negligible. Thus, three different domains are differentiated for each case study:

- Observation domain (D_{obs}), within which all documented overland flow paths were reconstructed.
- Watershed domain (D_{wsd}) representing the smallest watershed that contains the observation perimeter. The model results are cropped to this area.
- Simulation domain (D_{sim}) representing the buffered watershed domain, within which the simulations are carried out.

Table 4.4: Look-up table for relevant land use classes and corresponding Manning's roughness coefficients n, as recommended by McCuen (2016). The imperviousness is described by m (cf. Sect 4.2.3.5). It indicates, whether the corresponding cell is considered as being fully impervious ($m = 1$, no infiltration), partially impervious ($m < 1$, reduced infiltration) or completely pervious ($m = 0$, normal infiltration). Note that the rain falling on buildings did not contribute to the overland flow.

Land use	**Surface**	$\boldsymbol{n}$ ($\mathrm{sm}^{-1/3}$)	$\boldsymbol{m}$ (-)
Ley, meadow	Dense grass	0.240	0
Cropland	Conventional tillage without residue	0.090	0
Orchard	Woods without underbrush	0.200	0
Forest	Woods with light underbrush	0.400	0
Garden	Bermuda grass	0.410	0
Path, track	Graveled surface	0.012	0.75
Paved surface	Asphalt	0.012	1
Building	Smooth concrete	0.011	1

4.2.3.2 Primary input data

The main input for all four models is a DEM (Fig. 4.3). We used the DEM "swissALTI3D" as of 2013 with a regular grid size of 2-by-2 m, provided by the Swiss Federal Office of Topography (swisstopo, 2017a). Although, there are DEMs available with finer resolutions for some of the study sites, we used the aforementioned product, as it is homogeneous and available for whole Switzerland. As r.sim.water and MFD do not offer a direct option to integrate flow barriers such as buildings (cf. Table 4.1), the corresponding DEM was modified. All cells whose centroids are covered by a building, as specified by the land use, are elevated by at least 10 m.

The land use was assessed between July 2014 and June 2016. As the land use was observed shortly after each event that falls into this period, i.e., E3a, E3b, E4, E6 and E7 (cf. Table 4.2 and 4.3), the corresponding land use represent the conditions during these events. In contrast, the land use of the remaining case studies were assessed roughly three years after the date of occurrence, or more. Although there is a slight time shift, we assume that the mapped land use is still representative for the respective case study, as major land use changes are not expected at these study sites within the respective period. Firstly, the land use was digitized using orthophotos from the product "SWISSIMAGE" (swisstopo, 2017b). Secondly, the land use was verified in the field.

The surface roughness values were obtained by linking the land use with literature tables, i.e., with the comprehensive collection from McCuen (2016), as indicated in Fig. 4.3. The corresponding values are listed in Table 4.4.

The hourly rainfall rate is extracted from the product "CombiPrecip" provided by the Federal Office of Meteorology and Climatology (MeteoSwiss, 2014). The product combines radar and rain gauge measurements by means of a co-kriging with external drift (e.g., Sideris et al., 2014; Panziera et al., 2016). It has a spatial resolution of 1-by-1 km, a temporal resolution of one hour and is available from 2005 onwards (MeteoSwiss, 2014). As the case study sites are small, each study perimeter is covered by just a few cells. To reduce the influence of single cells that might contain outliers, the raster cells

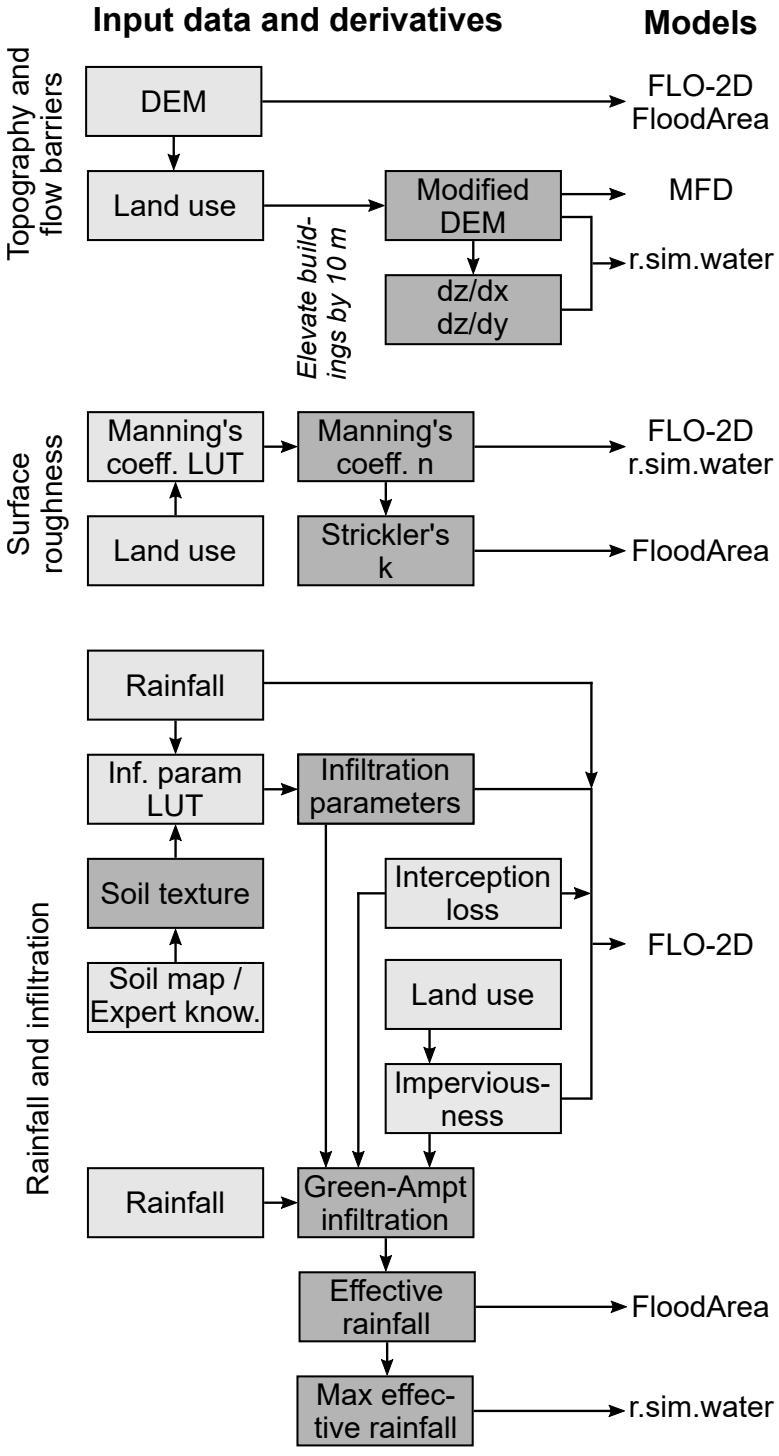

Fig. 4.3: Primary model input data (light gray boxes) as well as derivatives thereof (dark gray boxes). The look-up table (LUT) for Manning's coefficients is based on values from McCuen (2016), whereas the Strickler values are obtained by taking their inverse, i.e., $k = 1/n$. The LUT for the infiltration parameters is based on Rawls et al. (1983) and O'Brian (2009). The Green-Ampt infiltration with ponding was implemented and calculated externally (cf. Sect. 4.2.3.3).

covering each perimeter are buffered by one cell. Thereafter, the mean of these cells are calculated for each time step. Next, the triggering rainfall events are extracted from the rainfall records by considering a minimum inter-event time of $t_{min} = 6$ h and a minimum intensity threshold of $i_{min} = 0.1$ mmh^{-1}, which are in line with common literature values (e.g., Dunkerley, 2008). Consequently, at the beginning of each event, the rain intensity had been < 0.1 mmh^{-1} for at least six consecutive time steps of one hour each. Analogous, at the end of the event, it did not rain for at least six hours with an intensity ≥ 0.1 mmh^{-1}.

4.2.3.3 Infiltration

Out of all four models only FLO-2D allows the user to account for infiltration directly, while it cannot be modeled explicitly by FloodArea and r.sim.water, whereas MFD is not dependent on rainfall altogether (Table 4.1). Therefore, the following approach is chosen: The full potential of FLO-2D is exploited by using the integrated GA infiltration module. To feed the other two models with similar input, as recommended by Neal et al. (2012), the GA method is implemented in R (R Core Team, 2016). Therewith, spatially and temporally variable cumulative infiltration rates are calculated. Based on these values, effective rainfall rates are obtained that are used as model inputs for FloodArea and r.sim.water (Sect. 4.2.3.5). Hereafter, the implementation and parametrization of the GA method are briefly outlined.

Based on Green & Ampt (1911), the cumulative infiltration $F(t)$ (mm) at time t (h) can be expressed as

$$F(t) = Kt + \Psi \Delta\Theta \left(\frac{F(t)}{\Psi \Delta\Theta} + 1 \right) \quad , \tag{4.5}$$

whereas K is the hydraulic conductivity (mmh^{-1}), Ψ the wetting front soil suction head (mm), $\Delta\Theta = \Theta_f - \Theta_i$ (-) the difference between the final and initial soil moisture content. Thereby, an important assumption is that the water is ponded at the surface from the beginning of the steady rainfall. As this is generally not the case, Mein & Larson (1973) extended the GA infiltration method to account for the time until water starts to pond ($t = t_p$), at which time the cumulative infiltration depth equals the cumulative rainfall. Accordingly, the cumulative infiltration for steady rainfall after ponding time (i.e., $t > t_p$) is given by

$$F(t) = K(t - t_p) + F_p + \Psi \Delta\Theta \left(\frac{F(t)}{\Psi \Delta\Theta} + 1 \right) \quad , \tag{4.6}$$

whereas t_p denotes the ponding time (h) and $F_p = F(t)$ the cumulative infiltration (mm) at ponding time $t = t_p$. We then implemented the GA method following Chu (1978), who expanded the method for unsteady rainfall events. The interested reader may refer to Chu (1978), who provides a detailed derivation and applied examples of the method.

The required GA infiltration parameters were obtained as follows: We estimated each study site's dominant soil texture based on expert knowledge, except for the case studies E4 and E6 for which soil maps including soil texture classes were available. We estimated the hydraulic conductivity K, the wetting front soil suction head Ψ and the effective

porosity n_e using published regression parameter values from the comprehensive study by Rawls et al. (1983). Furthermore, it is assumed that the soils are saturated to a degree of $s_i = 30$, 50 or 80 % before each event under dry, normal or wet conditions, respectively. Each respective condition was set according to the observed antecedent rainfall (cf. Table 4.2 and 4.3). The change in soil moisture content is then estimated by $\Delta\Theta = n_e(s_f - s_i)$, while assuming that the soil's saturation after the event is always $s_f = 100$ %.

4.2.3.4 Interception

Canopy storage capacity depends on various factors and roughly amounts 1 mm (e.g., Ward & Robinson, 2000). Thus, the depletion of this storage is tiny in comparison to the total rainfall volumes of the corresponding case studies (cf. Table 4.2 and 4.3). Moreover, as the values of different land cover types are within the same order of magnitude, we simply consider a bulk interception loss of 1 mm. In FLO-2D this loss volume can be entered as a model parameter. For FloodArea and r.sim.water, we deduct the interception losses S (mm) from the total rainfall $P_t(t)$ (mm) to obtain a net rainfall $P_n(t)$ (mm) that reaches the ground, as follows.

$$P_n(t) = \begin{cases} 0, & P_t(t) \leq S \\ P_t(t) - S, & P_t(t) > S \end{cases} \tag{4.7}$$

4.2.3.5 Effective rainfall

As mentioned before, infiltration cannot be modeled directly by FloodArea and r.sim.water (cf. Sect. 4.2.3.3). Thus, to account for infiltration and interception losses, we compute effective rainfall rates, which are then used as model inputs. The effective rainfall is given by

$$P_e(t) = P_n(t) - (1 - m)F(t) \quad , \tag{4.8}$$

whereas P_e is the cumulative effective rainfall (mm), P_n is the net rainfall that considers an initial interception loss (mm, cf. Eq. 4.7), m is the imperviousness factor (cf. Table 4.4) and $F(t)$ is the cumulative infiltration (mm, Sect. 4.2.3.3). Note that an imperviousness factor can be set directly in FLO-2D's GA infiltration module for each individual cell (O'Brian, 2009). However, for FloodArea and r.sim.water, the imperviousness factors as specified in Table 4.4 are considered during the assessment of cell- and time-specific effective rainfall rates.

In FloodArea, spatial variable rainfall can be modeled by providing weighting factors (geomer, 2016), which can be thought of as runoff coefficients relating the hyetograph to cell-specific effective rainfall. Obviously, these coefficients are changing over time and space. They are defined as $c_{i,j,t} = P_e(i,j,t)/P_t(t)$. The spatially variable rainfall can then be modeled by creating a raster with cell values $c_{i,j}(t)$ for each time step t. The simulations can then be stopped after each time step and restarted with the runoff coefficients of the next time step. This procedure can be automated with batch scripts.

For r.sim.water, this procedure is not straightforward, as the simulations cannot be restarted based on results from a previous time step. Therefore, we choose the time step

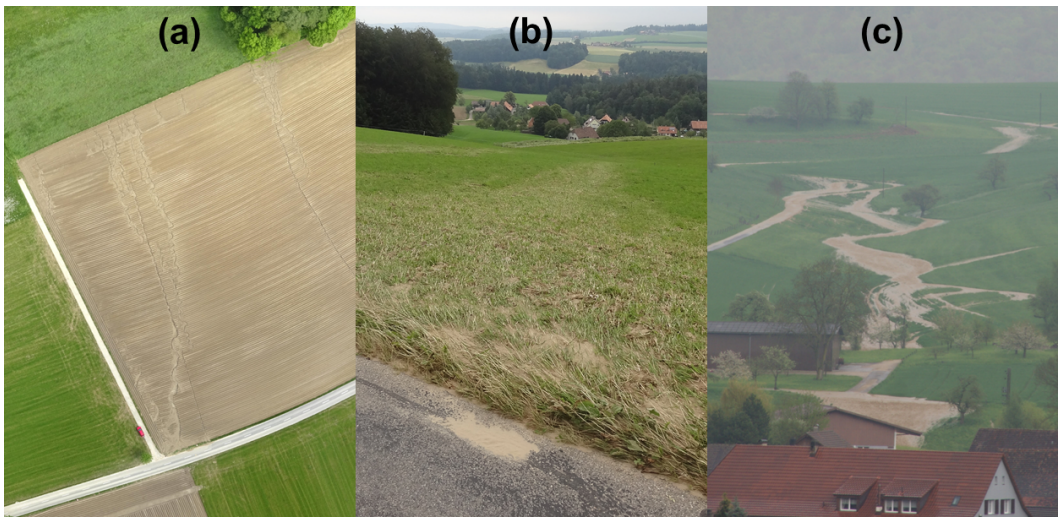

Fig. 4.4: Different sources used for reconstructing overland flow paths. (a) Orthophoto derived by means of a unmanned aerial vehicle (UAV) documenting traces of erosion in a field of the case study E6 (source: Elias Hodel, 16.05.2016). (b) Traces of overland flow in a field of the case study E3b that were mapped in the field (source: Daniel B. Bernet, 09.06.2015). (c) Photograph documenting actual overland flow of the case study E2 (source: Andrea Wanner-Staubesand, 02.05.2013).

with the highest effective rainfall rate and run the model with only this single spatially variable rainfall field.

4.2.3.6 Reconstruction of overland flow paths

Data sources that possibly indicate past SWFs include insurance claim records, disaster data bases, reports and recollections from affected people (Bernet et al., 2017, and references therein). However, for recent events, it is usually possible to reconstruct flow paths of SWFs based on their traces in the field, as exemplified by Fig. 4.4. Particularly in rural environments, overland flow usually leaves notable traces such as erosion marks, deposited sediments and flattened vegetation. For the purpose of this study, we have reconstructed discernible SWF traces based on field observations following the events of the case studies E3a, E3b, E4, E6 and E7, whereas for the remaining case studies, i.e., E1 and E2, the inundated areas were reconstructed based on external sources. Table 4.5 summarizes the source for the flow path's reconstructions along with associated limitations, as well as a qualitative confidence level of the data quality.

Irrespective of the data source, the flow paths were reconstructed and spatially localized. Using standard GIS software, the field assessment were then digitally stored. All overland flow traces and paths are considered as being wet. To assess the performance of the models, these areas are then compared to the model outputs, as outlined in the following section.

4.2.3.7 Model performance

Across various disciplines, map comparisons are a standard procedure to assess and compare model performances (e.g., Kuhnert et al., 2005; Foody, 2007; Bennett et al., 2013). However, there is not a single best method for this task. On the contrary, vast

Table 4.5: Exploited sources of information for reconstruction of inundated areas for each case study (cf. Tab. 4.2 and 4.3).

ID	Source	Quantity	Limitations	Confidence
E1	External map	Ponded water and water on the streets	No indication of flow paths, assessment methods unknown	Low
E2	Photographs	Flow paths and flood extent	Spatial localization of depicted flow paths	high
E3a,b	Field visits, aerial photos	Traces of flow (sediments, flattened vegetation)	Impossible to identify flow that left no traces	high
E4	Field visit	Traces of flow (sediments, flattened vegetation)	Impossible to identify flow that left no traces; Flow traces in forest difficult to detect	medium
E5	Video	Flow dynamics and extent of flood	Coverage limited to small area, low resolution	medium
E6	Field visit, aerial photos	Traces of erosion in bare field	Impossible to identify flow that left no traces	medium
E7	Field visit	Traces of erosion in bare field	Impossible to identify flow that left no traces; small observation perimeter compared to watershed	medium

tools including both quantitative as well as qualitative methods are recognized as being appropriate for this purpose (Kuhnert et al., 2005; Bennett et al., 2013). Thus, the model performance assessment have to be adapted to the models' objectives as well as to the characteristics of the available data, since the task is inherently case-specific (Bennett et al., 2013).

Along these lines, we compare the model outcomes and observations visually, as well as quantitatively. In terms of the latter, we use binary pattern performance measures based on the contingency table (Table 4.5), which are widely-used (e.g., Aronica et al., 2002; Schumann et al., 2009; Bennett et al., 2013; Stephens et al., 2014). However, more recently, Stephens et al. (2014) pointed out that these performance measures are all subjected to a varying degree of bias, which should be considered in subsequent conclusions. As we are using different measures conjunctively in this study and are more interested in the broader picture, the influence of this circumstance on our conclusions is negligible.

The binary pattern performance measures are based on the assessment whether a cell has been observed and/or simulated as wet or dry. All cells covered by an observed flow paths are considered as wet. For the simulation results, this information is inferred from the simulated maximum flow depths h_f (m) by applying an arbitrary threshold h_t (m). Thus, cells with a maximum flow depth below the threshold ($h_f < h_t$) are considered to be dry, while all other cells ($h_f \geq h_t$) are considered to be wet. We tested different threshold values and compared the model performance using the observations as the reference. Based on these results, we empirically chose a value of $h_t = 0.02$ m as this threshold value maximized the performance of all models.

In the following, we compare the models' results with observations, in addition to

Table 4.6: Contingency table of model prediction or observation (A) versus model prediction (B).

	Present (wet) in A	**Absent (dry) in A**
Present (wet) in B	Hits: $a = A_1B_1$	False alarms: $b = A_0B_1$
Absent (dry) in B	Misses: $c = A_1B_0$	Correct negatives $d = A_0B_0$

a comparison of the models among each other. The comparisons of the models with observations are constrained to the observation perimeter (D_{obs}), while the model comparison among each other is carried out within the whole watershed (D_{wsd}, cf. Sect. 4.2.3.1).

For the quantitative model comparison, the following binary pattern performance measures are used (e.g., Aronica et al., 2002; Pappenberger et al., 2007; Bennett et al., 2013), which are based on the contingency table (Table 4.5), :

$$\text{bias:} \quad m_1 = \frac{a+b}{a+c}, \quad m_1 \in [0,\infty], \quad \text{ideally } m_1 = 1 \tag{4.9}$$

$$\text{threat score:} \quad m_2 = \frac{a}{a+b+c}, \quad m_1 \in [0,1], \quad \text{ideally } m_2 = 1 \tag{4.10}$$

$$\text{hit rate:} \quad m_3 = \frac{a}{a+c}, \quad m_1 \in [0,1], \quad \text{ideally } m_3 = 1 \tag{4.11}$$

$$\text{false alarm rate:} \quad m_4 = \frac{b}{b+d}, \quad m_1 \in [0,1], \quad \text{ideally } m_4 = 0 \tag{4.12}$$

4.3 Results

4.3.1 Artificial surfaces

Despite the lack of a baseline, the applying the models to the selected artificial surfaces reveals interesting characteristics (Fig. 4.1). First and foremost, the incised street represents a prominent topographical structure that has a significant influence on the flow pattern. The street acts like a channel, which can collect incoming water and can be overtopped, if the channel is full or if the incoming water is not sufficiently deflected. Whether the street is overtopped or not, is discernible by the amount of dry cells directly to the south of the incised street, i.e., cells with a flow depth or flow accumulation below the flow threshold (dark red cells in Fig. 4.1). For each artificial surface, the pattern of these dry cells varies significantly among the model. In contrast, the pattern of dry cells north of the street is more similar among the models for each artificial surface, safe the ellipsoid, as discussed later. Thus, the street has a major influence on the distribution of dry and wet cells, respectively.

In more detail, r.sim.water does not predict a deflection of the water crossing the street on any surface. Quite the opposite is true for the flow accumulation calculated by MFD. For all surfaces safe the saddle, the street poses a complete or nearly complete flow barrier. FLO-2D and FloodArea, on the other hand, show a more differentiated picture, as water is overtopping where ever the flow depths are exceeding the street's incision. This is most apparent on the inverse ellipsoid, where FloodArea predicts a significant overtopping of the street's eastern end, unlike the other models. Thus, in this modeling exercise, the user's choice of a model does not only heavily influence the pattern of dry and wet cells south of the street, but also the corresponding flow paths.

The results of the hydrodynamic models do not only deviate substantially south of the street, but also on the street itself for each artificial surface. FLO-2D consistently predicts the highest flow depths on the street. FloodArea's results exhibit flow depths that lie mostly between the minimal values estimated by r.sim.water and the high values predicted by FLO-2D. However, as mentioned before, a striking difference of FloodArea

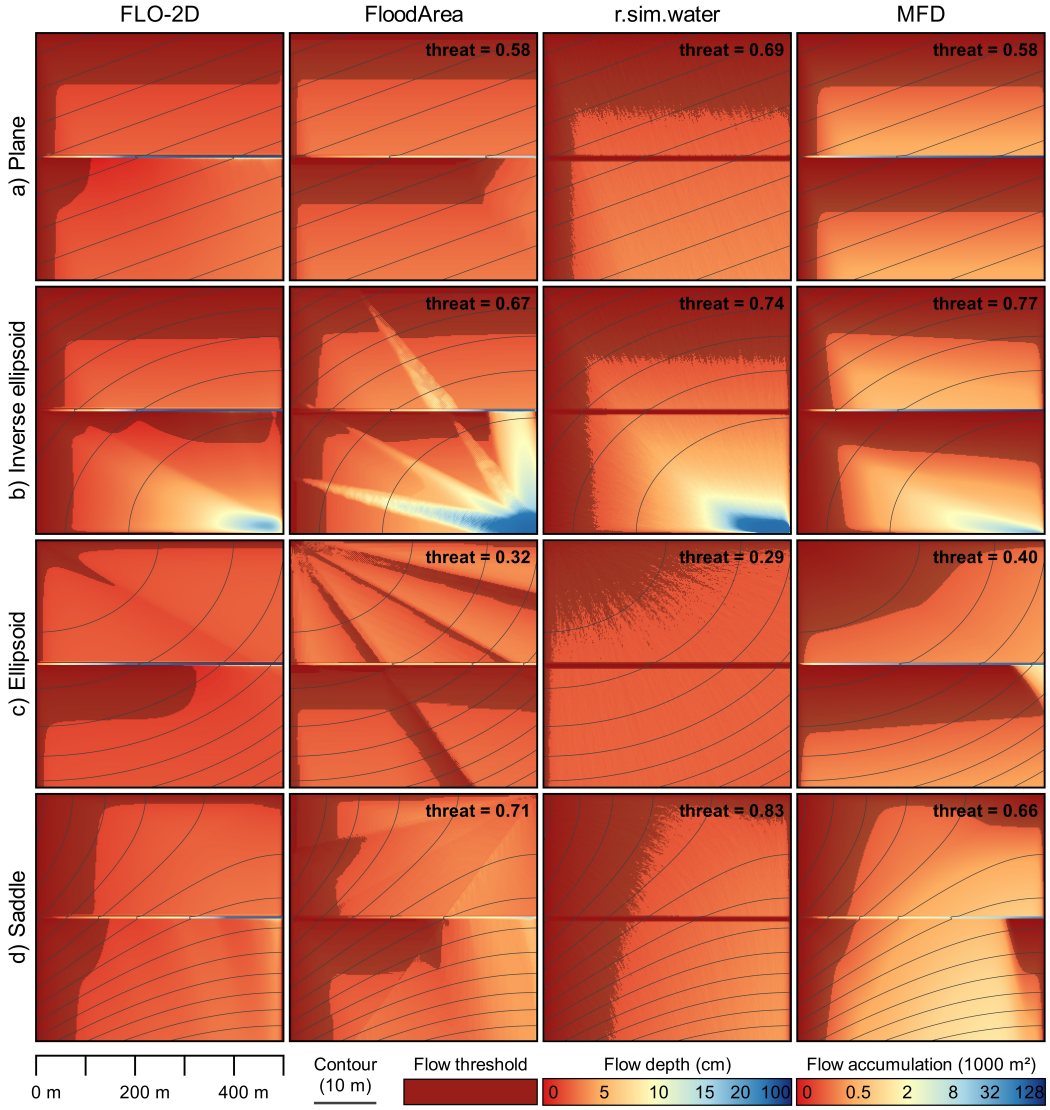

Fig. 4.5: Simulation results of the four different models applied to a parallel (a), a concave (b), a convex (c) and a combination of a convex and concave (d) artificial surface. The flow threshold for the hydrodynamic models (FLO-2D, FloodArea, r.sim.water) is a flow depth of 0.02 m, whereas the flow threshold for the flow accumulation algorithm (MFD) is an accumulation area of 250 m^2. Cells with values below the respective flow threshold are considered to be dry (dark red cells), while all other cells are considered to be wet. The indicated threat scores (threat, cf. Eq. 4.10) are obtained by comparing the models' predicted wet and dry cells to the binary pattern produced by FLO-2D, which is used as a reference.

compared to FLO-2D is the overtopping of the street's incision at the eastern side of the inverse ellipsoid. Compared to the other hydrodynamic models, r.sim.water predicts by far the lowest flow depths on the street for all surfaces. In fact, the flow depths on the street predicted by r.sim.water are below the wet/dry threshold of 0.02 m for all surfaces. Thus, the flow patterns south of the street are heavily influenced of how the models predict the flow over this topographical structure.

However, the flow patterns are also dependent on how the models simulate flow over the four different topographical forms. Specifically, the flow patterns on the ellipsoid (i.e., convex slope) of each single model is strikingly different from the other ones, which is reflected by the particularly low threat scores indicated in Fig. 4.1. Also the flow patterns in the northern half of the saddle seem to deviate slightly more among the models than the produced patterns on the plane (i.e., parallel slope) and the inverse ellipsoid (i.e., concave slope), respectively. This could be explained by the fact that the northern half of the saddle is characterized by convex forms that produce particularly different results among the models. Lastly, the flow pattern produced by FloodArea on the inverse ellipsoid is characterized by striking flow paths. FloodArea produces also sharp-edged flow paths on the ellipsoid and the saddle, however not as pronounced as on the inverse ellipsoid. These flow patterns might stem from the limitation of flow directions to 16 fixed angles by FloodArea's flow routing scheme (Tyrna et al., 2017).

4.3.2 Real-world case studies

The performance of the models applied to each case study is depicted in Fig. 4.6. The obtained threat scores (Eq. 4.10) are rather low and indicate that, overall, all models have a low performance for all case studies. The respective maximal threat score of the models lie between 0.318 and 0.344, which stem from the case study E2. For the same case study, the models produce the highest hit rates (Eq. 4.11), ranging between 0.566 and 0.788. Save a few exceptions, the hit rates are well below a value of 0.5 in all other case studies.

The bias is the fraction of simulated number of wet cells compared to the observed number of wet cells (Eq. 4.9). Thus, a bias greater than one indicates an overestimation of the wet cells by the model, whereas a bias below one shows the opposite. As presented in Fig. 4.6, all models overestimate the number of reconstructed wet cells for some case studies, but heavily underestimate them for others. As depicted in Fig. 4.6, the bias is correlated with the false alarm rates (Eq. 4.12). For each case study, models with a lower bias are also associated with a lower false alarm rate, and vice versa. The lowest absolute values are produced for the simulations with strong underestimations (bias $\ll 1.0$). This can be expected, since a particularly low bias value means that the number of modeled wet cells is much smaller than the observed number of wet cells. In this case, even if all modeled wet cells were misses, the false alarm rate would still be small, since the number of correct negatives is constantly high for all models. Hence, following Eq. 4.12, a low false alarm rate results.

Overall, we have identified three main issues limiting the models' performances, i.e., observational data of differing quality, insufficiently represented topographical structures and biased predictions of effective rainfall. In the following, we illustrate each of these issues with examples from the corresponding case studies.

The particularly low performance of all models applied to case study E1 can mainly be

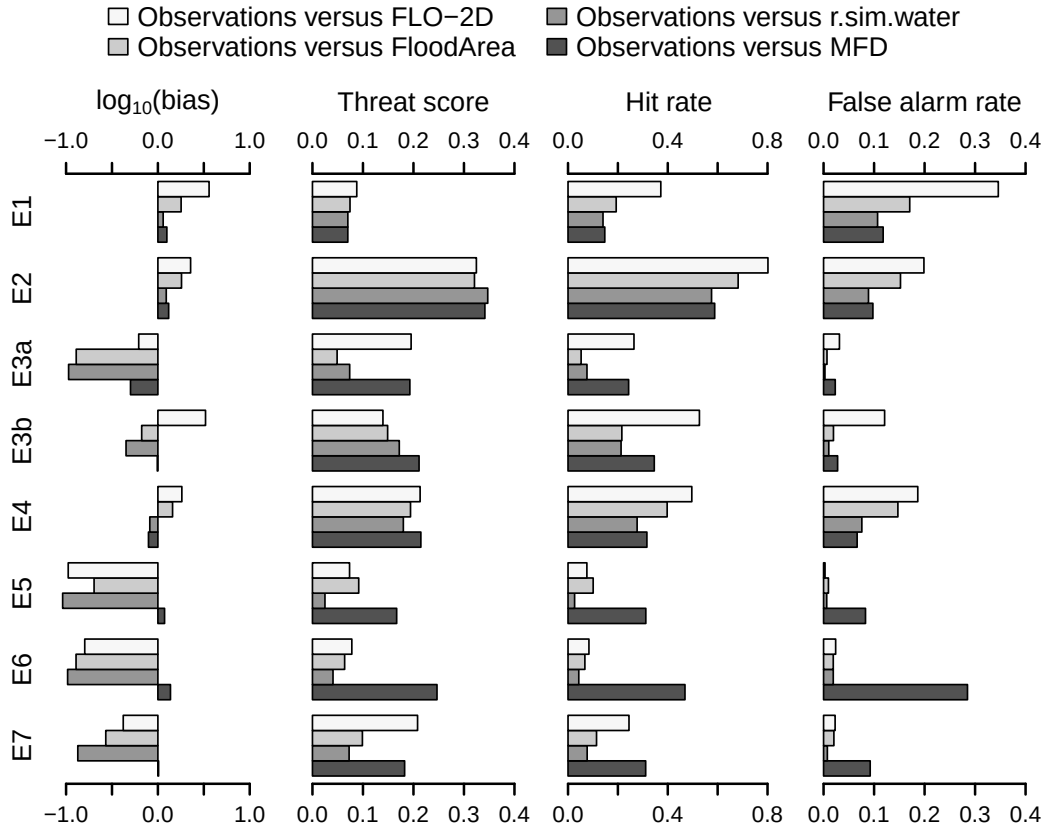

Fig. 4.6: Model performances of each model in comparison to the observed values evaluated within the observation domain (D_{obs}, Sect. 4.2.3.1). The binary pattern performance measures are defined in Eq. 4.9-4.12. Note that not the bias itself, but the common logarithm of the bias is displayed. The IDs (E1-7) indicate the corresponding case study, as summarized in Table 4.2 and 4.3.

attributed to poor observational data. Namely, the derivation of observed wet cells are based on an external map (Jordi + Kolb AG, 2008). Therein, areas with ponded water as well as water on the streets are mapped, while overland flow paths in the agricultural fields are not indicated (Table 4.5). Thus, the observations only capture areas that are small compared to the whole area that must have been inundated, as depicted by Fig. 4.7. As a consequence, the wet cells are overestimated, the false alarm rates are high and the threat scores are low for all models. Moreover, the map by Jordi + Kolb AG (2008) does not provide any ancillary information such as the applied mapping methods. Therefore, the map turns out to be an unsuitable source of information for the purpose of validating the models.

Applying the models to artificial surfaces has highlighted that topographical structures such as streets can have major effects on the produced flow paths (Sect. 4.3.1). How the models are predicting flow on streets in real-world case studies and how this influences the prediction of subsequent flow paths, can best be shown with results from the case study E2. All models perform best in this case study, as indicated by Fig. 4.6. The threat scores are similarly high for all models, whereas the other scores vary slightly more. For instance, FLO-2D produces the highest hit rate, however, at the expense of the highest false alarm rate and the highest overestimation. In contrast, r.sim.water

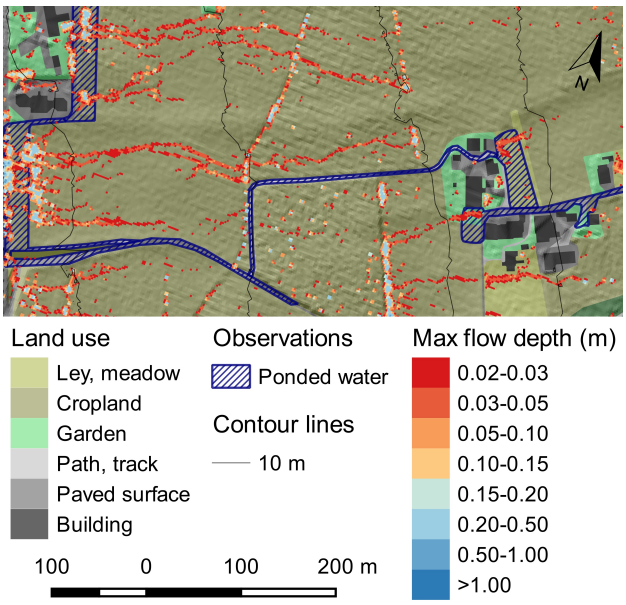

Fig. 4.7: Excerpt of the simulation results produced by r.sim.water applied to the case study E1. The observations inferred from an external map only capture areas where water was ponding or where the street's drainage system was overwhelmed, indicated by the hatched blue areas. Flow paths in the agricultural areas were not mapped. The accumulating water along what looks like trenches in the central part of the figure, are in fact caused by artifacts of the DEM. Note that the north direction is slightly tilted, as indicated.

exhibits the smallest bias and false alarm rate, however, at the expense of a smaller hit rate. Depending on the situation, one or the other configuration might be more desirable. The visual comparison confirms that all four models produce plausible results. As an example for the simulation results, the maximal flow depth predicted by FLO-2D are depicted in Fig. 4.8.

Based on the similar performance of all four models, the case study E2 is best suited for comparing the simulated flow paths in more detail. Namely, in most of the other case studies the models are associated with a greater range of bias values, i.e., the number of wet cells varies more among the models, which impairs the attribution of model differences. Fig. 4.9 illustrates the model comparison of the observed and simulated wet cells, as categorized according to the contingency table (Table 4.6).

According to all models, water mainly accumulates in the Thalweg, i.e., the path of lowest elevations along the hillslope (cf. Fig. 4.8 and 4.9). Thereby, the observed wet cells are captured well be all models, except MFD, which is not able the predict the ponding water towards the outlet of the observation domain. The main differences between the other models are that FLO-2D is overestimating the wet cells along the Thalweg more than FloodArea, which in turn overestimates the wet cells to a larger degree than r.sim.water. This is reflected by the respective bias values indicated in Fig. 4.9.

Overall, the models have difficulties predicting the water flowing on the streets. Foremost, the streets in the upper part of the domain were inundated, but were not simulated as such, which is reflected by the numerous misses in this area (red cells, Fig. 4.9). Compared to the other models, FLO-2D predicts the observed wet street cells

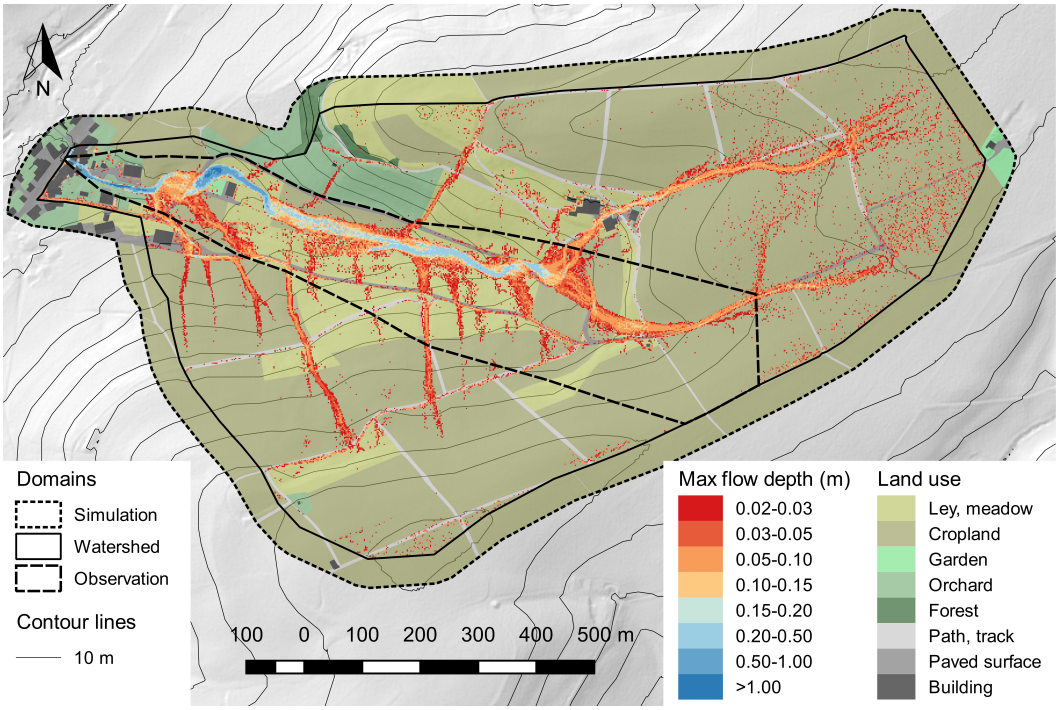

Fig. 4.8: Simulation result of FLO-2D applied to the case study E2. The maximal flow depths are categorized into discrete classes, as indicated in the legend. Considering the chosen water depth threshold, all cells that display a maximal water depth of $d \geq 0.02$ m are simulated as wet, whereas all other cells are predicted to remain dry.

better. This behavior could be expected based on the results from the models applied to artificial surfaces, since FLO-2D predicted consistently larger flow depths on the street than the other models (Sect. 4.3.1). Along the same lines, r.sim.water predicts the lowest number of wet street cells, which is also supported by the findings of the artificial modeling exercise. Interestingly, all models predict roughly the same places where water overtops the street's confinement and joins the main flow path in the Thalweg. Only one of these paths in the central part of the domain is predicted by FloodArea and FLO-2D, while the path is not indicated by r.sim.water and MFD. East thereof, a flow path could be observed that is not simulated by any model. Overall, this exemplifies that although the behavior may differ slightly between the models on a cell-by-cell basis, they all produce quite similar flow paths on a broader scale or, similarly fail to identify them.

As outlined introductorily, accurate predictions of effective rainfall are crucial for increased model performances, in addition to high-quality observational data and well-represented topographical structures. If a model predicts too little runoff, it usually leads to an underestimation of wet cells and, consequently, to a rather low performance. This issue is nicely exemplified by the case studies E3a and E3b observed at the same study site (cf. Table 4.1). As shown in Fig. 4.6, the number of wet cells are underestimated by all models in the first event (E3a). In particular, FloodArea and r.sim.water predict a much lower number of wet cells than the number of wet cells inferred from the observations. Consequently, the performance of these two models is particularly low for this case study. The performances are more balanced for the second observed event (E3b). However,

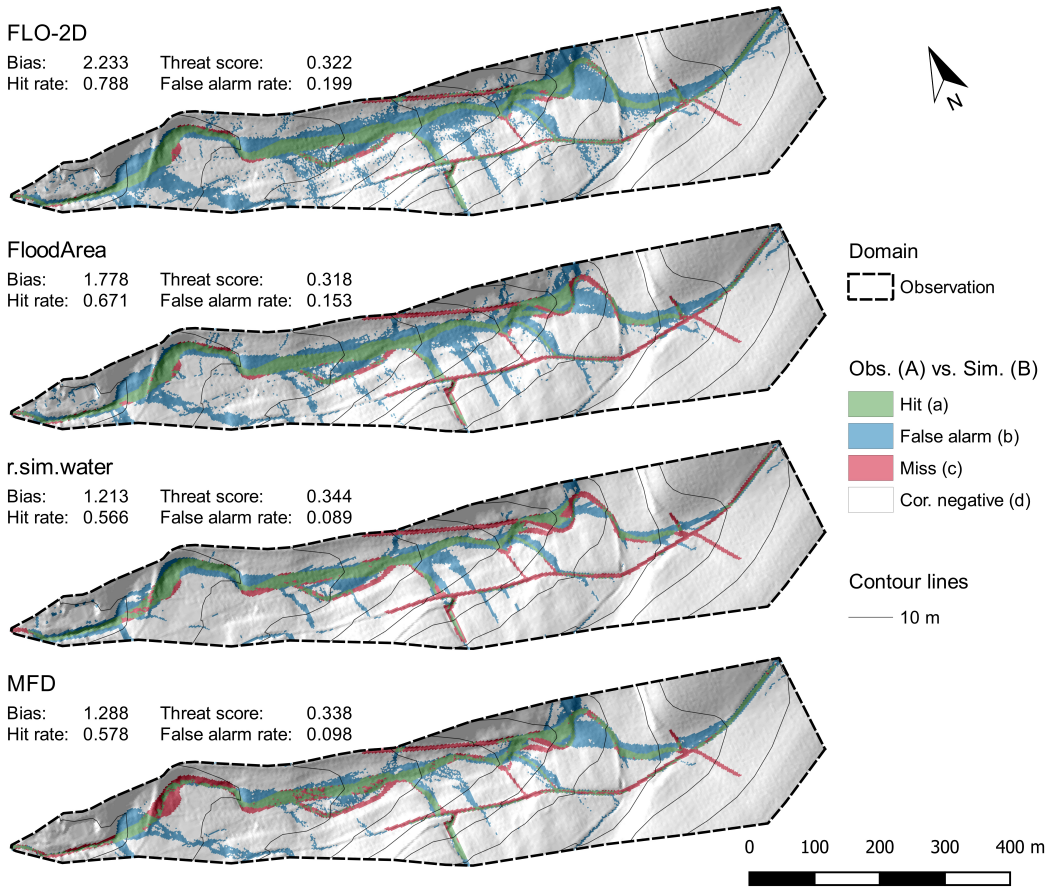

Fig. 4.9: Comparison of observed (obs.) and simulated (sim.) wet cells as categorized by the contingency table (Table 4.6) for each model applied to the case study E2. The definitions of hits, false alarms, misses and correct negatives can be found in Table 4.6. The whole study area (cf. Fig. 4.8) is clipped to the observation domain, as observations are unavailable outside of this domain. Note that the north direction is slightly tilted.

similarly to the case study E2, FLO-2D produces the highest hit rate, but also the highest false alarm rate, owed to the overestimated number of wet cells. Although, both case studies were triggered by thunderstorms, the rainfall intensities of E3a are moderate and the event spans over 13 hours, while E3b is associated with short and intense rainfall that is typical for thunderstorms (cf. Table 4.2).

Thus, we can observe that the hydrodynamic models, i.e., all except MFD, generally underestimate the number of wet cells for the case studies with low rainfall intensities. Namely, the said models exhibit an underestimation of the observed wet cells for the case studies E3a, E5, E6 and E7, as depicted in Fig. 4.6. This hints at the fact that the simulation of wet cells is less sensitive for case studies driven by intensive rainfall. In contrast, the mechanisms that lead to overland flow during the case studies with low rainfall intensities, are much more complex and badly captured by the chosen modeling approach of this study. Interestingly, the model MFD performs similarly for all case studies, since it is purely based on the DEM and, thus, independent of (event-specific) rainfall. As an example, the better performance of MFD compared to the other models is further illustrated by the case study E6, illustrated in Fig. 4.10.

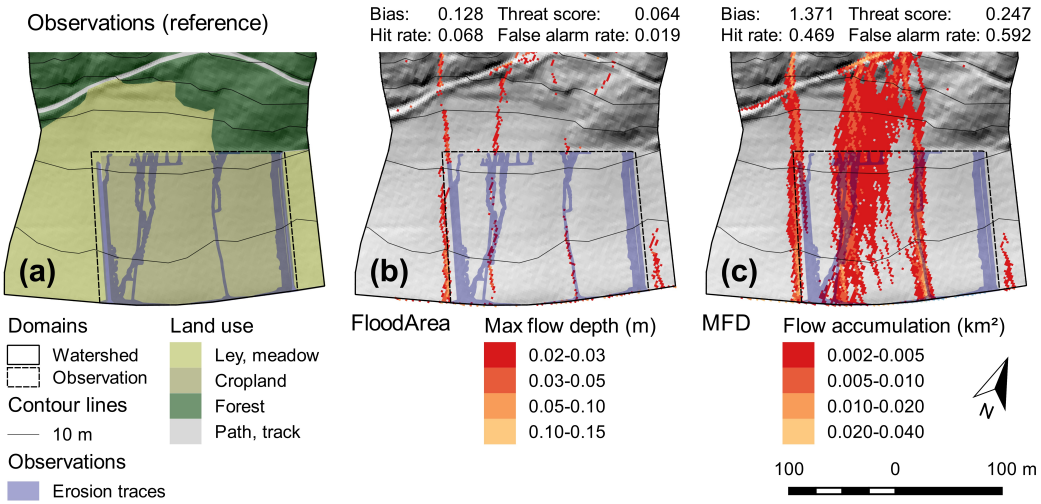

Fig. 4.10: Exemplary comparison of inundated areas inferred from documented traces of with flow depths predicted by FloodArea and flow accumulation calculated with MFD for the case study E6. (a) Flow paths inferred by means of a UAV in a patato field (cf. Fig. 4.4a). The land use is displayed in the background. (b) Maximal flow depth simulated by FloodArea. (c) Flow accumulation as predicted by MFD. Note that the north direction is slightly tilted for all sub-figures.

As highlighted by Fig. 4.10, the number of wet cells predicted by FloodArea is particularly low for the case study E6 within the observation domain, which is reflected by the performance measures' low values (Fig. 4.10b). Although the flow paths in the middle of the observation domain are vaguely indicated, it is apparent that too little effective rainfall is predicted, which leads to the exhibited underestimation of wet cells. In contrast, the flow paths predicted by MFD are a function of the respective catchment area of each cell, irrespective of the rainfall. Thereby, the two flow paths in the middle of the observation domain are covered. Notably, the flow path at the western border of the observation domain is shifted slightly westwards in comparison to the observations. This behavior can be attributed to the land management, that promotes flow at the western border of the potato field. The observed flow path at the eastern border of the observation domain is not captured by any model. Moreover, it should be noted that the flow over the bare potato field led to erosion, as depicted in Fig. 4.4a, which in turn may have a significant influence on the flow patterns. However, such effects cannot be captured with this study's modeling approach.

Until now, the models' performance has only been assessed by means of comparison to the reconstructed inundation areas. As indicated in Table 4.5, these observations are associated with a varying degree of confidence. Moreover, the example of the case study E1 has indicated that not all documents reporting inundated areas are suitable for model calibration and validation (Fig. 4.7). At the same time, for most case studies the observation domain is significantly smaller than the watershed domain (cf. Table 4.2-4.3). Thus, it is unclear how the models perform outside of the observation domain.

For that matter, we have compared the model results with each other, while using the results of the more sophisticated models as the corresponding reference values. Thereby, the capability of a simpler model to reproduce results from another more complex model can be assessed. As Fig. 4.11 indicates, FloodArea as well as MFD reproduce the

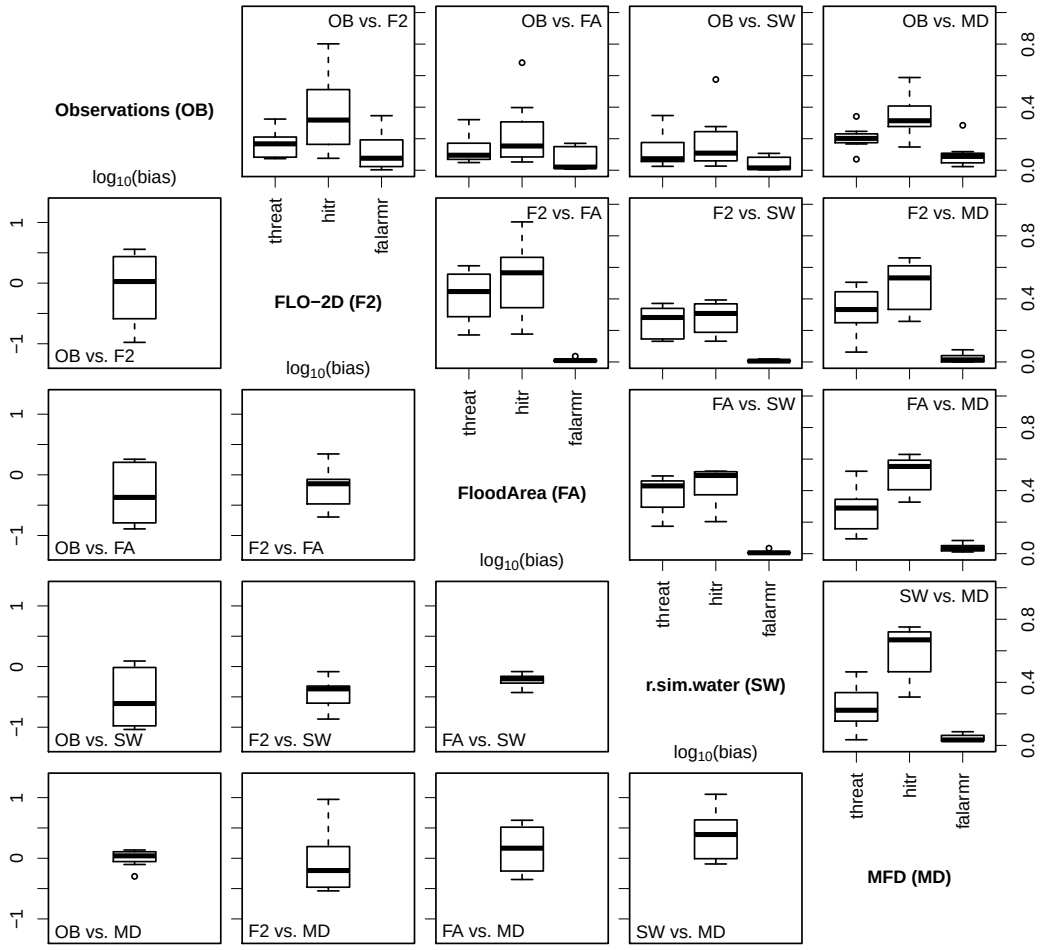

Fig. 4.11: Binary pattern performance measures of different pair-wise model and/or observation combinations. In the first row and the first column, the observations are compared with the model results within the observation domain (D_{obs}, Sect. 4.2.3.1). All other sub-figures show the comparison of different models within the watershed domain (D_{wsd}, Sect. 4.2.3.1). Each sub-figure is labeled with the abbreviated pairing, whereas the former label indicates the reference to which the latter is compared. As an example, the label "OB vs. SW" indicates the sub-figure, in which the observations are compared to the model results of r.sim.water. In the sub-figures above the diagonal, the performance measures are plotted, i.e., the threat score (threat, cf. Eq. 4.10), the hit rate (hitr, cf. Eq. 4.11) and the false alarm rate (falarmr, cf. Eq. 4.12). The bias (cf. Eq. 4.9) is plotted in the sub-figures below the diagonal. Note that not the bias itself, but the common logarithm of the bias is displayed.

results stemming from FLO-2D rather well. At the same time, the false alarm rates are particularly low. However, we also recognize that FloodArea generally underestimates the wet cells in comparison to FLO-2D. r.sim.water slightly underestimates the wet cells in comparison to FloodArea. However, the underestimation is limited to a small range indicating that the underestimation is similar in all case studies.

In addition to the comparison of the models among themselves, the first row and column of Fig. 4.11 also depicts the model performance in relation to the observations. Namely, it also displays the results shown in Fig. 4.6 in a different way, whereby the overall performance is better visualized. Thus, it depicts that the threat scores of all models are rather low, as discussed before. Moreover, it visualizes that the threat scores of the model MFD and FLO-2D are very similar, as well as the ones of FloodArea and r.sim.water, but at a lower level. Moreover, it visualizes the stronger tendency of FloodArea and r.sim.water to underestimate the wet cells, compared to FLO-2D. In comparison, MFD is by far the least biased of all the models.

4.4 Discussions

In this study, we have followed the procedure employed in practice by current SWF hazard assessments, which are based on uncalibrated, single deterministic simulations (cf. Meon et al., 2009; Tyrna & Hochschild, 2010; Kipfer et al., 2015; Tyrna et al., 2017). The results from the models applied to artificial surfaces and eight real-world case studies highlight that the models' performance could be increased if the model were properly calibrated. For instance, the model exercise on artificial surfaces (cf. Sect. 4.3.1) exemplified the need to calibrate the surface roughness. Namely, FLO-2D predicts rather high flow depths on the incised street, while r.sim.water predicts flow depth that are even below the chosen flow threshold of 0.02 m. Simulations with altered roughness values indicated that r.sim.water is rather sensitive to the street's chosen roughness value. Similarly, the flow depths on the street predicted by FloodArea are generally below those predicted by FLO-2D. A calibration of the roughness value could also improve the match between FLO-2D and FloodArea. This circumstance is also exhibited by applying the models in real-world case studies, whereby FloodArea and r.sim.water predict lower flow depths on the street (cf. Fig. 4.9 and Sect. 4.3.2).

The results from applying the models to a broad range of different settings indicates that the models' performance would still vary significantly, even if the models were calibrated. Namely, all models perform similarly well in the case study E2 (cf. Fig. 4.6), whereas properly calibrated models might perform even better. Yet, it is clear that a calibration could not bring the models' performances to a similar level in all case studies. On the one hand, this indicates that calibration and/or validation based on one single case study might be misleading. Thus, using various case studies covering a wide range of settings provides a more holistic picture of the models' performance. On the other hand, it also indicates that the models are not capable of capturing all relevant processes under diverse circumstances.

In fact, the results show that the hydrodynamic models tend to significantly underestimate the number of wet cells for the case studies associated with weak rainfall (cf. Fig. 4.6 and 4.10). Thus, the models do not predict sufficient runoff as compared to the observations, driven by an underestimation of the effective rainfall. More specifically, the

results indicate that the considered infiltration assessment methods (cf. Sect. 4.2.3.5) are not not capturing the governing processes well. Namely, saturation excess overland flow cannot be modeled by the applied methods, although this runoff generation mechanism is likely crucial for SWFs triggered by weak rainfall. Although SWFs are usually associated with heavy rainfall as mentioned before, results from Bernet et al. (2017) indicate that long lasting events with weak rainfall cause similar damage to buildings as short events with heavy rainfall. Thus, a model should be able to capture events characterized by heavy as well as weak rainfall to be suitable to reliably simulate SWFs in rural areas.

The two events observed at the same study site, i.e., case study E3a and E3b, show that SWFs can be triggered by heavier and weaker rainfall at the same location (cf. Table 4.2). Moreover, the case studies exemplify that the flow paths are not a static function of the topography, but are dependent on soil characteristics, land use, land management in addition to the rainfall input, of course. Along these lines, Ferreira et al. (2015) highlighted for instance that runoff generation mechanism are spatially and temporally highly variable. Certainly, there are established and emerging methods that could represent the runoff generation processes better (e.g., Schmocker-Fackel et al., 2007; Antonetti et al., 2016; Steinbrich et al., 2016). However, the consideration of such spatially highly variable processes are often impaired by the lack of appropriate data. Thus, for a better representation of the runoff generation processes, corresponding data are required. For the presented case studies such data were unavailable, as well as time-consuming and costly to collect.

The representation of topographical structures by the DEM is another aspect, which significantly influences the models' predictions (e.g., Sampson et al., 2012; de Almeida et al., 2016). As indicated by the model exercise on artificial surfaces, the models react sensitively on structures such as streets (Sect. 4.3.1). Moreover, applying the models to real-world case studies have pinpointed that the influence of such structures on the simulation results are governed more by the representation of such structures by the respective DEM than the choice of the model by the user. This is in line with findings stemming from more formal model comparisons, for instance from the benchmark study of urban flood models by Fewtrell et al. (2011). This issue is illustrated by Fig. 4.9, which indicates that the models predict the streets' overtopping at the same locations, while numerous of these flow paths could not be observed in reality. Thus, this behavior suggests that the streets confinements are not represented accurately enough by the DEM, supported by the fact that the rural environment of the case study E2 is characterized by single-lane streets with width in the same order as the DEM's resolution. In consequence, the channelizing effect of overland flow on streets is rather poorly captured by the models. Confronted with the same issue, Kipfer et al. (2012) proposed to incise all streets by a fixed depth. However, this measure most likely incapacitate the model to correctly reproduce the street's overtopping. Thus, a more common solution is to use a DEM with a finer resolution, if available (Wechsler, 2007; Dottori et al., 2013), as structures such as narrow streets are, thereby, generally better represented (Wechsler, 2007; Fewtrell et al., 2011; de Almeida et al., 2016). Nevertheless, as has been pointed out before, finer resolutions might also lead to inadequate confidence in the extremely precise model outputs (Dottori et al., 2013). Along these lines, it is crucial to note that the DEM itself is an imperfect representation of the reality, irrespective of its resolution (Wechsler, 2007; Abily et al., 2016). Just as DEMs with coarser resolutions, topographical models with finer resolutions are not flawless either and contain artifacts, which may cause

false results, as illustrated in Fig. 4.7. Therefore, the DEM needs to receive particular attention, i.e., it needs to be thoroughly pre- and post-processed, as other studies have indicated, as well (Hankin et al., 2008; Hunter et al., 2008; Tyrna et al., 2017).

The models may produce distinctly different results under certain circumstances, as highlighted by the models applied to the convex artificial surface characterized by diverging flow patterns (Fig. 4.5). However, in real-world applications such forms are likely less important in comparison to parallel and concave slopes, as exemplified by the case study E2, for instance, which is characterized by concave topography (cf. Fig 4.8). On such slopes, the models exhibit better model agreements (Fig. 4.5). Thus, in real-world applications, the model choice seems to play an inferior role compared to the previously discussed issues including the appropriate representation of effective rainfall and topographical structures. In other words, the model choice is generally not the most important factor determining whether the observed inundation area can be predicted well by the corresponding model, at least for events associated with heavy rainfall. However, it should be noted that this statement might be different for the prediction of flow depths and/or flow velocities.

As mentioned before, the hydrodynamic models, i.e., FLO-2D, FloodArea and r.sim.water, generally predict the number of wet cells less reliably for case studies associated with weak rainfall. An exception is the flow algorithm MFD, which produce the least biased results for all case studies (Fig. 4.11). Accordingly, MFD's performance is relatively robust in comparison to the other models. At the downside, the algorithm cannot consider ponding or backwater, as exemplified by the model's distinct underestimation of the inundated area towards the outlet of the study site E2 (Fig 4.9, MFD).

Lastly, the model performance is also highly dependent on the used data. Therefore, it is crucial to account for the uncertainties introduced by the input data, for instance by carrying out an appropriate uncertainty analysis (e.g., Pianosi et al., 2016). At the same time, the uncertainties need to be considered, which stem from the observational data that are used to condition and/or evaluate the models. For instance, if the observational data are a bad representation of the models' simulated quantity, the performance of the models are inevitably low, as exemplified by the case study E1 (Fig. 4.7 and Sect. 4.3.2). Yet, as mentioned before, there is little high-quality observational data available, which exhibit appropriate spatial and temporal resolutions suitable for model calibration and/or validation (e.g., Hunter et al., 2008; Blanc et al., 2012; Neal et al., 2012; Yu & Coulthard, 2015). Thus, in this study, we were forced to exploit different data sources, including external maps, eye witnesses' photographs and videos, mapped flood traces based on field visits partly supported by aerial photographs (cf. Table 4.5 and Fig. 4.4). Yet, the mapped quantity is not the same for each source. While the exploited photographs and videos represent a snapshot of the flow pattern at a certain instant during the respective SWF, reconstructions based on flood marks are constrained to areas where the flood has left discernible traces. For instance, overland flow with few suspended particles might not leave identifiable traces. In consequence, this likely leads to an underestimation of the actual inundated area. Accordingly, we assigned this data source with a lower (medium) confidence level, as indicated in Table 4.5. Despite the increased confidence level for overland flow reconstructed from photographs and videos, a similar bias might apply to this data source, as well. Namely, a bias is introduced if the picture is not taken at the instant of the maximal flood extent.

Therefore, just as the simulation outputs, the observational data should be regarded

as uncertain (Bennett et al., 2013; Stephens et al., 2014; Savage et al., 2016a). Thus, the representation of the observations and simulations as a crisp representation of the reality might be inappropriate. To address this issue, Pappenberger et al. (2007) applied a fuzzy set approach to measure the performance based on uncertain observational data. Thereby, slight shifts between observed and simulated wet cells could be accounted for. For simulated wet cells, it is straightforward to obtain a confidence level that a particular cell is wet by considering the simulated flow depths (Pappenberger et al., 2007). In contrast, this is not trivial for the observational data used in this study. Namely, ancillary data are required for this task. For instance, flood traces mapped in the field could be categorized according to the respective confidence that the corresponding area was in fact inundated.

Overall, this study pinpoints that the approach in flood hazard assessment based on single deterministic simulations with uncalibrated and/or unvalidated models is associated with manifold uncertainties. To reduce these uncertainties, an extensive uncertainty analysis could be carried out, e.g., as outlined by Pianosi et al. (2016). However, there are also alternative approaches that might be more suitable for simulating SWFs in rural areas, given the availability of high-resolution DEMs and a distinct lack of observational data. For instance, based on the finding that the simplest approach exhibits the most robust performance in this study, simple conceptual models, as termed by Teng et al. (2017), are promising. There are models that may overcome some of the limitations of the MFD, such as the incapability to simulate ponding water. At the same time, they are much less constraining in terms computational demand, owed to their simplicity. Thus, such simple conceptual models, as termed by Teng et al. (2017), can be applied to (almost) any scale and area, which makes them interesting candidates for regional or even nation-wide hazard assessments. Moreover, such models are predestined to be used in probabilistic modeling approaches (e.g., Merwade et al., 2008; Aronica et al., 2012; Savage et al., 2016a). Thus, the applicability of a probabilistic modeling approach in relation to SWFs in rural areas should be investigated in the future.

4.5 Conclusions and outlook

The main aim of this study was to test a SWF hazard assessment approach that is currently employed in practice and is based on single simulations with uncalibrated and/or unvalidated flood inundation models. For that matter, we applied four uncalibrated raster-based models to four characteristic artificial surfaces and eight real-world case studies. The models' application to the artificial surfaces exemplified that the flow patterns are heavily disturbed by streets, insofar as the prediction of inundated areas downslope of such structures are significantly influenced. Thus, there are large differences of how each model predicts these flow disturbances. Moreover, the modeling exercise has indicated that the models disagree most about the prediction of flow on the convex slope of an ellipsoid. The performances of the models applied to real-world case studies were assessed qualitatively as well as quantitatively in relation to inundated areas inferred from different sources. In summary, the performance of the selected grid-based hydrodynamic models indicates that they are not (yet) suited to be employed in an uncalibrated mode to reliably and deterministically predict inundations caused by SWFs in rural areas. Mainly, the models' performances are impaired by biased predictions of effective rainfall,

insufficient representation of topographical structures and observational data associated with varying quality and value.

To improve the prediction of SWF hazards, various approaches seem prospective. First of all, the deterministic modeling approach could be improved by incorporating a better prediction of the complex runoff generation mechanisms under various conditions. Moreover, the representation of topographical structures could be improved by considering DEMs with finer resolutions. Alternatively, irregular meshes and corresponding models could be used for a better representation of structures such as streets. At the same time, this study indicates that the models' calibration and/or their results' validation is imperative. For this task, the uncertainties of the observations, should be considered, as well. In general, the quantification and communication of the models' associated uncertainties are crucial, as the models' extremely precise outputs have indeed the potential to provoke overconfidence in their results, which may lead to inappropriate decisions in flood risk management (Dottori et al., 2013).

A different way forward would be to exploit simple conceptual models such as MFD. As a matter of fact, the sole dependence on the DEM by MFD turns out to be a slight advantage over the other models in this study. Thus, similar conceptual models could be tested that overcome some of the limitations of the MFD, while providing similarly robust results. The computational effort of such simple models is by far the least. Such approaches are therefore also interesting for the application to large areas, for instance in the context of regional or even national SWF hazard assessments. Yet, due to lower computational constraints, even the topographical data with the finest available resolutions might be exploited. Most importantly, such models could be applied in a probabilistic simulation framework, which could potentially better handle the lack of observational data in comparison to the current deterministic approaches.

Finally, this study highlighted once more that observational data are crucial irrespective of the chosen way forward. Thus, a standardized method to document and report SWFs in rural and urban areas is required and should be developed. At the same time, systematic observations should be put in place to lie the ground for future research, which is certainly necessary.

Acknowledgments

Funding from the Swiss Mobiliar supported the completion of this research. We thank the Federal Office of Topography for providing the corresponding spatial data, as well as the Federal Office of Meteorology and Climatology for providing the rainfall data. Moreover, we thank Mirjam Stawicki for supporting the field work, David Thöni for his modeling efforts during the initial phase of the study, Simona Trefalt for proofreading, and Guido Felder for revising the manuscript.

References

Abily, M., Bertrand, N., Delestre, O., Gourbesville, P., & Duluc, C.-M. (2016). Spatial global sensitivity analysis of high resolution classified topographic data use in 2D urban flood modelling. *Environ. Modell. Softw.*, *77*, 183–195. doi:10.1016/j.envsoft.2015.12.002.

Alder, S., Prasuhn, V., Liniger, H., Herweg, K., Hurni, H., Candinas, A., & Gujer, H. U. (2015). A

high-resolution map of direct and indirect connectivity of erosion risk areas to surface waters in Switzerland — A risk assessment tool for planning and policy-making. *Land Use Policy*, *48*, 236–249. doi:10.1016/j.landusepol.2015.06.001.

de Almeida, G. A. M., Bates, P., & Ozdemir, H. (2016). Modelling urban floods at sub-metre resolution: challenges or opportunities for flood risk management? *J. Flood Risk Manage.*, (pp. 1–11). doi:10.1111/jfr3.12276.

Andrieu, H., Browne, O., & Laplace, D. (2004). Les crues en zone urbaine: des crues éclairs? *La Houille Blanche*, (pp. 89–95). doi:10.1051/lhb:200402010.

Antonetti, M., Buss, R., Scherrer, S., Margreth, M., & Zappa, M. (2016). Mapping dominant runoff processes: An evaluation of different approaches using similarity measures and synthetic runoff simulations. *Hydrol. Earth Syst. Sc.*, *20*, 2929–2945. doi:10.5194/hess-20-2929-2016.

Aronica, G., Bates, P. D., & Horritt, M. S. (2002). Assessing the uncertainty in distributed model predictions using observed binary pattern information within GLUE. *Hydrol. Process.*, *16*, 2001–2016. doi:10.1002/hyp.398.

Aronica, G. T., Franza, F., Bates, P. D., & Neal, J. C. (2012). Probabilistic evaluation of flood hazard in urban areas using Monte Carlo simulation. *Hydrol. Process.*, *26*, 3962–3972. doi:10.1002/hyp.8370.

Barredo, J. I. (2009). Normalised flood losses in Europe: 1970–2006. *Nat. Hazard Earth Sys.*, *9*, 97–104. doi:10.5194/nhess-9-97-2009.

Bennett, N. D., Croke, B. F., Guariso, G., Guillaume, J. H., Hamilton, S. H., Jakeman, A. J., Marsili-Libelli, S., Newham, L. T., Norton, J. P., Perrin, C., Pierce, S. A., Robson, B., Seppelt, R., Voinov, A. A., Fath, B. D., & Andreassian, V. (2013). Characterising performance of environmental models. *Environ. Modell. Softw.*, *40*, 1–20. doi:10.1016/j.envsoft.2012.09.011.

Bernet, D. B., Prasuhn, V., & Weingartner, R. (2017). Surface water floods in Switzerland: what insurance claim records tell us about the caused damage in space and time. *Nat. Hazards Earth Syst. Sci. Discuss.*, (pp. 1–38). doi:10.5194/nhess-2017-136.

Blanc, J., Hall, J. W., Roche, N., Dawson, R. J., Cesses, Y., Burton, A., & Kilsby, C. G. (2012). Enhanced efficiency of pluvial flood risk estimation in urban areas using spatial-temporal rainfall simulations. *J. Flood Risk Manage.*, *5*, 143–152. doi:10.1111/j.1753-318X.2012.01135.x.

Castro, D., Einfalt, T., Frerichs, S., Friedeheim, K., Hatzfeld, F., Kubik, A., Mittelstädt, R., Müller, M., Seltmann, J., & Wagner, A. (2008). *Vorhersage und Management von Sturzfluten in urbanen Gebieten (URBAS): Schlussbericht des vom Bundesministerium für Bildung und Forschung geförderten Vorhabens*. Aachen, Deutschland: Hydrotec GmbH and Fachhochschule Aachen and Deutscher Wetterdienst. URL: http://www.urbanesturzfluten.de.

CEPRI (2014). *Gérer les inondations par ruissellement pluvial — Guide de sensibilisation*. Orléans, France: Centre Européen de Prévention du Risque d'Inondation. URL: http://www.cepri.net/Ruissellement_pluvial.html.

Chen, A. S., Evans, B., Djordjević, S., & Savić, D. A. (2012). A coarse-grid approach to representing building blockage effects in 2D urban flood modelling. *J. Hydrol.*, *426–427*, 1–16. doi:10.1016/j.jhydrol.2012.01.007.

Chu, S. T. (1978). Infiltration during an unsteady rain. *Water Resour. Res.*, *14*, 461–466. doi:10.1029/WR014i003p00461.

Conrad, O., Bechtel, B., Bock, M., Dietrich, H., Fischer, E., Gerlitz, L., Wehberg, J., Wichmann, V., & Böhner, J. (2015). System for Automated Geoscientific Analyses (SAGA) v. 2.1.4. *Geosci. Model Dev.*, *8*, 1991–2007. doi:10.5194/gmd-8-1991-2015.

Cook, A., & Merwade, V. (2009). Effect of topographic data, geometric configuration and modeling approach on flood inundation mapping. *J. Hydrol.*, *377*, 131–142. doi:10.1016/j.jhydrol.2009.08.015.

Coulthard, T. J., & Frostick, L. E. (2010). The Hull floods of 2007: implications for the governance and management of urban drainage systems. *J. Flood Risk Manage.*, *3*, 223–231. doi:10.1111/j.1753-318X.2010.01072.x.

Cutter, S. L., & Emrich, C. (2005). Are natural hazards and disaster losses in the U.S. increasing? *Eos Trans. AGU*, *86*, 381–389. doi:10.1029/2005EO410001.

Dottori, F., Di Baldassarre, G., & Todini, E. (2013). Detailed data is welcome, but with a pinch of salt: Accuracy, precision, and uncertainty in flood inundation modeling. *Water Resour. Res.*, *49*, 6079–6085. doi:10.1002/wrcr.20406.

Dunkerley, D. (2008). Identifying individual rain events from pluviograph records: A review with analysis of data from an Australian dryland site. *Hydrol. Process.*, *22*, 5024–5036. doi:10.1002/hyp.7122.

DWA (2013). *Starkregen und urbane Sturzfluten — Praxisleitfaden zur Überflutungsvorsorge* volume T1/2013 of *DWA-Themen*. Hennef, Deutschland: Deutsche Vereinigung für Wasserwirtschaft, Abwasser und Abfall (DWA).

Egli, T. (2007). *Wegleitung Objektschutz gegen meteorologische Naturgefahren*. Bern, Schweiz: Vereinigung Kantonaler Feuerversicherungen. URL: http://vkf.ch/VKF/Downloads.

Falconer, R. H., Cobby, D., Smyth, P., Astle, G., Dent, J., & Golding, B. (2009). Pluvial flooding: new approaches in flood warning, mapping and risk management. *J. Flood Risk Manage.*, *2*, 198–208. doi:10.1111/j.1753-318X.2009.01034.x.

Ferreira, C., Walsh, R., Steenhuis, T. S., Shakesby, R. A., Nunes, J., Coelho, C., & Ferreira, A. (2015). Spatiotemporal variability of hydrologic soil properties and the implications for overland flow and land management in a peri-urban Mediterranean catchment. *J. Hydrol.*, *525*, 249–263. doi:10.1016/j.jhydrol.2015.03.039.

Fewtrell, T. J., Bates, P. D., Horritt, M., & Hunter, N. M. (2008). Evaluating the effect of scale in flood inundation modelling in urban environments. *Hydrol. Process.*, *22*, 5107–5118. doi:10.1002/hyp.7148.

Fewtrell, T. J., Duncan, A., Sampson, C. C., Neal, J. C., & Bates, P. D. (2011). Benchmarking urban flood models of varying complexity and scale using high resolution terrestrial LiDAR data. *Phys. Chem. Earth*, *36*, 281–291. doi:10.1016/j.pce.2010.12.011.

Foody, G. M. (2007). Map comparison in GIS. *Prog. Phys. Geog.*, *31*, 439–445. doi:10.1177/0309133307081294.

Freeman, T. G. (1991). Calculating catchment area with divergent flow based on a regular grid. *Comput. Geosci.*, *17*, 413–422. doi:10.1016/0098-3004(91)90048-I.

Fuchs, S., Keiler, M., & Zischg, A. (2015). A spatiotemporal multi-hazard exposure assessment based on property data. *Nat. Hazard Earth Sys.*, *15*, 2127–2142. doi:10.5194/nhess-15-2127-2015.

Fuchs, S., Röthlisberger, V., Thaler, T., Zischg, A., & Keiler, M. (2017). Natural hazard management from a coevolutionary perspective: Exposure and policy response in the European Alps. *Ann. Am. Assoc. Geogr.*, *107*, 382–392. doi:10.1080/24694452.2016.1235494.

Gaitan, S., van de Giesen, N. C., & ten Veldhuis, J. A. E. (2016). Can urban pluvial flooding be predicted by open spatial data and weather data? *Environ. Modell. Softw.*, *85*, 156–171. doi:10.1016/j.envsoft.2016.08.007.

geomer (2016). *FloodAreaHPC-Desktop: ArcGIS-Extension for calculating flooded areas — User manual: Version 10.3*. Heidelberg, Germany: geomer GmbH and Ruiz Rodriguez+Zeisler+Blank. URL: http://www.geomer.de/fileadmin/templates/main/res/downloads/UserManualFloodArea10.pdf.

Grahn, T., & Nyberg, L. (2017). Assessment of pluvial flood exposure and vulnerability of residential areas. *Int. J. Disaster Risk Reduct.*, *21*, 367–375. doi:10.1016/j.ijdrr.2017.01.016.

Green, W. H., & Ampt, G. A. (1911). Studies on soil phyics. *J. Agric. Sci.*, *4*, 1. doi:10.1017/S0021859600001441.

Haghighatafshar, S., la Cour Jansen, Jes, Aspegren, H., Lidström, V., Mattsson, A., & Jönsson, K. (2014). Storm-water management in Malmö and Copenhagen with regard to climate change scenarios. *Vatten*, *70*, 159–168.

Hankin, B., Waller, S., Astle, G., & Kellagher, R. (2008). Mapping space for water: screening for urban flash flooding. *J. Flood Risk Manage.*, *1*, 13–22. doi:10.1111/j.1753-318X.2008.00003.x.

Horritt, M., & Bates, P. (2001). Effects of spatial resolution on a raster based model of flood flow. *J. Hydrol.*, *253*, 239–249. doi:10.1016/S0022-1694(01)00490-5.

Hunter, N. M., Bates, P. D., Neelz, S., Pender, G., Villanueva, I., Wright, N. G., Liang, D., Falconer, R. A., Lin, B., Waller, S., Crossley, A. J., & Mason, D. C. (2008). Benchmarking 2D hydraulic models for urban flooding. *P. I. Civil Eng.-Wat. M.*, *161*, 13–30. doi:10.1680/wama.2008.161.1.13.

Jakeman, A. J., Letcher, R. A., & Norton, J. P. (2006). Ten iterative steps in development and evaluation of environmental models. *Environ. Modell. Softw.*, *21*, 602–614. doi:10.1016/j.envsoft.2006.01.004.

Jongman, B., Kreibich, H., Apel, H., Barredo, J. I., Bates, P. D., Feyen, L., Gericke, A., Neal, J., Aerts, J. C. J. H., & Ward, P. J. (2012). Comparative flood damage model assessment: Towards a European approach. *Nat. Hazard Earth Sys.*, *12*, 3733–3752. doi:10.5194/nhess-12-3733-2012.

Jordi + Kolb AG (2008). *Schadenkarte Unwetter 2007*. Münsingen, Schweiz.

Kaźmierczak, A., & Cavan, G. (2011). Surface water flooding risk to urban communities: Analysis of vulnerability, hazard and exposure. *Landscape Urban Plan.*, *103*, 185–197. doi:10.1016/j.landurbplan.2011.07.008.

Kipfer, A., Kienholz, C., & Liener, S. (2012). Ein neuer Ansatz zur Modellierung von Oberflächenabfluss. In G. Koboltschnig, J. Hübl, & J. Braun (Eds.), *INTERPRAEVENT 2012 — Conference Proceedings* (pp. 179–189). International Research Society INTERPRAEVENT.

Kipfer, A., Schönthal, E., Liener, S., & Gsteiger, P. (2015). *Oberflächenabflusskarte Kanton Luzern: Bericht*. Bern, Schweiz: geo7 AG.

Kron, W., Steuer, M., Löw, P., & Wirtz, A. (2012). How to deal properly with a natural catastrophe database — analysis of flood losses. *Nat. Hazard Earth Sys.*, *12*, 535–550. doi:10.5194/nhess-12-535-2012.

Kuhnert, M., Voinov, A., & Seppelt, R. (2005). Comparing raster map comparison algorithms for spatial modeling and analysis. *Photogramm. Eng. Rem. S.*, *71*, 975–984.

Kundzewicz, Z. W., Kanae, S., Seneviratne, S. I., Handmer, J., Nicholls, N., Peduzzi, P., Mechler, R., Bouwer, L. M., Arnell, N., Mach, K., Muir-Wood, R., Brakenridge, G. R., Kron, W., Benito, G., Honda, Y., Takahashi, K., & Sherstyukov, B. (2014). Flood risk and climate change: global and regional perspectives. *Hydrolog. Sci. J.*, *59*, 1–28. doi:10.1080/02626667.2013.857411.

López-Vicente, M., Pérez-Bielsa, C., López-Montero, T., Lambán, L. J., & Navas, A. (2014). Runoff simulation with eight different flow accumulation algorithms: recommendations using a spatially distributed and open-source model. *Environ. Modell. Softw.*, *62*, 11–21. doi:10.1016/j.envsoft.2014.08.025.

Löwe, R., Urich, C., Sto. Domingo, N., Mark, O., Deletic, A., & Arnbjerg-Nielsen, K. (2017). Assessment of urban pluvial flood risk and efficiency of adaptation options through simulations — A new generation of urban planning tools. *J. Hydrol.*, *550*, 355–367. doi:10.1016/j.jhydrol.2017.05.009.

LUBW (2016). *Leitfaden kommunales Starkregenrisikomanagement in Baden-Württemberg*. Karlsruhe, Deutschland: Landesanstalt für Umwelt, Messungen und Naturschut Baden-Württemberg (LUBW). URL: http://www.lubw.baden-wuerttemberg.de/servlet/is/261161.

Maksivomić, Č., Prodanović, D., Boonya-Aroonnet, S., Leitão, J. P., Djordjević, S., & Allitt, R. (2009). Overland flow and pathway analysis for modelling of urban pluvial flooding. *J. Hydraul. Res.*, *47*, 512–523. doi:10.3826/jhr.2009.3361.

McCuen, R. H. (2016). *Hydrologic analysis and design*. (4th ed.). Hoboken, USA: Pearson Higher Education.

Mein, R. G., & Larson, C. L. (1973). Modeling infiltration during a steady rain. *Water Resour. Res.*, *9*, 384–394. doi:10.1029/WR009i002p00384.

Meon, G., Stein, K., Förster, K., & Riedel, G. (2009). *Untersuchung starkregengefährdeter Gebiete: Abschlussbericht zum Forschungsprojekt*. Braunschweig, Deutschland: Technische Universität Braunschweig and Leichtweiss-Institut für Wasserbau.

Merwade, V., Olivera, F., Arabi, M., & Edleman, S. (2008). Uncertainty in flood inundation mapping: current Issues and future directions. *J. Hydrol. Eng.*, *13*, 608–620. doi:10.1061/(ASCE)1084-0699(2008)13:7(608).

Merz, B., Kreibich, H., Schwarze, R., & Thieken, A. (2010). Review article — "Assessment of economic flood damage". *Nat. Hazard Earth Sys.*, *10*, 1697–1724. doi:10.5194/nhess-10-1697-2010.

MeteoSwiss (2014). *Räumliche Daten CombiPrecip*. Swiss Federal Office of Meteorology and Climatology. URL: http://www.meteoswiss.admin.ch/home/services-and-publications/produkte.subpage.html/en/data/products/2014/raeumliche-daten-combiprecip.html (last accessed 03.07.2017).

Mitasova, H., Thaxton, C., Hofierka, J., McLaughlin, R., Moore, A., & Mitas, L. (2004). Path sampling method for modeling overland water flow, sediment transport, and short term terrain evolution in Open Source GIS. In C. T. Miller, M. W. Farthing, G. F. Pinder, & W. G. Gray (Eds.), *Proceedings of the XVth International Conference on Computational Methods in Water Resources (CMWR XV)* (pp. 1479–1490). Chapel Hill, USA: Elsevier. doi:10.1016/S0167-5648(04)80159-X.

Neal, J., Villanueva, I., Wright, N., Willis, T., Fewtrell, T., & Bates, P. (2012). How much physical complexity is needed to model flood inundation? *Hydrol. Process.*, *26*, 2264–2282. doi:10.1002/hyp.8339.

Neteler, M., Bowman, M. H., Landa, M., & Metz, M. (2012). GRASS GIS: A multi-purpose open source GIS. *Environ. Modell. Softw.*, *31*, 124–130. doi:10.1016/j.envsoft.2011.11.014.

O'Brian, J. S. (2009). *FLO-2D Reference Manual: Version 2009*. Nutrioso, USA: FLO-2D Software Inc. URL: https://www.flo-2d.com/download/.

van Ootegem, L., Verhofstadt, E., van Herck, K., & Creten, T. (2015). Multivariate pluvial flood damage models. *Environ. Impact Asses.*, *54*, 91–100. doi:10.1016/j.eiar.2015.05.005.

Panziera, L., Gabella, M., Zanini, S., Hering, A., Germann, U., & Berne, A. (2016). A radar-based regional extreme rainfall analysis to derive the thresholds for a novel automatic alert system in Switzerland. *Hydrol. Earth Syst. Sc.*, *20*, 2317–2332. doi:10.5194/hess-20-2317-2016.

Pappenberger, F., Frodsham, K., Beven, K. J., Romanowicz, R., & Matgen, P. (2007). Fuzzy set approach to calibrating distributed flood inundation models using remote sensing observations. *Hydrol. Earth Syst. Sc.*, *11*, 739–752. doi:10.5194/hess-11-739-2007.

Pianosi, F., Beven, K., Freer, J., Hall, J. W., Rougier, J., Stephenson, D. B., & Wagener, T. (2016). Sensitivity analysis of environmental models: A systematic review with practical workflow. *Environ. Modell. Softw.*, *79*, 214–232. doi:10.1016/j.envsoft.2016.02.008.

Pilesjö, P., & Hasan, A. (2014). A triangular form-based multiple flow algorithm to estimate overland flow distribution and accumulation on a digital elevation model. *T. GIS*, *18*, 108–124. doi:10.1111/tgis.12015.

Pitt, M. (2008). *The Pitt Review: Learning lessons from the 2007 floods: An independent review by Sir Michael Pitt*. London, UK: Cabinet Office.

Planchon, O., & Darboux, F. (2002). A fast, simple and versatile algorithm to fill the depressions of digital elevation models. *Catena*, *46*, 159–176. doi:10.1016/S0341-8162(01)00164-3.

Quinn, P., Beven, K., Chevallier, P., & Planchon, O. (1991). The prediction of hillslope flow paths for distributed hydrological modelling using digital terrain models. *Hydrol. Process.*, *5*, 59–79.

R Core Team (2016). *R: A language and environment for statistical computing*. Vienna, Austria: R Foundation for Statistical Computing. URL: https://www.R-project.org.

Rawls, W. J., Brakensiek, D. L., & Miller, N. (1983). Green–Ampt infiltration parameters from soils data. *J. Hydraul. Eng.-ASCE*, *109*, 62–70. doi:10.1061/(ASCE)0733-9429(1983)109:1(62).

Röthlisberger, V., Zischg, A. P., & Keiler, M. (2017). Identifying spatial clusters of flood exposure to support decision making in risk management. *Sci. Total Environ.*, *598*, 593–603. doi:10.1016/j.scitotenv.2017.03.216.

Rözer, V., Müller, M., Bubeck, P., Kienzler, S., Thieken, A., Pech, I., Schröter, K., Buchholz, O., & Kreibich, H. (2016). Coping with pluvial floods by private households. *Water*, *8*, 304. doi:10.3390/w8070304.

Rüttimann, D., & Egli, T. (2010). *Wegleitung punktuelle Gefahrenabklärung Oberflächenwasser*. St. Gallen, Schweiz: Naturgefahrenkommission des Kantons St. Gallen.

Sampson, C. C., Bates, P. D., Neal, J. C., & Horritt, M. S. (2013). An automated routing methodology to enable direct rainfall in high resolution shallow water models. *Hydrol. Process.*, *27*, 467–476. doi:10.1002/hyp.9515.

Sampson, C. C., Fewtrell, T. J., Duncan, A., Shaad, K., Horritt, M. S., & Bates, P. D. (2012). Use of terrestrial laser scanning data to drive decimetric resolution urban inundation models. *Adv. Water Resour.*, *41*, 1–17. doi:10.1016/j.advwatres.2012.02.010.

Savage, J. T. S., Bates, P., Freer, J., Neal, J., & Aronica, G. (2016a). When does spatial resolution become spurious in probabilistic flood inundation predictions? *Hydrol. Process.*, *30*, 2014–2032. doi:10.1002/hyp.10749.

Savage, J. T. S., Pianosi, F., Bates, P. D., Freer, J., & Wagener, T. (2016b). Quantifying the importance of spatial resolution and other factors through global sensitivity analysis of a flood inundation model. *Water Resour. Res.*, *52*, 9146–9163. doi:10.1002/2015WR018198.

Schmocker-Fackel, P., Naef, F., & Scherrer, S. (2007). Identifying runoff processes on the plot and catchment scale. *Hydrol. Earth Syst. Sc.*, *11*, 891–906. doi:10.5194/hess-11-891-2007.

Schumann, G., Bates, P. D., Horritt, M. S., Matgen, P., & Pappenberger, F. (2009). Progress in integration of remote sensing–derived flood extent and stage data and hydraulic models. *Rev. Geophys.*, *47*, RG4001. doi:10.1029/2008RG000274.

Seibert, J., & McGlynn, B. L. (2007). A new triangular multiple flow direction algorithm for computing upslope areas from gridded digital elevation models. *Water Resour. Res.*, *43*. doi:10.1029/2006WR005128.

Sideris, I. V., Gabella, M., Erdin, R., & Germann, U. (2014). Real-time radar-rain-gauge merging using spatio-temporal co-kriging with external drift in the alpine terrain of Switzerland. *Q.J.R. Meteorol. Soc.*, *140*, 1097–1111. doi:10.1002/qj.2188.

Spekkers, M., Rözer, V., Thieken, A., ten Veldhuis, M.-c., & Kreibich, H. (2017). A comparative survey of the impacts of extreme rainfall in two international case studies. *Nat. Hazard Earth Sys.*, *17*, 1337–1355. doi:10.5194/nhess-17-1337-2017.

Spekkers, M. H., Kok, M., Clemens, F. H. L. R., & ten Veldhuis, J. A. E. (2014). Decision-tree analysis of factors influencing rainfall-related building structure and content damage. *Nat. Hazard Earth Sys.*, *14*, 2531–2547. doi:10.5194/nhess-14-2531-2014.

Steinbrich, A., Leistert, H., & Weiler, M. (2016). Model-based quantification of runoff generation processes at high spatial and temporal resolution. *Environ. Earth Sci.*, *75*, 1423. doi:10.1007/s12665-016-6234-9.

Stephens, E., Schumann, G., & Bates, P. (2014). Problems with binary pattern measures for flood model evaluation. *Hydrol. Process.*, *28*, 4928–4937. doi:10.1002/hyp.9979.

swisstopo (2017a). *swissALTI3D: The high precision digital elevation model of Switzerland*. Swiss Federal Office of Topography. URL: https://shop.swisstopo.admin.ch/en/products/height_models/alti3D (last accessed 03.07.2017).

swisstopo (2017b). *SWISSIMAGE: The digital color orthophotomosaic of Switzerland*. Swiss Federal Office of Topography. URL: https://shop.swisstopo.admin.ch/en/products/images/ortho_images/SWISSIMAGE (last accessed 03.07.2017).

Teng, J., Jakeman, A. J., Vaze, J., Croke, B., Dutta, D., & Kim, S. (2017). Flood inundation modelling: A review of methods, recent advances and uncertainty analysis. *Environ. Modell. Softw.*, *90*, 201–216. doi:10.1016/j.envsoft.2017.01.006.

Thieken, A. H., Kreibich, H., Müller, M., & Merz, B. (2007). Coping with floods: preparedness, response and recovery of flood-affected residents in Germany in 2002. *Hydrolog. Sci. J.*, *52*, 1016–1037. doi:10.1623/hysj.52.5.1016.

Tyrna, B., Assmann, A., Fritsch, K., & Johann, G. (2017). Large-scale high-resolution pluvial flood hazard mapping using the raster-based hydrodynamic two-dimensional model FloodAreaHPC. *J. Flood Risk Manage.*, *42*, 19. doi:10.1111/jfr3.12287.

Tyrna, B. G., & Hochschild, V. (2010). Modellierung von lokalen Überschwemmungen nach Starkniederschlägen. In J. Strobl, T. Blaschke, & G. Griesebner (Eds.), *Angewandte Geoinformatik 2010* (pp. 325–334).

Ward, R. C., & Robinson, M. (2000). *Principles of hydrology*. (4th ed.). London, UK: McGraw-Hill.

Wechsler, S. P. (2007). Uncertainties associated with digital elevation models for hydrologic applications: a review. *Hydrol. Earth Syst. Sc.*, *11*, 1481–1500. doi:10.5194/hess-11-1481-2007.

Yu, D., & Coulthard, T. J. (2015). Evaluating the importance of catchment hydrological parameters for urban surface water flood modelling using a simple hydro-inundation model. *J. Hydrol.*, *524*, 385–400. doi:10.1016/j.jhydrol.2015.02.040.

Zhou, Q., & Liu, X. (2002). Error assessment of grid-based flow routing algorithms used in hydrological models. *Int. J. Geogr. Inf. Sci.*, *16*, 819–842. doi:10.1080/13658810210149425.

Zhou, Q., Mikkelsen, P. S., Halsnæs, K., & Arnbjerg-Nielsen, K. (2012). Framework for economic pluvial flood risk assessment considering climate change effects and adaptation benefits. *J. Hydrol.*, *414–415*, 539–549. doi:10.1016/j.jhydrol.2011.11.031.

Part III

Synthesis

5 Conclusions

Surface water floods (SWFs) constitute a serious natural hazard that frequently causes substantial damage. With ever-growing population and wealth, the incurred adverse effects are expected to increase further in the future, possibly aggravated by climate change. So far, we know relatively little about most aspects of SWFs. Within this context, this thesis has made three main contributions: Firstly, a vast harmonized data set of flood claim records has been collated and methods have been developed, which allow to classify such spatially-explicit data according to the responsible flood type, i.e., SWFs or fluvial floods. Secondly, the relevance of SWFs has been demonstrated and quantified by analyzing the collated data set of registered damage to buildings in space and time. Lastly, a current SWF hazard assessment approach based on single deterministic flood simulations has been thoroughly tested, revealing that it is not (yet) fit to reliably predict inundations caused by SWFs in rural areas.

In this chapter, the findings related to the three main contributions of this thesis are first summarized in more detail. Thereafter, the main conclusions are drawn and an outlook is provided.

5.1 Summary of results

5.1.1 Classification scheme for spatially explicit flood damage

Before a certain flood process can be analyzed based on spatially explicit damage data, each data entry needs to be classified according to the responsible flood type. For that matter, a classification scheme has been developed to exploit the potential of flood claim records from insurance companies. The algorithm associates any flood damage with one of five classes, by relating the damage's known geographical location to flood maps as well as to the hydrological network. The following five classes are differentiated:

- A: Most likely surface water flood
- B: Likely surface water flood
- C: Fluvial flood or surface water flood
- D: Likely fluvial flood
- E: Most likely fluvial flood

The classification scheme is based on the general idea that objects affected by fluvial floods are necessarily clustered around the river network, while SWFs must be the cause for damaged objects located far away from any watercourse.

The method was developed in a pilot study based on data from four different Swiss public insurance companies for buildings (PICB) (cf. Sect. 2.2). Meanwhile, the data set was enlarged including a total of 14 PICB, in addition to data from the Swiss Mobiliar, a cooperative insurance company (CIC) (cf. Sect. 3.3.1). As the delivered flood damage records were heterogeneous, the data had to be harmonized. For instance,

deductibles needed to be explicitly accounted for in order to obtain total direct tangible losses. Furthermore, the loss values had to be corrected for inflation, so as to provide homogeneous values as of 2013. Most importantly, the data were geocoded based on the reported address, in case the delivered data from the respective insurance company did not contain corresponding coordinates already (cf. Sect. 3.3 for more details). Thus, it was possible to compile a vast, spatially explicit data set, including 63'117 flood damage claims covering 48 % of all Swiss buildings and periods of 10 to 33 years, depending on the data source.

The application of the initial scheme to the full data set highlighted a potential for improvements. Therefore, the method was refined before applying it to the extended data set (cf. Sect. 3.3.2): First of all, as the initial scheme disregarded topography altogether, a measure was developed called "altitude constrained Euclidean distance" (ACED), which combines the simplicity of Euclidean distances with an implicit consideration of topography. Accounting for the rivers' size turned out to be unessential, after the method had been applied to a larger data set, and was therefore dropped. Moreover, the incorporation of flood maps stemming from different sources was adjusted and the treatment of lakes was refined. Lastly, the terminology was amended based on the observation that terms related to SWFs are not well-defined on an international level. For that matter, the general term "overland flow", rooting in the translation of the frequently used German term "Oberflächenabfluss", was replaced by the more specific term "surface water flood" (cf. Sect. 3.2 for a detailed discussion of the terminology).

Overall, the refined classification scheme improved the categorization of individual damage claims, while the shares of claims per class were only slightly affected. It should be noted, though, that the presented numbers obtained with the initial method (Sect. 2.4) cannot be compared directly to those produced with the refined method (Sect. 3.4), because the considered time period is different and the numbers were not aggregated in the same way.

The classification scheme allows for an objective and pragmatic classification of any data set reporting flood damage, with the sole requirement of being spatially explicit. The scheme can be directly applied to such data sets in Switzerland, by using the corresponding published AECD percentile values (Table 3.4 in Sect. 3.3.2), ideally, but not necessarily, in combination with the corresponding flood maps. It remains to be tested, whether the percentile values are also representative for regions with similar geographical settings as the Swiss regions chosen for this thesis. Nevertheless, the scheme is applicable to other regions as well, but needs to be conditioned on corresponding damage data and adapted to the available flood maps.

The main limitation of the classification scheme is that it is not able to separate SWF claims from fluvial flood claims within fluvial flood zones. All claims located within such zones are being associated with fluvial floods, neglecting the fact that also surface water floods might have been the cause for the damage. However, a further differentiation is difficult, or often impossible, as additional data are missing. On the other hand, objects that are not in the vicinity of any watercourse can reliably be associated with SWFs. Consequently, the method provides a robust lower estimate of damage claims caused by SWFs.

5.1.2 Occurrence of surface water floods in space and time

The classified data set was analyzed with respect to the occurrence of SWFs in space and time. For that matter, the data were constrained to data from PICB, as they each hold a monopoly position within the respective canton, as opposed to CICs. Analyzing records from the latter mentioned source is therefore more challenging, as such data are subjected to certain (unknown) market shares. In contrast, the records from PICB cover virtually all buildings within the respective canton (cf. Sect. 3.3 or refer to Schwarze et al. (2011) for background information about the Swiss insurance system). To account for effects of socio-economic development on the damage data, relative number of claims and associated losses were assessed. For that matter, the absolute values were aggregated on regular grids and were then divided by the number of buildings or the total sum insured, respectively.

Overall, the analyses of the classified data have shown that 45 % of all damage claims could be associated with SWFs for the gapless period 1999–2013. The corresponding loss fraction was remarkably lower and amounted to 23 % of the total direct losses to buildings. The spatial distribution of the damage revealed large regional differences, whereas the patterns of number of claims were quite similar to the patterns of associated losses. The hilly lowlands of Switzerland were affected most by SWFs, both in terms of absolute and relative numbers. In contrast, the alpine areas were rather dominated by fluvial flood damage. Moreover, the damage is not evenly distributed within each region either. By considering relative values, the effect of higher absolute values driven by more densely populated areas could be accounted for. Temporally, the damage caused by SWFs is by far the highest in summer, while almost no damage is caused between October and April, save a few exceptions.

In all regions, the relative number of damage claims and associated losses do not exhibit upward trends within the period 1993–2013. Although the period is relatively short for such an analysis, the lacking trends indicate that the socio-economic development is the main driver of the increasing absolute damage values. Moreover, it pinpoints to the importance of considering such effects, when analyzing damage data.

SWF claims are more numerous for smaller events as opposed to fluvial flood claims, which are most numerous for the largest flood events, defined pragmatically as days with at least one registered damage of any class. In contrast, most of the associated losses are incurred during the largest events, irrespective of the flood type.

The losses related to SWFs are limited to a remarkably narrow range, while the losses associated with fluvial floods are skewed to a much higher degree. This clearly suggests that the losses caused by SWFs are not as dependent on the severity of the triggering event in comparison to the fluvial flood losses. Most likely, this circumstance is caused by differing flood impact mechanisms. SWFs are characterized by low flow depths, which lead to rather low damage ratios. In contrast, fluvial foods are associated with both low and high flow depths as well as with pronounced static (e.g., flooding from overtopping lakes) and dynamic flood impacts (e.g., from debris flows). Hence, fluvial flood damage ratios vary within a much larger range from frequent low values to values around one indicating a building's complete destruction, observable during the most severe events.

5.1.3 Modeling surface water floods in rural areas

In practice, the hazard of SWFs is commonly assessed by using single realizations of a deterministic flood inundation model. As data for a thorough model evaluation are usually lacking, such models are often applied in an uncalibrated and unvalidated mode. To test this approach, three raster-based hydrodynamic models were selected, i.e., "FLO-2D", "FloodArea", and "r.sim.water", whereas each model is associated with a different level of model complexity. In addition, the models were complemented by a simple flow accumulation algorithm, i.e., the multiple flow direction algorithm "MFD" (cf. Sect. 4.2.1 for details).

The models were tested in two steps. Firstly, the models were applied to four artificial surfaces, i.e., to a parallel slope of an inclined plane, a convex surface defined by an ellipsoid, a concave slope given by the ellipsoid's inverse and a saddle, representing the combination of a convex and a concave surface. Additionally, an artificial street was incised into the corresponding digital elevation model (DEM). For this exercise, the models were fed with a constant rainfall intensity of 50 mmh^{-1} for one hour, while neglecting all losses such as infiltration, interception, etc. Secondly, the models were applied two eight real-world case studies that cover a wide range of different geographical and meteorological settings. The models were then validated with reconstructions of inundated areas based on various data sources. For that task, commonly used binary pattern performance measures were exploited.

The modeling exercise with artificial surfaces exemplified that the flow is significantly disturbed by structures such as streets, whereby each model simulated this flow disturbance differently. The predicted flow depth on the street highlighted the need for calibrating the corresponding roughness values obtained from linking the land use to common literature values. Namely, r.sim.water produced flow depths on the street below the chosen dry/wet threshold of 0.02 m for all surfaces, while FLO-2D predicted flow depths exceeding 0.5 m. The pattern of inundated areas, i.e., the pattern of cells with a flow depth above the threshold value, agreed better in the regions upslope of the street. In general, the model spread was largest for simulations on the convex slope, which are characterized by diverging flow. The models' (undisturbed) flow patterns agreed better for simulations on the other slope forms.

Without exception, all models exhibited generally low performances for all real-world case studies. Above all, the results indicate that the uncalibrated models are not able to reliably predict inundations of rural areas within a wide range of settings. Hence, the models need to be calibrated to improve the models' prediction skills under the corresponding circumstances. When such an approach is employed for SWF hazard assessments, special attention should therefore be payed to the introduced uncertainties in the observational data, the input data as well as the simulated results.

In more detail, the performance of the hydrodynamic models was better for events associated with more intense rainfall. In contrast, too little effective rainfall was estimated for the other events, which led to biased results and, consequently, particularly low performances. The flow accumulation algorithm MFD was less biased, as the algorithm's prediction of wet/dry cells is not dependent on rainfall. Overall, MFD slightly outperformed the other models. On the downside, MFD does not route any water, so that the estimated flow accumulation area has to be converted to the desired quantity, e.g., to flow depths. Yet, this conversion is generally not universal, but may depend on

the specific settings.

5.2 Conclusions and outlook

The classification scheme presented in this thesis is a pragmatic algorithm, which allows to separate spatially explicit flood damage records of insurance companies. The differentiation of five classes with various levels of confidence provides additional information and qualitatively reflects the uncertainty associated with the claims' classification.

The presented algorithm might be of use for various applications. For instance, insurance and re-insurance companies could classify their data sets to obtain new insights about their portfolio with respect to SWFs. Furthermore, insurance companies may apply the scheme in case of a damage to provide prior knowledge, enabling a more efficient and reliable damage assessment during the claim settling process. However, the utility of the scheme is not limited to insurance data, but can basically be applied to any spatially explicit data containing unclassified flood damage records.

For Switzerland, the reported distance percentile values (Table 3.4 in Sect. 3.3.2) can be used directly, save for Southern Switzerland and the Western Inner Alps. For these two regions, values could be estimated based on the other regions' values. An open question is, whether these values are also representative for other regions embedded in a similar geographical context. Thereby, the geographical setting does not only encompass the physical characteristics such as topography, geology, pedology, hydrology and meteorology, but likewise, societal factors determining how flood risks are managed, how the settlements are built and protected against fluvial hazards. These combined factors determine the distribution of fluvial flood damage in the landscape, which in turn is the basis for the classification scheme. Thus, prior to the application of the scheme to other regions, it should be adapted to the local or regional context. The minimum requirements are a representative number of damage records, fluvial flood maps, in addition to a DEM, and a spatial data set representing the river network.

Obviously, the classification is dependent on the representation of the hydrological network. Specifically, the spatial data's implicit (or explicit) definition of a watercourse also determines what is considered to be a SWF or fluvial flood, respectively. For instance, if a spatial data set contains only large rivers, damaged objects located outside of the flood maps might be associated with SWFs, albeit they were caused by overtopping streamlets. In contrast, if a spatial data set contains artificial channels and large sewers, claims classified as fluvial flood damage might in fact have been caused by a SWF following the definition by Falconer et al. (2009), for instance. These pointed examples illustrate the classification scheme's pragmatism, which is necessary, however, as to make the algorithm applicable to large data sets, since a detailed manual classification is not feasible in such cases. Nevertheless, the dependence of the classification on the respective spatial data should always be considered. Thus, it highlights the need for transparent and consistent definitions of all involved processes using unequivocal terminology, as advocated by this thesis.

The results of this thesis unambiguously demonstrate that SWFs are a significant natural hazard in Switzerland. Although anecdotal evidence has suggested that SWFs are causing substantial damage, a quantification of the relevance has been lacking, so far. Overall, 45 % of the damage claims can be associated with SWFs. Hence, SWFs

are responsible for almost as many damaged buildings as are fluvial floods. As the classification scheme provides a lower estimate of SWF damage, the numbers are likely even higher in reality. At the same time, SWFs "only" account for 23 % of the total flood losses to buildings. The lower loss share of SWFs is due to a lower and narrower distribution of losses per claim in comparison to fluvial floods. Nevertheless, based on the presented loss values, SWFs are ranked among the costliest natural hazards in Switzerland (cf. Imhof, 2011; Hausmann et al., 2012) and, thus, are certainly a serious concern for our society.

Remarkably, the median of yearly losses caused by SWFs is slightly higher than the median of yearly fluvial flood losses. In fact, SWFs cause quite regular losses with a distinct seasonality peaking in the summer months. At the same time, increased losses are always constrained to certain areas. This is exemplified by the time series of normalized damage within the period 1993–2013 (Fig. 3.14 in Sect. 3.4), indicating that the regions were never simultaneously affected to a similar degree. Although certain regions are significantly more affected by SWFs than others, e.g., the Swiss lowlands in comparison to the alpine regions, damage has been registered in all regions. It should be kept in mind, however, that by analyzing damage data, only damaging SWFs can be observed, as opposed to floods in the hydrological sense (Barredo, 2009). Thus, even more so, the data indicate that SWFs can occur practically anywhere in the landscape.

Given the distributed manner and the suddenness with which SWF occur (Yu & Coulthard, 2015), the affected people are often taken by surprise. As the damage number and associated losses are in fact increasing in absolute numbers, mostly attributable to socio-economic development, it is not surprising that the media coverage is seemingly increasing, as well. As society is frequently reminded about the hazard of SWFs due to the relatively high recurrence of SWFs, this might support the required political process to advance and establish measures to better manage SWF risks.

However, the tools for assessing such risk still have to be developed, tested and established. Moreover, strategies need to be elaborated with which the hazard can be managed most efficiently. Given the distributed occurrence of SWFs, it is obviously not reasonable to protect the built environment with area protection (Kron, 2009), unlike for fluvial floods. However, owing to the rather low flow depths associated with SWFs, damage could often easily be prevented.

Manifold types of measures are potentially suitable to reduce adverse impacts of SWFs on our society, including, but not limited to, informational, organizational, political, ecological, agronomic, technical, and structural measures. In particular, potential measures include raising awareness among all stakeholders, compiling hazard or risk maps supporting the consideration of SWFs in spatial planning and development, drafting and enforcing building codes, reducing overland flow generation through agronomic measures and improved drainage systems in rural and urban areas, implementing technical measures to retard overland flow, and physically protect objects, wherever necessary. Thus, the options to better start managing SWF risks in an holistic manner are manifold. However, to be able to make well-informed decisions, SWFs have to be better understood, in the first place. So far, relatively little is known about the main drivers and influencing factors of SWFs. Moreover, as highlighted by this thesis, SWFs do not occur as an isolated process, but are highly inter-linked with other flood processes in a complex interplay. Hence, SWFs should not be regarded as a separate process, but as an integrated part of the catchments.

A better understanding of the involved processes and their (inter-) dependencies is imperative for enhancing existing prediction tools or devising new ones that can be employed for hazard assessments. The need for improving commonly used instruments has been demonstrated by the modeling exercises presented in this thesis. However, the endeavor to develop more reliable tools for hazard assessments should not be focused only on advancing deterministic approaches, but should exploit the whole range of promising tools such as probabilistic methods or simple conceptual models, as well.

After all, the central problem with modeling SWFs is an issue of scale. While small-scale features may determine a flood's flow path and, ultimately, may be decisive whether a certain object is affected or not, the data available for calibration and validation are often either inexistent altogether or only available at a much coarser scale. Therein lies a scale-asymmetry, as models are able to make predictions at extremely fine scales, supported by the increasing availability of corresponding DEMs, while there are practically no observational data available to evaluate such models (Refsgaard et al., 2016). There are some examples, though, that have addressed this problem. For instance, Cea et al. (2014) have used observations of water depth and velocities at high resolution to evaluate a two-dimensional overland flow model at a plot scale.

Thus, a prerequisite for a better understanding of SWFs, as well as better tools to predict this natural hazard, are appropriate data. Specifically, SWF events should be systematically observed and registered at a high spatial resolution. Although the demand for better observational data is not new (e.g., Blanc et al., 2012; Spekkers et al., 2014; Yu & Coulthard, 2015), little progress has been made along these lines. Thus, major efforts are needed to institutionalize and promote the collection of data regarding SWFs. In fact, this study exemplifies that Switzerland, as well as many other countries, have an extremely broad and dense observation network constituted by the insurance companies' portfolios. Of course, such data may contain sensible information, however, such constraint should not be the reason for leaving such data treasures unexploited. Nevertheless, the quality of the insurance companies' records could be improved, as well. For instance, the insurance companies might start to explicitly differentiate flood types during the claim settling process. Apparently, efforts in this direction have been undertaken in practice. Namely, the Swiss Association of Public Insurance Companies that collects damage records from its members has introduced a new damage cause category with which SWFs can be identified (M. Imhof, personal communication, 2017). However, further-reaching improvements are desirable, such as the collection of ancillary data including flow depths, deposited sediments, event descriptions, etc. Additionally, emerging data sources in combination with data mining techniques are promising (e.g., Eilander et al., 2016; Huang et al., 2017) and should be exploited, as well. Last but not least, test fields in SWF prone areas could be set up for long-term monitoring of SWFs, similar to the gauging system of watercourses.

However, not only better and more data are required, but also enhanced methods for an adequate treatment and interpretation thereof. Namely, even the best available observational data are associated with a degree of uncertainty, just as simulation results are, too. Thus, along with improving the data situation related to SWFs, all sources of uncertainties should be quantified and considered, including those of observational data.

References

Barredo, J. I. (2009). Normalised flood losses in Europe: 1970–2006. *Nat. Hazard Earth Sys.*, *9*, 97–104. doi:10.5194/nhess-9-97-2009.

Blanc, J., Hall, J. W., Roche, N., Dawson, R. J., Cesses, Y., Burton, A., & Kilsby, C. G. (2012). Enhanced efficiency of pluvial flood risk estimation in urban areas using spatial-temporal rainfall simulations. *J. Flood Risk Manage.*, *5*, 143–152. doi:10.1111/j.1753-318X.2012.01135.x.

Cea, L., Legout, C., Darboux, F., Esteves, M., & Nord, G. (2014). Experimental validation of a 2D overland flow model using high resolution water depth and velocity data. *J. Hydrol.*, *513*, 142–153.

Eilander, D., Trambauer, P., Wagemaker, J., & van Loenen, A. (2016). Harvesting social media for generation of near real-time flood maps. *Procedia Eng.*, *154*, 176–183. doi:10.1016/j.proeng.2016.07.441.

Falconer, R. H., Cobby, D., Smyth, P., Astle, G., Dent, J., & Golding, B. (2009). Pluvial flooding: new approaches in flood warning, mapping and risk management. *J. Flood Risk Manage.*, *2*, 198–208. doi:10.1111/j.1753-318X.2009.01034.x.

Hausmann, P., Kurz, C., & Rebuffoni, G. (2012). *Floods in Switzerland — an underestimated risk*. Zurich, Switzerland: Swiss Re.

Huang, Q., Cervone, G., & Zhang, G. (2017). A cloud-enabled automatic disaster analysis system of multi-sourced data streams: An example synthesizing social media, remote sensing and Wikipedia data. *Comput. Environ. Urban Syst.*, *66*, 23–37. doi:10.1016/j.compenvurbsys.2017.06.004.

Imhof, M. (2011). *Analyse langfristiger Gebäudeschadendaten: Auswertung des Datenbestandes der Schadenstatistik VKF*. Bern, Schweiz: Interkantonaler Rückversicherungsverband. URL: http://irv.ch/IRV/Download.

Kron, W. (2009). Überschwemmungsüberraschung: Sturzfluten und Überschwemmungen fernab von Gewässern. *Wasserwirtschaft*, *6*, 15–20.

Refsgaard, J. C., Højberg, A. L., He, X., Hansen, A. L., Rasmussen, S. H., & Stisen, S. (2016). Where are the limits of model predictive capabilities? *Hydrol. Process.*, *30*, 4956–4965. doi:10.1002/hyp.11029.

Schwarze, R., Schwindt, M., Weck-Hannemann, H., Raschky, P., Zahn, F., & Wagner, G. G. (2011). Natural hazard insurance in Europe: Tailored responses to climate change are needed. *Env. Pol. Gov.*, *21*, 14–30. doi:10.1002/eet.554.

Spekkers, M. H., Kok, M., Clemens, F. H. L. R., & ten Veldhuis, J. A. E. (2014). Decision-tree analysis of factors influencing rainfall-related building structure and content damage. *Nat. Hazard Earth Sys.*, *14*, 2531–2547. doi:10.5194/nhess-14-2531-2014.

Yu, D., & Coulthard, T. J. (2015). Evaluating the importance of catchment hydrological parameters for urban surface water flood modelling using a simple hydro-inundation model. *J. Hydrol.*, *524*, 385–400. doi:10.1016/j.jhydrol.2015.02.040.

Acknowledgements

The path that has led to the conclusion of this thesis seemed sometimes indefinitely long, and too short at other times. Along this exciting, rewarding, enriching, but also challenging, convoluted, and tough journey, a long list of people have been supporting me in one way or another, to whom I would like to express my sincere gratitude. Additionally, I would like to mention a few individually:

I greatly thank my "doctoral father" and supervisor Rolf Weingartner, borrowing a term translated directly from German. Indeed, Rolf has been a great father to me, giving most valuable advice and inspiring inputs, supporting me whenever needed, but at the same time, letting me develop and pursue my own ideas. Secondly, I thank my co-supervisor Volker Prasuhn, whom I could probably call my "doctoral uncle", adhering to the same terminology. Likewise, Volker has greatly supported and guided me, and I am really thankful for his down-to-earth perspective, in the truest sense of the word.

I am deeply thankful for the productive, enriching, supportive and humorous microcosmos in the office 415, created by its rather permanent residents Veronika Röthlisberger, Simona Trefalt, Andreas Zischg, and Markus Mosimann as well as, formerly, Hannes Suter.

My thanks extend further to the whole team of the Mobiliar Lab and the group of hydrology for all the support, inputs, great discussions, in addition to the much appreciated distractions during lunch and coffee breaks.

Also, I thank Margret Möhl, Tom Reist, Basil Ferrante, Manuel Bart, Isabella Geissbühler, Milka and Dragan Nikolic, as well as all the other benevolent elves working in the background, making sure everything is running smoothly.

My deepest gratitude goes to all my dear friends, relatives, brothers, and parents. Without their advice, reassurance, understanding, motivation, humor, and support — including both tangible as well as intangible means, in both explicit as well as implicit ways — this thesis certainly would not have come to be.

Finally, above all, I express my deepest gratitude to Rose, who has been, and is, amazing in so many ways.

Declaration of consent

on the basis of Article 28 para. 2 of the RSL 05 phil.-nat.

Name/First name	Bernet, Daniel Benjamin
Matriculation number	05-920-434
Study program	PhD in Climate Sciences Bachelor ☐ Master ☐ Dissertation ☒
Title of the thesis	On the occurrence and modeling of surface water floods
Supervisors	Prof. Dr. R. Weingartner and Dr. V. Prasuhn

I declare herewith that this thesis is my own work and that I have not used any sources other than those stated. I have indicated the adoption of quotations as well as thoughts taken from other authors as such in the thesis. I am aware that the Senate pursuant to Article 36 para. 1 lit. r of the University Act of 5 September, 1996 is authorized to revoke the title awarded on the basis of this thesis. I allow herewith inspection in this thesis.

Bern, 12 September 2017 Daniel Benjamin Bernet